A MODEL-BASED APPROACH FOR THE DEVELOPMENT OF A BIOELECTROCHEMICAL SENSOR FOR BIOCHEMICAL OXYGEN DEMAND IN WASTEWATER

BY

CHRISTINE M McCARTHY

THESIS

Submitted in partial fulfillment of the requirements
for the degree of Master of Science in Environmental Engineering in Civil Engineering
in the Graduate College of the
University of Illinois at Urbana-Champaign, 2015

Urbana, Illinois

Adviser:

Professor Roland Cusick

Abstract

Bioelectrochemical systems such as microbial fuel cells and microbial electrolysis cells are currently being researched for many different environmental engineering applications. Some of these applications include wastewater treatment coupled with electricity generation, wastewater treatment coupled with hydrogen production, powering of remote sensors, and as sensors for biochemical oxygen demand or volatile fatty acids. After introducing bioelectrochemical systems and the basic principles and mechanisms of their operation, this thesis will focus on a model-based approach to developing a sensor based on a microbial electrolysis cell to characterize wastewater biochemical oxygen demand.

In a microbial electrolysis cell, a microbial biofilm growing on the anode of an electrochemical cell catalyzes the oxidation of organic matter and uses the anode as a terminal electron acceptor for respiration, thereby generating a measurable current. A polarization curve measures the response of the current generated to changes in the anode potential. In this study, four continuously operated microbial electrolysis cells with two different anode materials with differing surface properties have been used to model the relationship between acetate concentration in the bulk liquid and the shape of a polarization curve generated using low scan cyclic voltammetry. In terms of Monod kinetics, the anode potential determines the limitation placed on microbial respiration rate by the affinity of the electron acceptor for electrons, and is analogous to the effect of oxygen concentration on growth rate in an aerobic system. The Butler-Volmer Monod model is used to relate substrate concentration, anode potential, and generated current. Polarization curves generated at a range of different acetate concentrations were used to estimate the kinetic parameters of the model and to test its capability to predict substrate concentration. The results of this characterization of anode respiring biofilm respiration kinetics, presented in Chapter 3, show that this approach can differentiate between different substrate concentrations and that the fit and predictive capability of the model can be improved by optimizing the choice of anode materials and electrochemical techniques. This approach differs from other studies which attempt predict substrate concentration using only whole-cell current or total charge generated.

Emphasis has also been placed on developing a sensor that is inexpensive and easy to operate, with the idea that such a sensor could allow better process monitoring and optimization at small or resource-limited wastewater treatment plants. To address this, a control and data acquisition system based on the Arduino Uno, an inexpensive microcontroller, was also developed.

This study shows that an approach based on characterizing the kinetic parameters of an anode respiring biofilm in a microbial electrolysis cell and using the Butler-Volmer Monod model to estimate substrate

concentration holds promise. To the best of this author's knowledge, this is the first study to test the predictive capability of a kinetic model for bio-anode polarization curves. Other studies, discussed in Chapter 2, which have developed bioelectrochemical sensors for biochemical oxygen demand, chemical oxygen demand, specific substrates, or other wastewater quality parameters or conditions have shown that sensors based on microbial electrolysis cells and microbial fuel cells can correlate these parameters or conditions with current or total charge generated, and that such sensors have good long term stability and reasonably low response times. However, these biosensors are often subject to thermodynamic limitations on current production, leading to a very low upper detection limit. Furthermore, these previously developed biosensors do not account for the limitations that anode potential can impose on microbial respiration. A sensor based on a three-electrode microbial electrolysis cell and a kinetic respiration model for anode respiring biofilms such as the Butler-Volmer Monod model addresses the issues of thermodynamic limitations and anode potential effects. Future work to include characterization of the effects of other environmental conditions such as temperature, pH, and solution electroconductivity and to further refine the electrochemical techniques and electrode materials could be expected to dramatically improve biosensing capabilities for applications in wastewater treatment process monitoring and optimization.

Acknowledgements

I would like to express my sincere gratitude to everyone who has helped me survive my graduate program and/or contributed to the work described in this thesis. This was a very challenging project, and certainly not a something that I completed entirely on my own. It would not have been possible without the contributions, support, and advice of many others.

I would especially like to thank my adviser Dr. Roland Cusick, who has devoted a significant amount of his time and resources to both this project and my own academic development. I could not have hoped for a better mentor during my time at the University of Illinois and I appreciate his dedication and enthusiasm, his understanding when I made mistakes, and his encouragement and advice when I was stuck. I have learned so much from him and would have missed out on so much if he had not taken a chance by accepting me as his student.

I would also like to thank Dr. Joshua Peschel and his students Meng Han and Adam Burns. Meng helped with the development of the early control system prototypes and code, and Adam helped to design and build PCBs and code the Arduino sketches. Thanks also to Elzabad Kennedy who contributed to later versions of the control system code.

My gratitude also goes to Bruce Rabe and everyone at the Urbana wastewater treatment plant. I was allowed access to samples and plant facilities, given advice on performing a BOD_5 test, and a location is being provided for future setup of field-study equipment.

Thanks also to Patrick Kiely, Nicholas Phelan, and Jack Ambler of Island Water Technologies for their collaboration. It was invaluable to bounce ideas off of them and discuss problems, progress and results on a regular basis.

Finally, I want to thank my family for their support, especially my parents and my husband Scott who put up with me living two states away for two years so that I could obtain my master's degree.

Partial funding for this project was provided by an Innovation Grant from the department of Civil and Environmental Engineering.

Table of Contents

List of Acronyms

AD	Anaerobic digestion
ADC	Analog to digital converter
ARB	Anode respiring bacteria
AS	Activated sludge
ASCE	American Society of Civil Engineers
BES	Bioelectrochemical system
BOD	Biochemical oxygen demand
BOD_5	Five day biochemical oxygen demand
BVM	Butler-Volmer Monod model
CA	Chronoamperometry
CEM	Cation exchange membrane
COD	Chemical oxygen demand
CV	Cyclic voltammetry
DO	Dissolved oxygen
EDL	Electrical double layer
EET	Extracellular electron transport
ET	Electron transfer
LSCV	Low-scan cyclic voltammetry
LSV	Linear sweep voltammetry
MDG	Millennium development goal
MEC	Microbial electrolysis cell
MFC	Microbial fuel cell
PCB	Printed circuit board
SCMFC	Single-chamber air cathode MFC
SPI	Serial-peripheral interface
TEA	Terminal electron acceptor
VFA	Volatile fatty acid

List of Symbols

$A = anode\ surface\ area$
$C = capacitance$

$D_B = diffusivity\ of\ substrate\ in\ the\ biofilm$
$D_L = diffusivity\ of\ sustrate\ in\ the\ liquid\ phase$
$E = anode\ potential\ [V]$
$E_A = anode\ potential$
$E_{KA} = anode\ potential\ where\ j = \frac{1}{2} j_{max} \quad [V]$
$E_{S/P} = theoretical\ Nernst\ anode\ potential$
$E_X^{0'} = formal\ potential\ of\ redox\ component$
$F = Faraday^{'}s\ constant$
$I_{ex} = max\ anodic\ current\ at\ equilibrium$
$I_{max} = maximum\ possible\ current$
$J_{B,\Delta x} = mass\ flux\ through\ bioflim\ differential\ element$
$J_L = rate\ of\ mass\ flux\ through\ stagnant\ liquid\ film$
$K_1 and\ K_2\ are\ lumped\ parameters\ in\ the\ BVM\ model$
$K_A = half - saturation\ concentration\ of\ e^-\ acceptor\ \left[\frac{g\ BOD}{m^3}\right]$
$K_M = substrate\ affinity\ constant$
$K_P = product\ inhibition\ constant$
$K_S = half - saturation\ e^-\ donor\ concentration$
$L_f = active\ biofilm\ thickness\ \ [m]$
$R_{ext} = external\ resistance\ [\Omega]$
$P = Products\ (CO_2, H^+)$
$R = ideal\ gas\ constant$
$S = e^-\ donor\ (substrate)\ concentration$
$S = Substrate$
$S_A = concentration\ of\ e^-\ acceptor$
$S_{B,0} = substrate\ concentration\ at\ the\ liquid/biofilm\ interface$
$S_{L,\infty} = substrate\ concentration\ in\ the\ bulk\ liquid$
$T = temperature\ [K]$
$X_C = redox\ component\ complex$
$X_{OX} = redox\ component$(for example NAD^+)
$X_f = concentration\ of\ active\ biomass\ \left[\frac{g\ VSS}{m^3}\right]$
$X_{red} = reduced\ redox\ component$
$f = \frac{F}{RT}$
$f_e{}^o = fraction\ of\ electrons\ used\ for\ catabolism$
$j_{max} = \gamma_s q_{max} X_f L_f f_e{}^o = maximum\ current\ density\ \left[\frac{A}{m^2}\right]$
$k^0 = standard\ heterogeneous\ rate\ constant$

$k_i = reaction\ rate\ constant$

$q_{max} = maximum\ specific\ rate\ of\ substrate\ utilization\ \left[\frac{g\ BOD}{g\ VS \cdot d}\right]$

$r_{ut} = rate\ of\ substrate\ utilization\ per\ anode\ surface\ area\ \left[\frac{g\ BOD}{m^2 \cdot d}\right]$

$\gamma_s = term\ for\ converting\ mass\ of\ substrate\ to\ coulombs$

$\propto = transfer\ coefficient$

$p = power\ density\ \left[\frac{W}{m^2}\right]$

$\eta = E_A - E_{S/P} = anode\ overpotential\ (BVM\ model)$

$\eta = E - E_{KA} = anode\ overpotential\ (Nernst - Monod\ model)$

Chapter 1: Introduction

The goal of this work was to develop a near real-time biochemical oxygen demand (BOD) sensor for wastewater treatment applications based on a microbial electrolysis cell (MEC). Desired characteristics of the sensor were that it be accurate, low cost, robust, and small in size. The sensor can be viewed as having two basic components: the bioelectrochemical system that generates an amperometric response to BOD concentration and the data acquisition and control system.

BOD is a standard method for quantifying the amount of biodegradable organic contamination in a water sample. Releasing wastewater with a high BOD into a natural water can result in a significant drop in the amount of dissolved oxygen (DO) in the water because as microbes consume the organic matter, many of them also consume oxygen. In surface waters, excessive oxygen consumption due to discharges of high-BOD wastewater can cause fish kills and other water quality problems associated with low DO.

The test used to quantify BOD at wastewater treatment plants and determine compliance with regulations is the five day BOD (BOD_5) test. As the name suggests, the test requires a five day incubation period before results can be obtained (Eaton et al. 1995). Because of the five day lag time, the BOD_5 test is not useful for process monitoring and control at wastewater treatment plants. In addition to the delayed results, the BOD_5 test requires a well-equipped laboratory and well-trained personnel. Due to these shortcomings of the BOD_5 test, a continuous real-time BOD sensor would be very useful at wastewater treatment plants, especially if it was inexpensive and easy to operate. Such a sensor would not replace the BOD_5 test, which is required for regulatory compliance, but would provide a steady stream of measurements useful for informing or even automating process decisions.

1.1 Motivation

Wastewater treatment plays a very important role in protecting human health and the environment, and together with improvements in drinking water treatment, is credited with improving human health and lifespans over the past century as well as minimizing human impacts on the environment (van Loosdrecht and Brdjanovic 2014). However, according to a joint report by the World Health Organization and UNICEF, at the end of 2011 more than 2.5 billion people worldwide, or more than one third of the world population, still lacked access to an improved sanitation facility (WHO/UNICEF 2013). Despite the fact that progress is being made and 1.9 billion people have gained access to improved sanitation since 1990, the millennium development goal (MDG) for sanitation is one of the few MDGs that is completely off track to be met by the 2015 deadline (WHO/UNICEF 2013).

Because sanitation is closely linked to both human and environmental health, expanding access to sanitation and maintaining or improving the operation of existing sanitation facilities is imperative. In industrialized countries, large and centralized sanitation facilities are characteristic of most wastewater treatment systems. However, in a recent article, van Loosdrecht and Brdjanovic (2014) discuss why in the developing world such facilities have not been widely implemented and in many cases where attempts were made, the implementation failed. The high up-front cost of such facilities is a major barrier in many places. Reasons for the lack of success where attempts have been made to implement large-scale sanitation infrastructure in the developing world vary from case to case, but may include failure to account for the local conditions such as temperature and waste characteristics, lack of experienced operators, poor planning and oversight, and a lack of cost recovery and infrastructure asset management programs. van Loosdrecht and Brdjanovic (2014) suggest that in many places in the developing world, decentralized facilities that are smaller, simpler, and managed by the community may provide a viable solution. In addition to reducing costs and need for complex equipment, plants utilizing anaerobic digestion or aerobic granular sludge combined with other technologies for enhanced water and nutrient recovery could provide other benefits and resources to their communities, such as biogas for fuel, nutrients for fertilizing crops, or potable water (van Loosdrecht and Brdjanovic 2014).

Even in the United States, where nearly everyone has access to improved sanitation, much of the wastewater treatment infrastructure is aging. The American Society of Civil Engineers estimates that $298 billion needs to be invested in wastewater infrastructure over the next 20 years. Of this sum, 15% – 20% needs to be invested in wastewater treatment plants and 80% – 85% is needed for pipe and sewer mains (ASCE 2013). The ASCE asserts that much of the US's wastewater treatment infrastructure is in poor condition and that aging pipes and inadequate plant capacity results in the discharge of about 900 billion gallons of untreated wastewater each year (ASCE 2013). In addition, much of the wastewater infrastructure in the US is based on large, centralized facilities that may be vulnerable to large-scale unexpected interruptions. One example of this occurred in 2012 when coastal flooding caused by Hurricane Sandy resulted in the discharge of 11 billion gallons of untreated or partially treated wastewater to the surface waters of the eight hardest-hit states, with the majority of the damage occurring in New York and New Jersey. Many communities had impaired or non-functioning wastewater treatment facilities for a time after the storm, ranging from hours to months (Kenward 2013).

Often, local communities bear the financial burden associated with maintaining and upgrading sanitation infrastructure. In the United States and elsewhere, this often means that in communities with limited resources, even where sanitation facilities exist they may be outdated, inefficient, and insufficient in capacity. Optimization of wastewater treatment processes requires continuous real-time monitoring of

process indicators such as BOD concentration, temperature, pH, and total suspended solids (TSS). While affordable and reliable sensors are widely available for most of these parameters, such is not the case for BOD. Not only is frequent BOD_5 testing not economically feasible for many communities, but standard methods for BOD take too long to be practical for this purpose.

The goal of this project was to reduce the resources needed for real-time monitoring and optimization of wastewater treatment by developing an inexpensive, real-time BOD sensor that can operate under conditions found in typical wastewater treatment plants, including a range of BOD concentrations, pH, and temperature. If combined with a control system, the sensor could also allow for more automation of wastewater treatment and make smaller decentralized wastewater treatment infrastructure more practicable in both the developing and developed world.

Chapter 2: Background and Literature Review

2.1 Development and history of bioelectrochemical systems

Microbial fuel cells (MFCs) and electrolysis cells (MECs) are currently being researched for a variety of applications including renewable energy from wastewater (Liu et al. 2004; Min and Logan 2004; Puig et al. 2011; Rabaey and Verstraete 2005; Sonawane et al. 2014), power sources for remote sensors (Donovan et al. 2011; Yu et al. 2011), as biosensors for monitoring and optimizing wastewater treatment and anaerobic digestion (AD) processes (Chang et al. 2004; Di Lorenzo et al. 2009; Kaur et al. 2013; Kim et al. 2003), and even as microbial supercapacitors (Ren et al. 2015). MFCs and MECs are electrochemical cells which use microbes as biocatalysts in an anaerobic anode chamber to oxidize substrate and transfer electrons to a solid anode. In terms of microbial respiration, the substrate acts as the electron donor and the anode as the terminal electron acceptor. In an MFC, the electrons then move through an external circuit, where the electrical current can power a load, to the cathode where they reduce O_2. Though O_2 is typical, other oxidants such as ferricyanide (Pham et al. 2004) and nitrate (Fang et al. 2011) can also be used. Protons generated during the oxidation of substrate at the anode travel to the cathode through a membrane that separates the anode chamber from the cathode chamber, where they reduce O_2 to form H_2O (Logan 2008a). The membrane is permeable to protons while not allowing O_2 into the anode chamber.

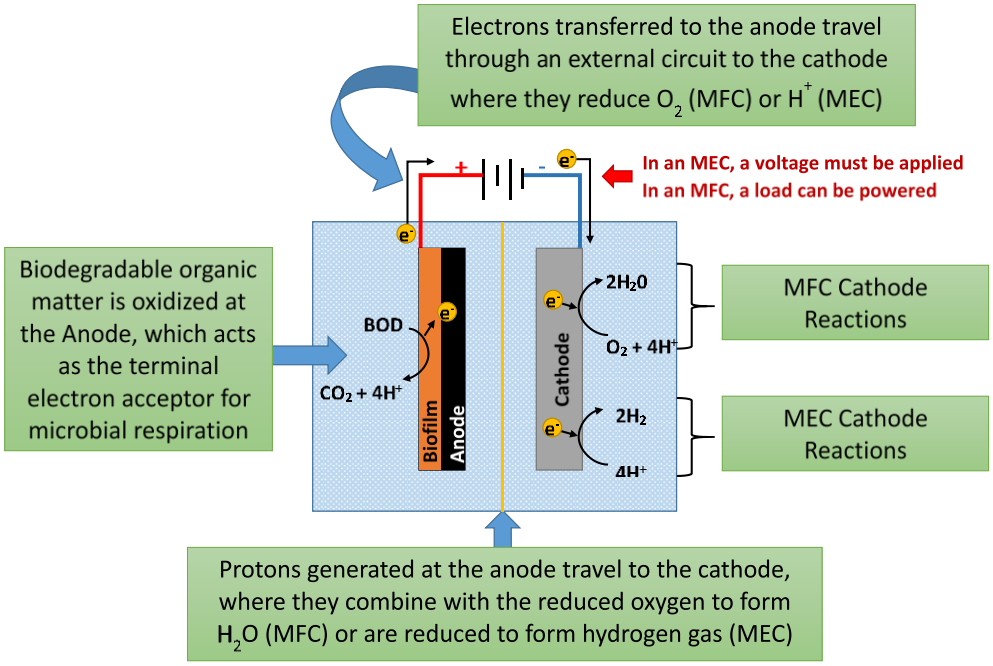

Figure 1: Electrochemical reactions and electron flow in an MEC vs an MFC.

Single chamber MFC designs also exist which use an air cathode and do not require a membrane (Di Lorenzo et al. 2009; Liu and Logan 2004). For both MFCs and MECs, it is necessary to maintain anaerobic conditions in the anode chamber so that oxygen does not act as a competing electron acceptor. MECs are similar to MFCs at the anode, however at the cathode no oxidant is required and instead H^+ is reduced to hydrogen gas. Because there is no need for oxygen at the cathode in an MEC, a membrane separating the anode and cathode is not required, simplifying the design and construction compared to an MFC. In an MEC, the formation of hydrogen gas at the cathode does not proceed spontaneously unless a small voltage is applied to the electrodes. Figure 1 shows a diagram of a typical two-chamber MFC with a membrane and aqueous cathode and illustrates the key differences between MFCs and MECs. MECs are promising for biosensor applications and are also often used for modeling anode biofilm behavior (Torres et al. 2008b) because the anode potential can be controlled, allowing for the application of electrochemical techniques such as chronoamperometry, cyclic voltammetry, and linear sweep voltammetry. An MFC has inefficiencies because of rate limitations due to internal resistance and thermodynamic limitations on the cell voltage (Logan 2008b).

Bacteria that can respire by transferring electrons directly to an anode in an MFC or MEC are referred to collectively as anode respiring bacteria (ARB). While most microbes rely on intracellular electron transfer to soluble terminal electron acceptors (TEAs) such as oxygen, nitrate, sulfate, and others, ARB are unique in that they are exoelectrogens capable of extracellular electron transfer (EET) to reducible solids.

It has been known for decades that certain strains of bacteria can respire by using solid minerals such as Fe(III), Mn(III), and Mn(IV) oxides (Lovley and Phillips 1988; Myers and Nealson 1988). Previously, use of solid minerals as a terminal electron acceptor for respiration was believed to occur only through use of soluble electron shuttles or direct contact of cell membrane embedded cytochromes with the mineral substrate (Rabaey and Rozendal 2010). The earliest MFCs relied on the addition of soluble electron transfer (ET) mediators to carry electrons from within microbial cells to the anode (Park and Zeikus 2000; Roller et al. 1984), with thionine, methyl viologen, 2-hydroxy-1, 4-naphtoquinone, neutral red being some examples of commonly used ET mediators (Kim et al. 2002). The disadvantage of having to add a chemical to mediate ET is obvious, and furthermore, many of the common mediators are toxic to microorganisms, resulting in poor long-term stability (Chang et al. 2004). In 1999 the first study to demonstrate that Fe(III)-reducing *Shewanella putrefaciens* bacteria could transfer electrons directly to an anode in an MFC was published (Kim et al. 1999a). Since the discovery in 2005 that some species of bacteria such as *Geobacter sulfurreducens* (Reguera et al. 2005) and *Shewanella oneidensis* (Gorby et al. 2006) have electrically conductive pili-like structures, dubbed ‘nanowires’, capable of EET over long distances, there has been an immense amount of excitement and research regarding what can be learned

about these microbes and their applications in bioelectrochemical systems (BES). The distance of EET via nanowires can range from nanometers to more than a centimeter. Measurements of *S. oneidensis* MR-1 nanowires have shown them to have conductivity comparable to silicon over distances of hundreds of nanometers, with transport rates of up to 10^9 electrons per centimeter (El-Naggar et al. 2010), and nanowires are believed to be responsible for electron transport from microbes living in an anoxic layer of marine sediment to an aerobic layer more than 1 cm away (Nielsen et al. 2010).

It was long assumed by many researchers that all bacterial nanowires are pili with embedded cytochromes that allow for electron hopping along the length of the structure. However, it has recently been shown that in *S. oneidensis* these nanowires are actually extensions of the cell's outer membrane and periplasm, and the exact molecular structure and mechanism of electrically active *Geobacter* species' nanowires is still under investigation (Pirbadian et al. 2014). However, it is believed likely that *Geobacter sulfurreducens* utilize type IV pili along with outer membrane c-type cytochromes B and Z (OmcB and OmcZ) when respiring on an anode (Richter et al. 2009). It has also been shown that when these organisms grow as a biofilm on the anode of an electrochemical cell such as a microbial fuel cell (MFC) or microbial electrolysis cell (MEC), a conductive matrix is formed with the movement of electrons being driven by redox gradients (Snider et al. 2012).

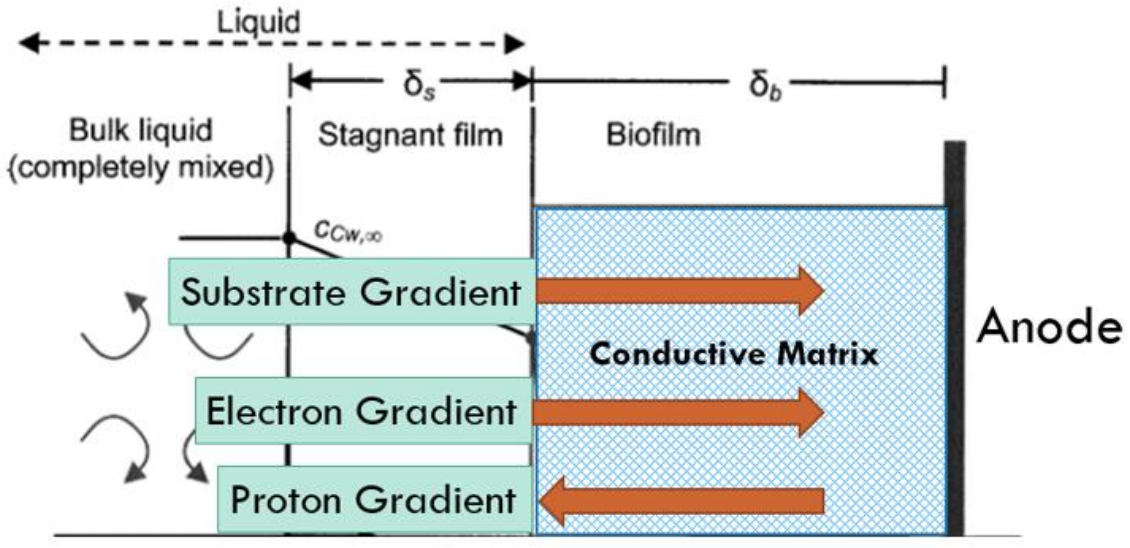

Figure 2: Some important features of an anode biofilm. The red arrows represent the direction of diffusion.

The conductive matrix within an anode respiring biofilm acts as an extension of the anode surface and allows electron transfer from anywhere within the biofilm, regardless of the electron transfer mechanism utilized. Because of this, not only the nanowire producers, but even ARB that use other mechanisms such as electron shuttling can transfer electrons to the anode via the conductive matrix, eliminating the need to

be in direct contact with the surface of the electrode (Torres et al. 2008b). This eliminates distance from the anode as a limitation on biofilm thickness. Thicker biofilms have been associated with higher current output in MFCs and MECs (Lee et al. 2009; Reguera et al. 2006), but such biofilms are still limited by the rate of substrate diffusion into the biofilm, the rate of proton transport out of the biofilm, and the potential of the anode (Lee et al. 2009; Torres et al. 2008a). The proton transport rate can play an important role because if protons leave the biofilm more slowly than they are generated, a pH gradient will exist within the biofilm which can affect electron transfer kinetics because low pH is inhibitory to ARB respiration (Lee et al. 2009). In addition to a proton gradient which drives protons toward the surface and out of the biofilm and a substrate gradient that drives mass transport of substrate into the biofilm, an electron gradient will also exist within an anode biofilm, which drives electron diffusion toward the anode (Snider et al. 2012). The electron gradient can also be viewed as a gradient in the redox state of the biofilm. Figure 2 illustrates some of the key characteristics of an anode biofilm.

2.2 Microbial BOD sensors

2.2.1 Aerobic microbial BOD sensors

The first study regarding the development of a microbial BOD sensor was published in 1977 (Karube et al. 2009), and since then numerous papers about biosensor development have been published in the literature. A 2002 review of microbial BOD sensors (Liu and Mattiasson) divided the sensors that have been developed into two categories: biofilm-based sensors and respirometer-type sensors, and focused on the former. These rapid response sensors can only directly determine the amount of short-term BOD, and additional methods or calibration are required to relate the sensor readings to long term BOD values such as BOD_5. Despite this shortcoming of BOD biosensors, the authors of the review assert that short term BOD values are an important parameter for wastewater treatment process control because of their ability to provide almost immediate feedback on the process state.

Most of the biofilm-type BOD sensors reviewed by Liu and Mattiasson are similar in their design: whole microbial cells are immobilized between two membranes and placed in close proximity to an appropriate transducer that can convert a physical phenomenon such as change in DO concentration or emission of light into an electrical or optical signal. Figure 3 shows a schematic of a typical design for a microbial BOD sensor. An oxygen electrode is the transducer used for the majority of published microbial BOD sensor designs. The sensor response is typically taken as the difference in current from the oxygen electrode before and after the addition of a sample. This difference may be measured as the steady state difference, where the current is allowed to reach equilibrium before each reading requiring about 15 to 20 minutes for each BOD measurement and 15 to 60 minutes in between measurements, or the initial-rate

method can be used which measures the change immediately following addition of the sample, requiring only 15 to 30 seconds for each measurement and less than 10 minutes of recovery between samples. According to Liu and Mattiasson's review, both the steady-state and initial-rate methods have good reproducibility and good correlation with BOD_5 values, but sensors using the initial-rate method have higher sensitivity in addition to faster response times.

Other differences in the various published designs for biofilm-type microbial BOD sensors include the type of microbial cells used, ranging from pure cultures of various species to quantified mixtures of two or more species to a consortium derived from activated sludge (Liu and Mattiasson 2002). Pure cultures have the advantage of stable performance over time, but the limited affinity of a pure culture for all of the substrates that could be found in a wastewater sample reduces the overall detection of BOD. In contrast, a mixed community can detect a wider range of substrates, but the response may change over time as the proportions of different species in the community change. In addition to sensors based on live microbes, some have also been developed using heat-killed microbial cells, thereby reducing maintenance requirements for the sensor (Liu and Mattiasson 2002).

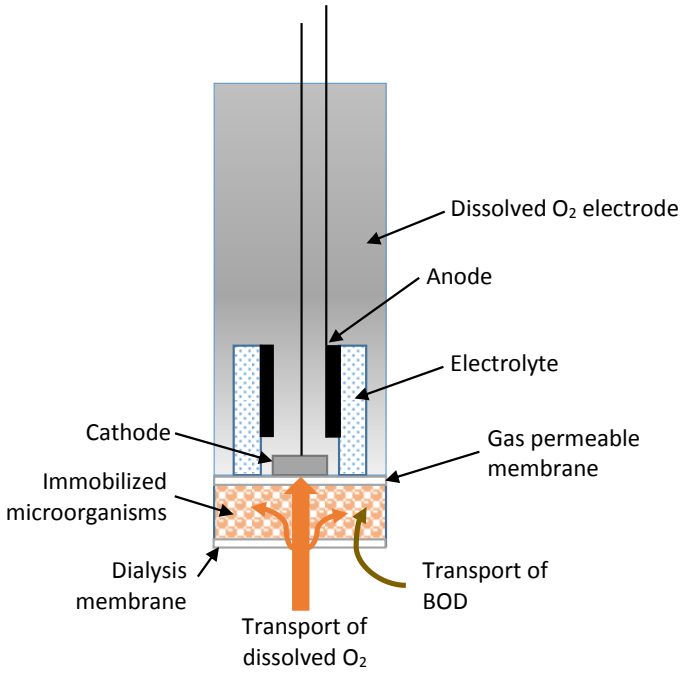

Figure 3: Typical microbial BOD sensor design as described by Liu & Mattiasson (2002).

The performance of the sensor designs reviewed by Liu and Mattiasson varied in terms of measuring range, response time, repeatability, operational stability, and precision with respect to BOD_5 values. The lowest BOD measuring range reported was from 0.5-10 mg/L (Chee et al. 1999), while the highest was

from 17-1275 mg/L (Riedel and Uthemann 1994). Response times ranged from 0.25 (Riedel et al. 1988) to 60 minutes (Tan and Wu 1999) and repeatability from ±1.3% (An et al. 1998) to ±20% (Chee et al. 2000). Operational stability ranged from 7 days (Preininger et al. 1994) to 140 days (Qian and Tan 1998). The ratios of measured BOD to BOD_5 values vary depending on the type of microbes and type of substrate used, but ranged from 0.65 (Yang et al. 1996) to 2.81 (Liu et al. 2000). The weaknesses of BOD biosensors in general were identified by Liu and Mattiasson as: 1) lack of reliability across wastewaters with varied compositions, 2) susceptibility to toxic compounds that may be found in wastewaters, 3) lack of robustness, 4) complex maintenance requirements, and 5) lack of standardization and recognition of use by regulatory bodies.

Riedel et al. (1998) developed a BOD sensor using a pure culture of *Arxula adeninivorans* immobilized in polyvinyl alcohol on an oxygen electrode. The authors stress the importance of using a pure culture for obtaining reproducible results, as well as using a microorganism that can metabolize a broad range of substrates. However, because any pure culture will have a limited variety of usable substrates, the sensor developed by Riedel et al. reported lower BOD values than the standard BOD_5 test for most of the real wastewater samples tested. The *A. adeninivorans* cells were mixed with polyvinyl alcohol and spread onto a capillary membrane. After drying, the resulting "microbial membrane" was added to the Teflon membrane of an oxygen electrode in a cell with a gold cathode. Current production was measured at -600 mV vs. Ag/AgCl for 70 s, with 5 min between each sample. The sensor was calibrated with glucose standards, and sensor response had a linear relationship with BOD_5 in the range of 13 to 550 mg/L of BOD. For a range of pure organic substrates, the ratio of the sensor's BOD value to the BOD_5 value ranged from 0.11 for glycerol to 4.68 for ethyl alcohol. When tested on real wastewater samples from various sources including municipal wastewater, manure, and landfill seepage, 70% of the time the developed sensor was within 30% of the BOD_5 value.

Chee et al. (1999) developed a sensor using an immobilized pure culture of *Pseudomonas putida* on an oxygen electrode which was calibrated using artificial wastewater. This sensor had a lower detection limit of 0.5 mg/L of BOD and response time of 2 to 15 minutes. However, the useful life of the immobilized *P. putida* cells was less than 10 days. Sensor readings were taken by placing the sensor into a phosphate buffer solution and allowing the current to reach equilibrium, after which the sample was added to the buffer solution and the sensor was again allowed to equilibrate. The sensor response was taken as the difference in equilibrium current before and after sample addition. Because the authors were interested in detecting very low BOD concentrations in natural water samples such as river water, the sensor was calibrated and tested with very low levels of BOD. The sensor response was found to be linear with respect to increasing BOD concentration between 0 and 10 mg/L. The sensor was found to be highly

sensitive to temperature and pH, with the optimums being pH 7 and 35^0C. Similar to other sensors relying on a pure culture, sensor BOD values for natural water samples were typically lower than BOD_5 values.

Kim et al. (1999) developed a sensor similar to that of Riedel et al. (1998) using a pure culture of *Serratia marcescens* and investigated the influence of the presence of heavy metal ions in unbuffered samples on the sensitivity of the sensor. The sensor was built by filtering the cultured cells onto a Teflon membrane, covering them with a gas-permeable membrane, and placing this on a DO probe. Their sensor was found to have decreased sensitivity in the presence of Cd^{2+}, Zn^{2+}, Cu^{2+}, and Ag^{+}, while Pb^{2+} and Mn^{2+} had negligible impact. Treating the Teflon membrane with graft polymerization of sodium styrene sulfonate to add a coating of polystyrene sulfonic acid (PSSA) decreased the impact of Zn^{2+} on the sensor, as did using cells that had been cultured in the presence of $ZnSO_4$, however, the treatment increased the sensitivity of the sensor response to pH.

Tan and Wu (1999) developed a biosensor using a commercially available BOD seeding mixed culture and compared the performance of the sensor when using live vs. thermally killed cells. The cells were killed by being heated to 280^0C for 165 s, which left enough active enzymes to catalyze the oxidation of organic matter. The sensor was calibrated using a standard glucose-glutamic acid BOD check solution, and the sensor response was found to be linear with respect to BOD_5 up to 45 mg/L. They found that the sensor using thermally killed cells could be more easily stored and had similar sensitivity, but required longer response and recovery times compared to an otherwise equivalent sensor using living cells. The response times for the thermally killed cell sensors was 45-60 minutes, compared to 35-50 minutes for the living cell sensors, and recovery times were 45 and 30 minutes, respectively. The sensor BOD measurements were lower than BOD_5 values regardless of whether living or thermally killed cells were used.

A BOD sensor similar to other sensors using microorganisms on an oxygen electrode was developed by Rastogi et al. (2003). This sensor made use of a carefully selected consortium of microorganisms instead of pure culture. Operation of the sensor was similar to that of Chee et al. (1999). The sensor was calibrated with glucose-glutamic acid solutions and was found to have a linear relationship with BOD_5 up to a concentration of 90 mg/L. The sensor was tested with dilutions of industrial wastewater from dairy, distillery, and tannery operations. The sensor showed reasonable agreement with BOD_5 values, but in some cases the predicted values for a given sample differed significantly depending on the degree of dilution.

Nakamura et al. (2007) developed a BOD sensor and method referred to as BOD_{DM}. This double mediator system relied on additions of *Saccharomyces cerevesiae* yeast cells, potassium cyanoferrate, and

meniadone into a small stirred cell with two screen-printed carbon electrodes. The cell potential was poised at 900 mV for three seconds, and the response was taken as the current output at the end of that time. Disadvantages of this system included the need to add chemical mediators and suspended cells as well as a surfactant to prevent adsorption of meniadone to the carbon electrodes, which decreased the response of the sensor with subsequent use.

Velling et al. (2009) investigated the effect of different calibration methods for a biofilm based oxygen electrode sensor using microorganisms from activated sludge. The steady-state and dynamic response methods were also compared. The constructed sensor had a detection range of 14-255 mg/L of BOD. For the steady state regime, 12-15 minutes were required for measurement, followed by 20-50 minutes of recovery time.

2.2.2 MEC and MFC based BOD sensors

One major issue with the types of aerobic oxygen electrode BOD sensors described in the previous section is poor long-term operational stability and repeatability. MFC and MEC based sensors provide a possible solution, with many studies having demonstrated operational stability over a period of several months (Di Lorenzo et al. 2009) to numerous years (Gil et al. 2003; Kim et al. 2003).

Kim et al. (1999b) used a pure culture of *Shewanella putrefaciens* strain MR-1 in a mediator-less MFC as a biosensor for lactate. The anode chamber contained a suspension of the bacteria which was kept well-mixed and anoxic by sparging with nitrogen gas and was separated from the cathode chamber by a cation exchange membrane (CEM). Graphite plate was used for the anode and an external circuit containing a 500 Ω resistor connected the anode to the reticulated vitreous carbon cathode. The sensor's response was taken as the steady-state current after the addition of 1 mL of lactate solution to the 19 mL of bacterial suspension in the anode chamber. This was repeated with various known concentrations of lactate to create a calibration curve, which was linear with respect to current in the range of 2 to 25 mM. Solutions of glucose and acetate did not produce a signal, while formate and pyruvate solutions generated a positive signal. This indicates that the range of substrates that can be detected are limited to those that can be utilized as electron donors by the pure culture bacteria.

Though not originally intended to act as biosensors, three mediator-less two-chamber MFCs which had already been operating for 3 years and are also described by Kim et al. (2004) were used by Gil et al. (2003) to examine the correlation between various operational parameters and current production. The MFCs had graphite felt electrodes separated by a CEM and were inoculated using activated sludge and anaerobic digester sludge and fed wastewater from a starch processing plant diluted with a solution of 50 mM phosphate buffer and 100 mM NaCl. One of the parameters investigated was influent COD

concentration and the authors suggested that the MFC system could be used as a BOD sensor based on their findings of a linear relationship between current generation and COD up to 50 mg/L and between total charge generated and COD up to 400 mg/L,. Other parameters that were investigated included pH, external resistance, catholyte aeration rate and DO, and electrolyte composition of the catholyte.

Kim et al. (2003) developed an MFC-based BOD sensor, building on their previous work with *S. putrefaciens* MFCs (Kim et al. 1999a; Kim et al. 1999b) and utilizing the same two-chamber MFCs described by Kim et al. (2004) and optimized by Gil et al. (2003). The MFCs, which had been operating for 4 years when the study began, were fed dilutions of wastewater from a starch processing plant which at full-strength had 1200 mg/L of COD and 520 mg/L of BOD. The relationship between total charge generated and BOD was found to be linear up to 206 mg/L, but the linear range was much smaller when the calibration was based on the maximum current generated. Measurements repeated over the period of a year varied from ±3% to ±12%, which is comparable to the repeatability achieved by aerobic biofilm-type sensors (Liu and Mattiasson 2002), and is also comparable to the ±15.4% reproducibility that is considered acceptable for the BOD_5 test (Eaton et al. 1995). Response times ranged from 30 min or less for samples with very low BOD to 10 h for samples with more than 200 mg/L BOD. When samples of wastewater were measured using both the MFC biosensor and the standard methods BOD_5 test, the values obtained were in close agreement. However, these tests were carried out with the same diluted wastewater used for calibration. If wastewater samples with a more variable composition were used, the agreement between measurements made with the MFC biosensor and the BOD_5 test would likely have decreased.

An MFC based biosensor for estimating BOD in samples with very low concentrations was developed by Kang et al. (2003) and its performance compared to the biosensor developed by Kim et al. (2003). The "oligotroph-type" fuel cell was operated at 33 °C and inoculated with river sediment. Throughout the enrichment period which lasted for 8 weeks the MFC was fed river water with a COD of 5 ± 1.2 mg/L. At the end of the enrichment period the current production had stabilized at 0.01 mA. The graphite felt anode and platinum-coated graphite felt cathode were separated by a cation exchange membrane and each chamber had a void volume of 20 mL. The electrodes were connected through an external circuit containing a 500 Ω resistor. Because the current was very low, the design minimized the area of the cation exchange membrane to lessen the amount of oxygen diffusing into the anode chamber while still meeting proton exchange requirements at the cathode. The oligotroph-type MFC had higher current output and higher coulombic efficiency than the MFC developed by Kim et al. (2003) when samples with very low BOD were fed. However, the correlation between BOD and current was different when the feed was changed from river water to artificial wastewater containing glucose and glutamic acid, leading the

authors to suggest that an MFC intended for use as a BOD sensor should be enriched and calibrated with fuel as similar as possible to the samples it will be used to analyze.

Chang et al. (2004) developed a BOD sensor based on a mediator-less MFC. The anode and cathode both consisted of graphite felt and the electrodes were separated into two chambers by a CEM. The catholyte consisted of aerated tap water and the anode chamber was fed a synthetic wastewater which was a modification of the glucose-glutamic acid check solution used in the BOD_5 test. Inoculum was activated sludge from a municipal wastewater treatment plant. The MFC was operated in amperometric mode, where current output is measured with the MFC under a constant load (10 Ω resistor) in the external circuit connecting the anode and cathode. The sensor's response was only linear up to 100 mg/L BOD, but higher concentrations could be measured by decreasing the pumping rate. The BOD concentration of the synthetic wastewater was varied from 20 to 200 mg/L, and 60 minutes was required after changing the concentration for the current output of the MFC to reach a new steady-state. The response of the sensor remained about the same, with variability of less than 10% for the same BOD concentration regardless of whether that concentration had been preceded by a higher or lower concentration. The sensor had good stability and had been operating for more than a year when the study was published. Repeated measurements varied by 10% or less. If the MFC was starved for a prolonged period a long recovery period was required to reach the current densities obtained before the starvation. The longer the starvation, the longer the recovery. Only 30 min was required after a 3 h starvation, but 80 h was required for recovery after a 270 h starvation period. Interestingly, the authors showed that protein synthesis is not involved in recovery by using chloramphenicol to inhibit protein synthesis after a prolonged starvation period and observing that the current still returned to its previous level after enough time had passed. Chang et al. also observed that the current could be limited by the flowrate of aerated water into the cathode chamber at high BOD concentrations.

Some of the limitations of the Chang et al. (2004) sensor include the inefficiencies of an MFC and the need to pump a separate air-saturated solution into the cathode chamber, as well as the low range of BOD that could be detected without dilution. This sensor also does not account for BOD from different types of substrates, anode potential, temperature effects, or pH effects. In a follow-up study, Moon et al. (2004) found that reducing the volume of the MFC could dramatically improve the dynamic response time of the sensor, with a 5 mL MFC needing only 5±1 min for an increase in BOD and 11 min for a decrease. Another follow-up study by Chang et al. (2005) improved the biosensor performance by adding azide and cyanide to act as respiration inhibitors and prevent other electron acceptors such as oxygen and nitrate from competing with anode respiration.

Another MFC based biosensor for estimating BOD was developed by Kumlanghan et al. (2007). An MFC with anode and cathode compartments separated by a proton exchange membrane was constructed and then calibrated and tested using a glucose solution. The anaerobic consortium of microorganisms acting as the biocatalysts for ET to the anode were grown in a separate reactor and replaced in the MFC for each new sample analysis, with the consortium from the previous analysis being returned to the separate anaerobic reactor. The pH in the separate anaerobic reactor was maintained at 7.5. The cathode chamber was continuously aerated to provide oxygen for reduction at the cathode which contained a solution of 25 mM phosphate buffer, 80 mM NaCl, and 10 mM HCl. The biosensor and separate anaerobic reactor were operated at 37^0C and the signal was taken as the steady state voltage drop across an 800 Ω resistor in the external circuit connecting the anode to the cathode before and after injection of the sample. The response time of the sensor was 3-5 minutes, and the response was found to be linear up to 25 g/L of glucose. Disadvantages of this biosensor system included the pumping and aeration requirements, the need to recalibrate frequently to account for changes in the anaerobic consortium, the need to maintain a separate anaerobic reactor, the high operating temperature, and the need for frequent cleaning of the proton exchange membrane.

Di Lorenzo et al. (2009) developed a BOD sensor based on a single-chamber air cathode microbial fuel cell (SCMFC). An air-cathode MFC has significant advantages over aqueous cathode MFCs because there is no need to circulate, aerate, or regenerate the catholyte and the supply of oxidant at the cathode is less likely to be rate limiting. The sensor was initially fed a synthetic wastewater consisting of nutrients and varying amounts of glucose to obtain the desired BOD, and was later also tested with dilutions of wastewater from the primary clarifier of a municipal wastewater treatment plant with 175±50 mg/L BOD. Anaerobic sludge was used for the inoculum and the BOD of the synthetic wastewater was 1000 mg/L until a stable current output was obtained with the anode and cathode connected in a circuit with a 500 Ω resistor. Stable current was obtained after 4 weeks, after which no more inoculum was fed and the BOD of the synthetic wastewater was decreased to 200 mg/L. At various flow rates, the COD removal efficiency varied from 17% for the highest flow rate to 97% for the lowest. However, coulombic efficiencies were low at 4 to 6%, indicating that much of the COD removal was not related to current production.

In the development of their SCMFC biosensor, Di Lorenzo et al. examined the effect of the external resistance on the response time of the sensor, since external resistance can have a limiting effect on MFC dynamic performance (Kang et al. 2003; Kumlanghan et al. 2007). External resistances ranging from 50 to 500 Ω were tested with an influent COD of 100 mg/L. Once a stable current was reached, the flow of influent was interrupted and the solution from inside the anode chamber was recirculated to induce

starvation while still promoting good mixing within the anode chamber. This was continued until the current decreased to 0.015±0.05 mA. It was found that as the external resistance was reduced, the time needed for current to reach a new steady sate was also reduced, so an external resistance of 50 Ω was chosen for further testing and calibration of the biosensor. Resistances lower than 50 Ω were not used because the cell potential was not stable and current production was decreased. The sensor response was then calibrated based on influent CODs ranging from 50 to 1000 mg/L. The sensors were each fed a consistent influent COD concentration until a stable current was reached, which was taken as the sensor response. The sensors were then starved until current decreased to 0.015±0.05 mA before a new influent concentration was fed. The response of the sensor was found to be linear up to 350 mg/L of COD when calibrated based on steady-state current, which is much higher than the linear response of the sensor developed by Chang et al. (2004). Other studies had correlated COD with the total amount of charge generated rather than current, with a linear response up to 250 mg/L COD (Gil et al. 2003; Kim et al. 2003). When the sensor developed by Di Lorenzo et al. was calibrated using this method, the linear range was extended up to 500 mg/L COD, although the response in this range was slightly less linear than when the sensor was calibrated based on steady-state current, with an R^2 value of 0.93 compared to 0.96 for current-based calibration.. The greater linear range for both calibration methods is most likely due to more oxygen availability at the cathode of the single-chamber MFC.

Di Lorenzo et al. also investigated the effect of hydraulic retention time (HRT) on the dynamic response of their single-chamber MFC sensor. HRT was reduced to 27 min by building a new MFC with a similar design but 75% less volume in the anode chamber. At the same flowrate, the original design had an HRT of 109 min. When compared with the larger volume SCMFC, the smaller SCMFC had a significantly reduced response time for either an increase or a decrease in COD concentration. In the case of an increase, the time to reach a steady-state current was decreased from 4 h to 40 min and in the case of a decrease the time was reduced from 8.8 h to 2 h. Slower response times in the case of a decrease in COD have been reported in other studies as well (Moon et al. 2004). The lower volume SCMFC also exhibited a much higher coulombic efficiency of 56 ± 5% compared to 6 ± 0.5% for the higher volume SCMFC. The smaller SCMFC biosensor was calibrated using dilutions of real wastewater and then used to measure the COD of unknown samples of real wastewater. When the measurements were compared with COD measurements made using the standard method they were in very close agreement, with all of the SCMFC biosensor measurements falling within the standard deviation range of the standard method measurements.

Temperature was found to have a very large impact on the sensor response of the SCMFC biosensor. When tested with real wastewater, the sensor response at 30^0C was about 72% higher than at 25^0C and

96% higher than at 20^{0}C. Additionally, the response time was much faster at 30^{0}C, approaching the HRT of 27 min, while close to 40 min or more was required at 20 and 25^{0}C.

The SCMFC-based sensor developed by Di Lorenzo et al. exhibited good operational stability over a period of 7 months. During that period, the sensor was operated continuously with an influent COD of 200 mg/L and the current generation varied by no more than 15%. The reproducibility was also good, with a coefficient of variation of 0.56%. It was shown by Liu and Logan (2004), however, that even with a Nafion membrane separating the anode chamber from the air cathode as was used by Di Lorenzo et al., a significant amount of O_2 is able to diffuse into the anode chamber of an SCMFC, providing a competing electron acceptor and reducing the performance. The authors express interest in evaluating whether the performance of the SCMFC biosensor could be improved by adding respiratory inhibitors as was done by Chang et al. (2005) to improve the performance of their two-chamber MFC biosensor.

Modin and Wilén (2012) developed a BOD sensor based on a single-chamber MEC with no membrane separating the anode from the cathode. The applied voltage reduces some of the limitations on current generation present in an MFC, such as internal resistance and supply of oxidant at the cathode, allowing the ARB to respire at their full capability. Additionally, the lack of a membrane reduces the problem of developing an acidic pH in the anode chamber due to the limit of the rate at which protons can cross the membrane into the cathode chamber. A graphite rod was used as an anode and the cathode was a gas-diffusion electrode which enclosed one side of the reactor. Because of the gas diffusion cathode, the cell could function as either an MFC or an MEC, depending on whether a voltage was applied. The MEC was inoculated with a mixture of aerobic and anaerobic sludge from a wastewater treatment plant and fed with a solution of 20 mM acetate and nutrients. The sensor response was taken as the total charge generated by a batch-wise feeding of a sample and was calibrated with various concentrations of acetate. In this way, the linear range of the sensor was extended up to 1280 mg/L BOD. However, samples with high concentrations required response times as long as 20 h. A BOD concentration of 320 mg/L was the highest that could be measured in 5 h or less. After calibration, the sensor was also tested with other substrates including propionate, glucose, and ethanol. Though the amount of current initially generated was much higher for acetate, the total amount of charge generated per unit of BOD over the reaction period was not necessarily less for other substrates, as similar coulombic efficiencies were measured for each of the different substrates for samples with relatively low BOD. For higher substrate concentrations the coulombic efficiency for acetate was greater than for the other substrates. It is interesting to note that no effort was made to exclude oxygen from the MEC, and the samples fed into the reactor were saturated with air. Because oxygen was present to compete with the anode as a TEA, it is likely that coulombic efficiencies, which ranged from 23% to 59%, could have been higher if oxygen were not present.

Excluding oxygen might have improved the performance of the MEC biosensor, especially when measuring very low BOD concentrations.

Kaur et al. (2013) studied the ability of two-chamber MFCs with acclimated communities to detect specific volatile fatty acids (VFAs), namely acetate, propionate, and butyrate. Three MFCs were constructed with carbon paper anodes and platinum-coated cathodes. The cathode chambers were filled with 50 mM phosphate buffer and continuously aerated. The anode and cathode chambers were separated by a CEM and the electrodes were connected by an external circuit containing a 1000 Ω resistor. The anodes were inoculated with anaerobic digester sludge from a municipal wastewater treatment plant. All of the MFCs were operated at 30^0C and each was fed a different VFA to acclimate the communities of ARB to a specific electron donor. The start-up time for the MFCs fed butyrate and propionate were much longer at more than 500 h, compared to 100 h for the acetate-fed MFC. After the current generation had stabilized, the current, power, and coulombic efficiency of the propionate and butyrate MFCs were also much lower. Each MFC was tested for response to all three VFAs. The acetate-fed MFC demonstrated no sensitivity to propionate and butyrate, while the propionate-acclimated MFC was sensitive only to propionate, and the butyrate-fed MFC was sensitive to all three VFAs. Cyclic voltammetry was used to observe variation in oxidation and reduction peaks for each of the MFCs at various concentrations of each VFA. A linear relationship between peak oxidation current and VFA concentration was found at low concentrations of up to 20 mg/L. Furthermore, the anode potential at which oxidation peaks occurred differed for each of the three MFCs when fed their acclimated substrate, allowing for the possibility of differentiating between the different VFAs. In subsequent work, Kaur et al. (2014) found that start-up time, power and current generation, stability, sensitivity, repeatability, and recovery time could all be improved with modifications to the anode.

In contrast to studies like those previously described which looked to use MFCs or MECs to measure BOD, COD, or even specific VFAs, Xu et al. (2014) developed an MFC biosensor that could act as an early warning system for an activated sludge (AS) process. Rather than measuring a specific metric, changes in current generation, anode potential, and cell potential were used to diagnose problems such as organic overloading shock, ammonia overloading shock, and toxic shock. The MFC biosensor was part of a system which also included software and electronics for continuous monitoring of the AS process.

2.3 Existing models for anode respiring biofilm kinetics

2.3.1 Nernst-Monod Model

The Nernst-Monod model is a modified version of Monod kinetics, where a Nernst-Monod term incorporates the Nernst Equation to modify the Monod Equation with an anode as the TEA. Equation 1 is

the Monod Equation for substrate utilization rate in a case where the concentration of e^- acceptor is limiting the microbial respiration rate in a biofilm (Torres et al. 2008b).

Equation 1

$$r_{ut} = q_{max} X_f L_f \left(\frac{S_A}{K_A + S_A}\right)$$

Where:

$r_{ut} = rate\ of\ substrate\ utilization\ per\ surface\ area\ \left[\frac{g}{m^2 \cdot d}\right]$

$q_{max} = maximum\ specific\ rate\ of\ substrate\ utilization\ \left[\frac{g}{g\ VS \cdot d}\right]$

$X_f = concentration\ of\ active\ biomass\ \left[\frac{g\ VSS}{m^3}\right]$

$L_f = active\ biofilm\ thickness\ [m]$

$K_A = half - saturation\ concentration\ of\ e^-\ acceptor\ \left[\frac{g}{m^3}\right]$

$S_A = concentration\ of\ e^-\ acceptor$

The analogous case for an anode biofilm is when microbial respiration is limited by the anode potential (i.e. the rate at which the anode can accept electrons). For this case, r_{ut} is replaced by the electron transfer rate per unit area in the form of current density, j, and the Monod term, $\left(\frac{S_A}{K_A+S_A}\right)$, is replaced by the Nernst-Monod term, $\left(\frac{1}{1+exp\left[-\frac{F}{RT}(E-E_{KA})\right]}\right)$, as shown in Equation 2 (Torres et al. 2008b).

Equation 2

$$j = j_{max}\left(\frac{1}{1 + exp\left[-\frac{F}{RT}(E - E_{KA})\right]}\right)$$

Where:

$j_{max} = \gamma_s q_{max} X_f L_f {f_e}^o = maximum\ current\ density\ \left[\frac{A}{m^2}\right]$

$\gamma_s = term\ for\ converting\ mass\ of\ substrate\ to\ coulombs$

${f_e}^o = fraction\ of\ electrons\ used\ for\ catabolism$

$F = Faraday's\ constant$

$R = ideal\ gas\ constant$

$T = temperature\ [K]$

$E = anode\ potential\ [V]$

$E_{KA} = anode\ potential\ where\ j = \frac{1}{2} j_{max}\quad [V]$

Equation 2 can be modified for the case where availability of both e^- donor (substrate) and e^- acceptor (anode) are rate-limiting. When availability of substrate and anode potential must both be considered, this can be done by including both a Monod term for the substrate, and a Nernst-Monod term to represent the anode's affinity for electrons as shown in Equation 3 (Lee et al. 2009).

Equation 3

$$j = j_{max}\left(\frac{S}{K_S + S}\right)\left(\frac{1}{1 + exp\left[-\frac{F}{RT}(\eta)\right]}\right)$$

Where:

$S = e^- \ donor \ concentration$

$K_S = half - saturation \ e^- \ donor \ concentration$

$\eta = E - E_{KA} = anode \ overpotential$

Current generated is proportional to the amount of substrate consumed with respect to time, so Equation 3 can also be expressed in terms of substrate utilization rate, as shown in Equation 4.

Equation 4

$$r_{ut} = q_{max} X_f L_f \left(\frac{S}{K_S + S}\right)\left(\frac{1}{1 + exp\left[-\frac{F}{RT}(\eta)\right]}\right)$$

K_S and E_{KA} can be determined experimentally. For an anode biofilm, E does not vary significantly throughout the thickness of the biofilm if it contains a conductive matrix, but S will vary with depth into the biofilm because it is limited by the diffusion rate. For this case, the Nernst-Monod model does not have an analytical solution but can be approximated using the finite difference method as was done by Lee et al. (2009).

2.3.2 Butler-Volmer Monod

The Butler-Volmer Monod (BVM) model is more complex than Nernst-Monod, and was shown by its developers to provide a better fit to experimental anode biofilm polarization curves based on the F-test for goodness of fit (Hamelers et al. 2011). The model is based on the premise that the rate of substrate conversion into products (CO_2, H^+, e^-) by the ARB is determined by enzyme kinetics, and the Butler-Volmer model is incorporated to represent the kinetics of electron transfer to the anode. The enzyme kinetics are modeled by breaking them down into three reversible reactions.

The first reaction shows the formation of a redox component complex (X_C) from substrate and a redox component. In the second reaction, X_C is reduced and CO_2 and H^+ are formed as products. In the third reaction, the reduced redox component becomes oxidized again by transferring its electron to the anode. Figure 4 illustrates the enzymatic model for substrate oxidation and electron transfer.

Equation 5

$$S + X_{OX} \underset{k_2}{\overset{k_1}{\rightleftarrows}} X_C$$

Equation 6

$$X_C \underset{k_4}{\overset{k_3}{\rightleftarrows}} P + X_{red}$$

Equation 7

$$X_{red} \underset{k_6}{\overset{k_5}{\rightleftarrows}} X_{OX} + e^-$$

Where:

$S = Substrate$

$X_{OX} = redox\ component$ (for example NAD^+)

$X_C = redox\ component\ complex$

$X_{red} = reduced\ redox\ component$

$P = Products\ (CO_2, H^+)$

$k_i = reaction\ rate\ constant$

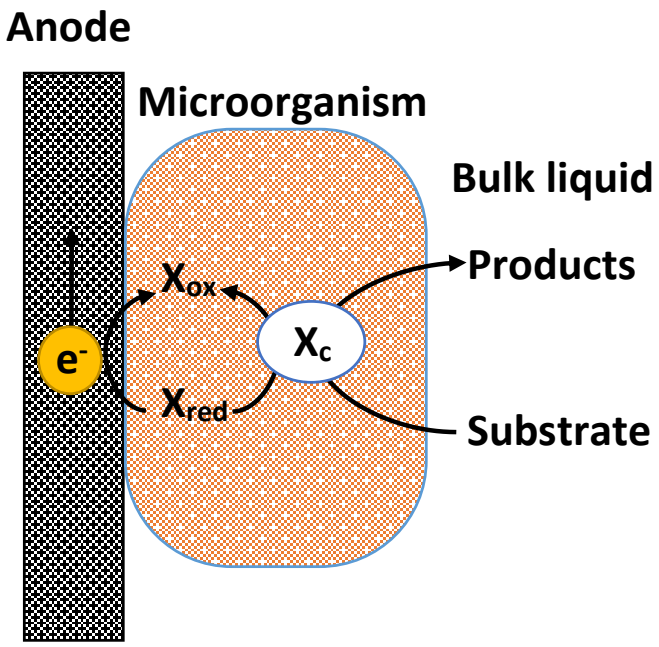

Figure 4: Simple model of ARB enzyme kinetics as described by Hamelers et al. (2011).

The system can then be described with a set of mass balances, shown in Equation 8 through Equation 10, by assuming that whether complexed, oxidized, or reduced the total amount of redox component remains constant within the cell.

Equation 8

$$\frac{d}{dt}X_{ox} = -k_1 S X_{ox} + k_2 X_c + (k_5 X_{red} - k_6 X_{ox})$$

Equation 9

$$\frac{d}{dt}X_{red} = k_3 X_c - k_4 P X_{red} - (k_5 X_{red} - k_6 X_{ox})$$

Equation 10

$$X_c = X_T - X_{ox} - X_{red}$$

The Butler-Volmer model is then applied to describe the dependence of electron transfer rates (k_5, k_6) on anode potential as shown in Equation 11 and Equation 12.

Equation 11

$$k_5 = k^0 exp\left[(1-\propto) f(E_A - E_X^{0'})\right]$$

Equation 12

$$k_6 = k^0 exp\left[-\propto f(E_A - E_X^{0'})\right]$$

Where:

$k^0 = standard\ heterogeneous\ rate\ constant$

$\propto = transfer\ coefficient\ (typically \sim 0.5)$

$f = \frac{F}{RT}$

$E_A = anode\ potential$

$E_X^{0'} = formal\ potential\ of\ redox\ component$

The current that is observed from the anode is given by the difference between the forward and backward current as shown in Equation 13.

Equation 13

$$I = nF(k_5 X_{red} - k_6 X_{ox})$$

Equation 11 and Equation 12 can be substituted into Equation 13:

Equation 14

$$I = nF\left(k^0 exp\left[(1-\propto) f(E_A - E_X^{0'})\right] X_{red} - k^0 exp\left[-\propto f(E_A - E_X^{0'})\right] X_{ox}\right)$$

In order to obtain an interpretable solution to the model, a number of parameters are introduced:

Equation 15

$$K_M = (k_2 + k_3)/k_1$$

Equation 16

$$K_P = (k_2 + k_3)/k_4$$

Equation 17

$$I_{max} = nFX_t k_3$$

Equation 18

$$I_{ex} = nFX_T k^0 \exp[-(1-\alpha) f(E_X^{0'} - E_{S/P})]$$

Equation 19

$$K_1 = \frac{I_{max}}{I_{ex}}\left(1 + P\frac{k_4}{k_3} + \exp\left(-f\left(E_X^{0'} - E_{s/p}\right)\right)\right)$$

Equation 20

$$K_2 = \frac{\mathrm{k_3}}{\mathrm{k_2}}\left(1 + \frac{K_P}{P}\right)$$

Where:

$K_M = substrate\ affinity\ constant$

$K_P = product\ inhibition\ constant$

$I_{max} = maximum\ possible\ current$

$I_{ex} = max\ anodic\ current\ at\ equilibrium$ $(when\ anodic\ and\ cathodic\ current\ are\ equal)$

$K_1 and\ K_2\ are\ lumped\ parameters$

$E_{S/P} = theoretical\ Nernst\ anode\ potential$

Equation 19 introduces K_1, a lumped parameter which can be interpreted as the ratio of the biochemical reaction rate to the electrochemical reaction rate. K_2, introduced in Equation 20, is another lumped parameter which represents enzyme-substrate oxidation kinetics and is expected to be substantially larger than 1. Substituting Equation 10 into Equation 8 and Equation 9 results in two differential equations for X_{ox} and X_{red}. Assuming steady state conditions and combining Equation 8 through Equation 20 results in the Butler-Volmer Monod model:

Equation 21: The BVM Model

$$I = I_{max}\frac{1 - e^{-fn}}{K_1 e^{-(1-\alpha)f\eta} + K_2 e^{-fn} + \left(\frac{K_M}{S} + 1\right)}$$

Where:

$\eta = anode\ overpotential\ (E_A - E_{S/P})$

By rearranging Equation 21, the similarities and differences with the Nernst-Monod model can be more easily seen. Equation 22 shows that, like the Nernst-Monod model, the BVM model can be separated into two factors, with the first representing the influence of anode potential on current production and the second representing the influence of substrate concentration.

Equation 22

$$\frac{I}{I_{max}} = \left(\frac{1 - e^{-f\eta}}{K_1 e^{-(1-\alpha)f\eta} + K_2 e^{-f\eta} + 1} \right) \left(\frac{S}{\frac{K_M}{K_1 e^{-(1-\alpha)f\eta} + K_2 e^{-f\eta} + 1} + S} \right)$$

2.4 Electrochemical techniques and equipment

Because MECs combine a two or three-electrode electrochemical cell with a biological component, a number of voltammetric techniques can be used to study and characterize an anode respiring biofilm. Three-electrode systems typically contain an anode as the working electrode (WE), a cathode as the counter electrode (CE), and a reference electrode. During an electrochemical experiment in a three-electrode system, it is the WE that is controlled based on the potential of a reference electrode, while in a two-electrode system the WE can be controlled based on cell voltage (the difference in potential between the WE and CE).

Three-electrode systems in particular offer significant advantages over MFCs or two-electrode MECs because anode potential can be controlled relative to a known potential, allowing for better control and comparison between different datasets and methods. Both two and three-electrode MECs allow rate limitations due to internal resistance and thermodynamics to be overcome by applying a voltage to the cell, ensuring that the respiration of the anode biofilm is the only rate-limiting step (Rimboud et al. 2014). The elimination of other rate limitations gives MECs significant advantages over MFCs for many applications.

2.4.1 Equipment

A potentiostat is the instrument typically used to control an electrochemical cell and run electrochemical experiments. Potentiostats contain complex electronic circuitry based around the use of operational amplifiers to control the potential of a working electrode (Bard and Faulkner 2001). Though less expensive potentiostats have been developed (Friedman et al. 2012), most cost thousands of dollars per channel, with each channel having the capability to control a single electrochemical cell. Though they are expensive, user-friendly software is often included with numerous pre-programmed techniques and user

customizable settings. Data visualization and analysis tools are also commonly included in the software package. A potentiostat is considered to be indispensable in almost any electrochemistry laboratory.

2.4.2 Techniques

Open circuit voltage

Open circuit voltage (OCV) is a technique where WE potential is measured rather than controlled with the circuit connecting the WE and CE open so that no current can flow.

Chronoamperometry

Chronoamperometry (CA) is a technique that can poise the potential of a WE relative to a reference electrode for a specified period of time. Increasing or decreasing the anode potential will increase or decrease its affinity for accepting electrons. The anode is typically the WE in an MEC, and by poising it within the correct range of potentials, anode respiring biofilms can be grown and maintained over a period of time while collecting data on current generation. CA can be used to observe changes in current production over long periods of time as the biofilm develops or over shorter periods of time as it increases or decreases with substrate concentration. Figure 5 shows an example of how a WE is controlled with respect to time in a CA experiment.

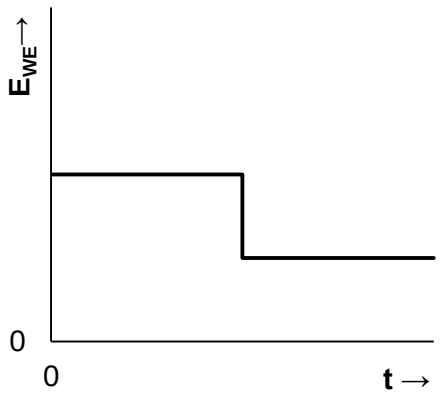

Figure 5: Example of a chronoamperometry experiment where a WE is poised at the same potential for a specified period of time, after which it can be poised at a different potential for a specified period of time.

Hamelers et al. (2011) used CA to generate polarization curves for evaluating the BVM model's fit in comparison to the Nernst-Monod model, as well as to evaluate how the anode potential during the day preceding the polarization curve experiment affected the biofilm's kinetic parameters, K_1 and K_2, when fitting the BVM model to the voltammetry data. They generated a polarization curve by poising the anode potential for two minutes at a time in steps of 0.05 V and recording the current at the end of each step.

CA was also similarly used by Torres et al. (2007) to generate polarization curves. A biofilm anode was poised at each potential for 45 minutes and steady-state current was measured by averaging the last 20 minutes of data for each anode potential step. Torres et al. (2008a) again used CA to generate polarization curves by poising the biofilm anode for 30 minutes at each potential and averaging the final 10 minutes of each potential step.

Linear sweep voltammetry

Linear sweep voltammetry (LSV) is another technique which can be used to determine the response of current production to changes in working electrode potential. In characterizing an anode respiring biofilm, LSV can be used to construct polarization curves. As shown in Figure 6, the potential of the working electrode is increased linearly with respect to time. The sweep rate depends on the application, but is typically much slower when working with a bio-anode than it would be for other electrochemical experiments in order to allow for steady state current to be measured. Sweep rates of 1 or 2 mV/s are common for MEC experiments (Torres et al. 2010).

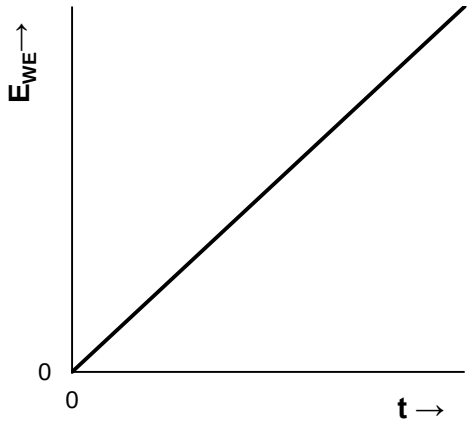

Figure 6: An example of how WE potential is controlled with respect to time during an LSV experiment.

Cyclic voltammetry

Cyclic voltammetry (CV) is similar to LSV in that the potential of the working electrode is swept in a linear fashion with respect to time. However, in a CV experiment, when the anode potential reaches a selected value the scan is reversed. The reversal can be repeated multiple times, with each set of an upward and downward sweep constituting one cycle. An example of how the potential of a WE is controlled with respect to time during a CV with two cycles is shown in Figure 7. Like LSV sweep rates, sweep rates used in cyclic voltammetry experiments with biofilm anodes are typically 1 to 2 mV/s. These

sweep rates are quite slow compared to rates that are usually used in electrochemistry experiments, so CVs at the slower rates are sometimes referred to as low-scan cyclic voltammetry (LSCV).

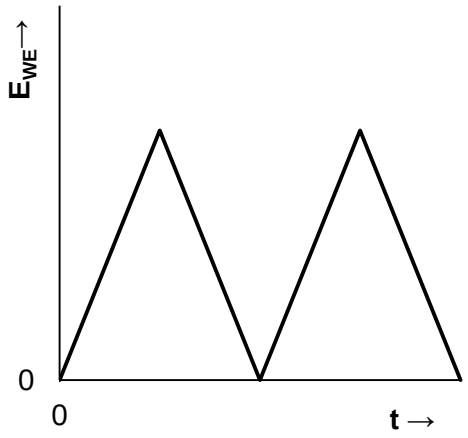

Figure 7: An example of how WE potential is controlled relative to time during a CV experiment with two cycles.

CV has been utilized extensively in MEC research for generating polarization curves (Lee et al. 2009; Torres et al. 2008b; Yoho et al. 2014), evaluating anode biofilm response to different substrates (Kaur et al. 2013), and investigating the roles of specific cytochromes in EET (Richter et al. 2009).

Chapter 3: MEC Biofilm Characterization

3.1 Experimental design

The purpose of the biofilm characterization experiments was to test the predictive capabilities of the BVM model. Anode respiring biofilms were characterized based on their respiration rate, measured as current, at various anode potentials and substrate concentrations using electrochemical techniques such as open circuit voltage, linear sweep voltammetry, cyclic voltammetry, and chronoamperometry.

3.1.1 Reactor designs

Experiments were carried out for MEC reactors with anodes constructed from heat-treated (450 °C, 1 h) carbon mesh (Graphite Store, Buffalo Grove, IL) or isomolded graphite plate (Graphite Store). Both types of anode were paired with a 2.5 x 3 cm stainless steel mesh cathode (38 x 38 0.0065" diameter, Gerard Daniel Worldwide, Hanover, PA). Titanium mesh (30 x 30 0.004" diameter, Unique Wire Weaving Co., Hillside, NJ) was used as a current collector for the carbon mesh anodes. Figure 8 shows the electrode assembly for a carbon mesh anode MEC.

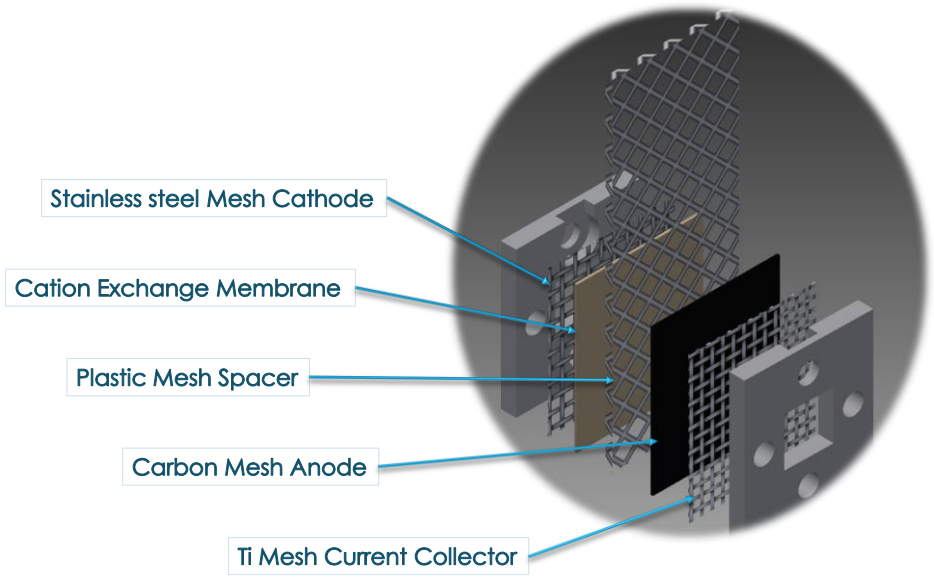

Figure 8: Electrode assembly for MECs with carbon mesh anodes.

The CEM (Membranes International, NJ) shown in Figure 8 was added to the design not to regulate ion transport, but to alleviate problems with the electrodes being shorted together by fibers from the carbon mesh fraying and coming into contact with the cathode. The assembly was sandwiched together between plastic frames with an open area of 1 cm^2 and secured with plastic machine screws.

Initially, five carbon mesh electrode-pairs were placed within a single column reactor as shown in Figure 9. The void volume of the reactor was 590 mL. The column also contained three Ag/AgCl reference electrodes (BASi, West Lafayette, IN) and was packed with plastic biofilm carriers (Hel-X, Germany) with a total surface area of 0.47 m^2 to encourage growth of microbial biofilms that would create a BOD gradient as the influent moved up through the column. This gradient was also to be characterized so that the upper BOD detection limit could be increased for a sensor of similar design. However, in this multi-electrode configuration it was found that each anode could not be truly controlled and characterized independently from one another as would be required for a sensor based on measuring and modeling the respiration of the ARB on each anode separately. This was due to the requirement that all of the cathodes be shorted together and grounded, allowing interaction between the separate electrode-pairs both through the cathodes and through the solution. The column reactor was used to inoculate the biofilm anodes, but no useful characterization experiments were carried out with this reactor and the best-performing anode biofilms were transferred to their own individual reactors for characterization.

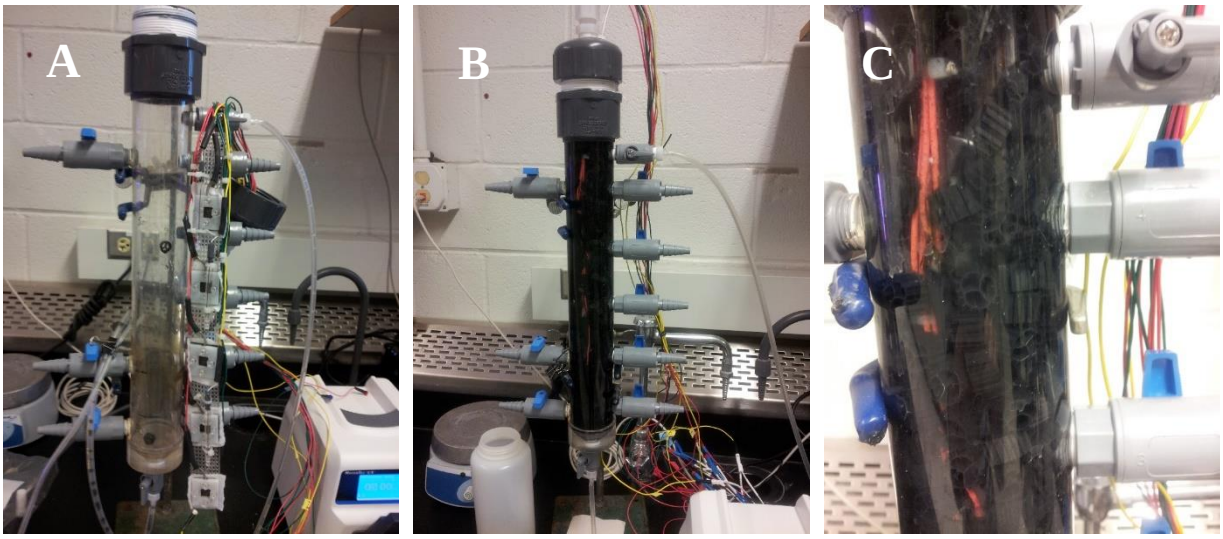

Figure 9: Original column reactor with 5 electrode-pairs and sampling ports at each electrode. A) Electrode assembly, B) column reactor packed with biofilm carriers, C) close-up of biofilm carriers.

In hopes of being able to use a multi-electrode-pair design by better isolating the electrode-pairs from one another, a new modular reactor was designed. The new design allowed for each electrode-pair to be in a separate chamber with only a small channel allowing flow of water and substrate from one chamber to the next. A prototype of this design is shown in Figure 10. Unfortunately, this design did not alleviate the problem of interaction between the different electrode-pairs and the prototype reactor was instead used in the development and testing of the control and data acquisition system described in Chapter 4.

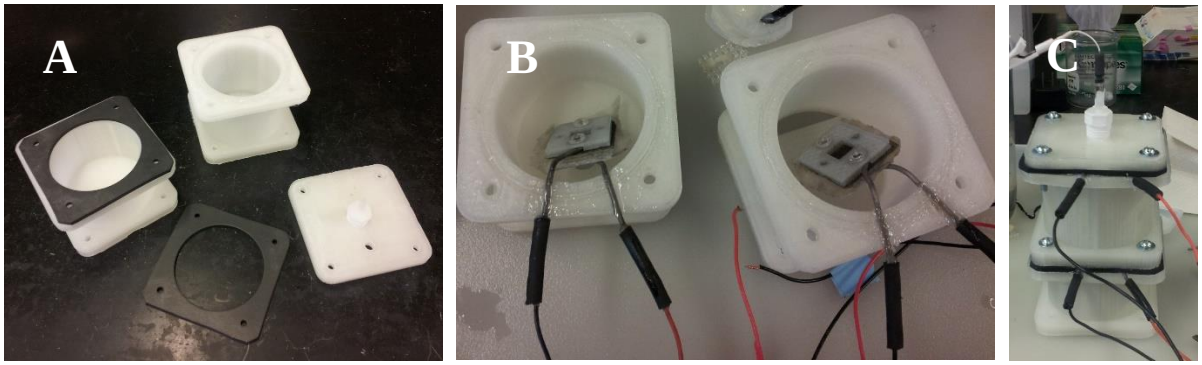

Figure 10: The prototype two-chamber system with carbon mesh anodes as shown in Figure 8. A) 3-D printed ABS plastic components, B) individual chambers with electrode-pair assembly, C) assembled two-chamber reactor.

Due to the problems found with using a reactor containing multiple electrode-pairs in the same bulk liquid, individual electrode-pairs were transferred into 100 mL bottles as shown in Figure 11.

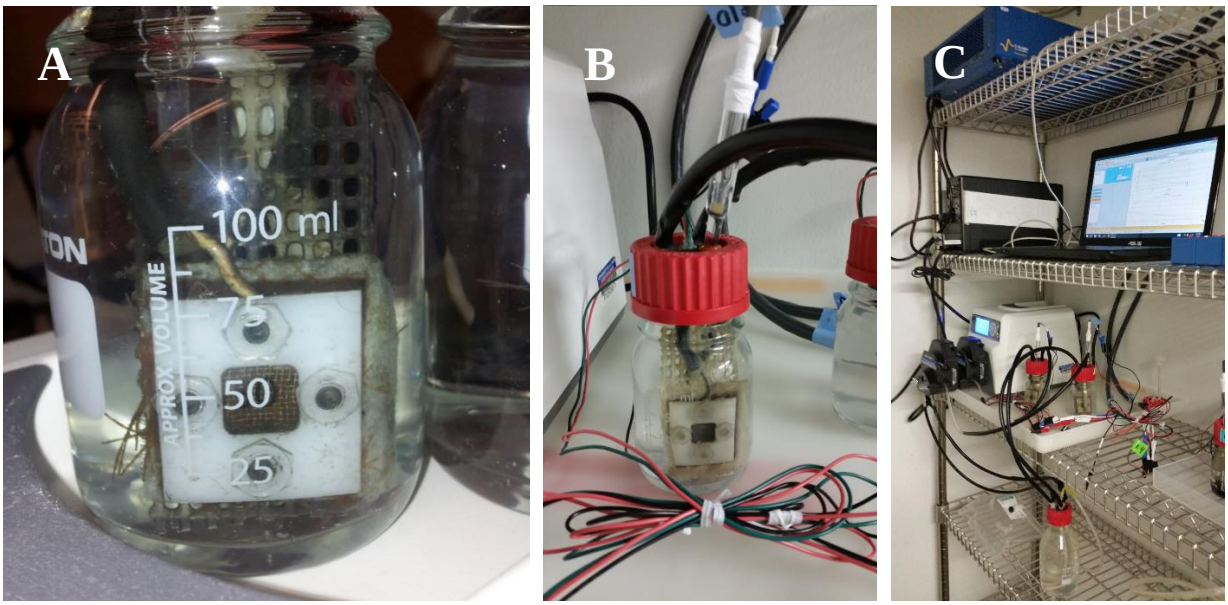

Figure 11: Carbon mesh anode MEC reactors. A) Close-up view of the anode side of an inoculated MEC reactor, B) MEC reactor with reference electrode, electrode lead wires, C) setup with two MECs, potentiostat, pump, and recirculation reservoir.

The individual carbon mesh anode MEC reactors each contained a reference electrode and could be set up in two configurations: 1) a modified batch mode where multiple MECs could recirculate (Masterflex peristaltic pump, Cole Parmer) media to and from a common reservoir in order to maintain uniform environmental conditions and microbial communities between multiple reactors; and 2) a single-pass mode where influent could be pumped from a common reservoir through each individual MEC to a waste reservoir. The modified batch mode was used for growth and maintenance of the biofilms, while the

single-pass mode was used for characterization experiments. In both modes the hydraulic retention time (HRT) was 1 h.

The design and setup of the graphite anode MEC reactors was similar to that of the individual carbon mesh anode MEC reactors. The primary differences between the two designs were that plastic frames and a titanium mesh current collector were not used in the electrode assembly for the graphite anode MECs. Instead, the graphite plate was coated with ABS plastic excepting a 1 cm^2 open area and a small area underneath a machine screw for contact with the titanium wire lead to the external circuit. The open area of the anodes were sanded with fine-grit sandpaper and buffed smooth with lint-free paper. The electrode assembly for a graphite anode MEC is shown in Figure 12.

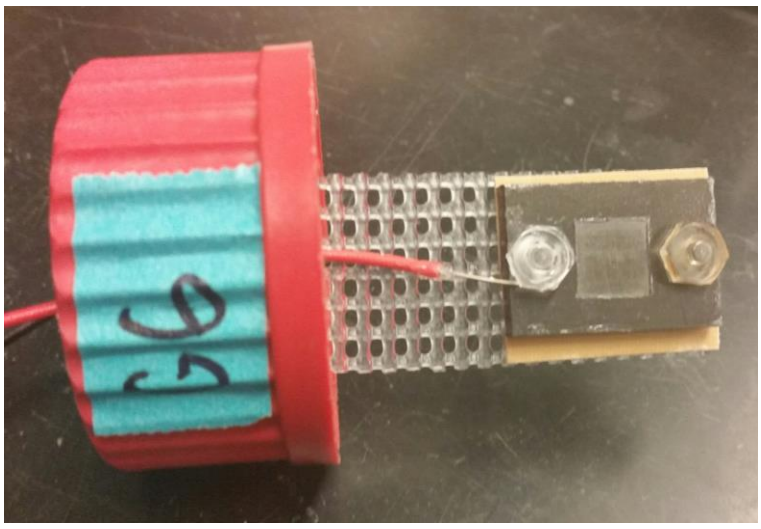

Figure 12: Electrode assembly for a graphite anode MEC reactor.

As with the carbon mesh anode MECs, the graphite anode electrode assemblies were placed into individual 100 mL bottles with Ag/AgCl reference electrodes and tubing allowing for pumping of media to and from a reservoir shared by two MEC reactors (modified batch setup), or from a shared reservoir through two MEC reactors and into a waste collection reservoir (single-pass setup).

3.1.2 Methods

Anode biofilm growth and maintenance

The first reactor to be constructed and inoculated was the column reactor containing five electrode-pairs with anodes made of carbon mesh. The reactor was inoculated in batch mode with 10% by volume sludge from a municipal wastewater treatment plant's anaerobic digester (Urbana, IL) and 10% by volume effluent from a previous attempt to inoculate the column reactor (see discussion in section 3.3.1). 20 mL

of synthetic wastewater concentrate as described by Pell and Nyberg (1989) was added to the sludge and sodium acetate was added for a concentration of 150 mg/L, with the balance being tap water. Organic components of the media came from the synthetic wastewater concentrate, which in addition to inorganic compounds to add nutrients and alkalinity, contained 26.25 g of casein hydrolysate, 26.25 g of meat extract, and 17.50 g of urea per 1 L of concentrate. Each of the next four batches consisted of 10% effluent from the previous batch diluted with synthetic wastewater and 150 mg/L of sodium acetate. The initial COD of the first batch of media was 1170 mg/L (Hach Test 'N Tube colormetric method) after filtration through a 0.2 μm syringe filter (Pall Life Sciences). After five batches (35 days) the amount of synthetic wastewater concentrate and acetate were decreased for an influent COD of approximately 357±14 mg/L (10% by volume previous batch effluent, 5 mL of synthetic wastewater concentrate and 75 mg/L of sodium acetate). Each batch lasted until current production leveled off close to zero, indicating that the reactor had become substrate limited and current production was primarily due to endogenous respiration. During inoculation the media was recirculated from the bottom to the top of the column at a rate of 5 mL/min. The reactor was inoculated at room temperature, approximately 23 °C.

The five electrode-pairs in the column were connected to a multi-channel potentiostat (BioLogic VMP3, France) with the anodes as the WE and the cathodes as the CE. The electrode-pairs were connected to the potentiostat in a 'CE to ground' configuration, where all of the cathodes were shorted together and connected to the potentiostat's ground. This configuration also required a change in the settings for the EC-Lab software (BioLogic) provided with the potentiostat. CA was used to poise the potential of each anode at -0.36 V vs. Ag/AgCl (-0.15 vs. SHE), which corresponds to the midpoint potential, E_{KA}, for *G. sulfurreducens* respiring on acetate (Srikanth et al. 2008).

After the anode biofilms were well established and stable with a consistent level of current production when fed the same media, an investigation of the interactions between electrode-pairs was carried out. For one part of this investigation, all of the electrode-pairs were on separate channels in a standard configuration. The CEs were not grounded together, and the external circuit of each electrode-pair was isolated from the others. Four of the electrodes were monitored using OCV, while the remaining electrode-pair was run through a series of techniques: 1) CA, 2) LSV, 3) OCV, and 4) CA. For the second part of the investigation, all of the electrode-pairs were connected to the potentiostat in CE to ground configuration. Four of the electrode-pairs were poised at midpoint potential using CA, while the fifth was run through the same series of techniques as for the first part.

Based on the investigation of the electrode-pair interactions, and determination that the modular design described in section 3.1.1 did not alleviate the problem, the two electrode-pairs with the highest current production were selected and placed into separate MEC reactors as described in section 3.1.1. These

reactors were placed in a temperature-controlled room at 30 °C and fed (per 1 L of media): 10 mL of synthetic wastewater concentrate, 100 mg sodium acetate, 10 mL of trace mineral stock solution (per 1 L: 1.5 g nitrilotriacetic acid, trisodium salt, 3.0 g $MgSO4{\cdot}7\,H2O$, 0.5 g $MnSO4{\cdot}H2O$, 1.0 g NaCl, 0.1 g $FeSO4{\cdot}7\,H2O$, 0.1 g $CaCl2{\cdot}2\,H2O$, 0.1 g $CoCl2{\cdot}6\,H2O$, 0.13 g ZnCl2, 10 mg $CuSO4{\cdot}5\,H2O$, 10 mg $AlK(SO4)2{\cdot}12\,H2O$, 10 mg H3BO4, 2.5 mg $Na2MoO4{\cdot}H2O$, 2.4 mg $NiCl2{\cdot}6\,H2O$, and 0.25 mg $Na2WO4{\cdot}2\,H2O$) as described in Yoho et al. (2014), and 10 mL of Kao and Michayluk vitamin solution (100x, Phyto Technology Laboratories). Typical COD values for fresh media were approximately 540 mg/L. The electrode-pairs were connected to individual channels of a multi-channel potentiostat (VSP, BioLogic) in a standard configuration with the anodes as the WE and were controlled using the included EC-Lab software.

The graphite anode MEC reactors were inoculated and maintained similarly to the carbon mesh MECs in a room controlled at 30 °C. They were inoculated with media that differed somewhat from that used for the carbon mesh anode MECs and had a COD of 1300 mg/L. The inoculation media consisted of (per 1 L): 50% by volume MEC effluent, 5 mL of anaerobic digester sludge, 250 mg sodium acetate, and 10 mL synthetic wastewater concentrate, 10 mL Kao & Michayluk vitamin solution, 10 mL trace mineral stock solution, and with deionized water for the balance. Subsequent batches were the same but with the inoculum (MEC effluent and anaerobic digester sludge) replaced by 100 mL of effluent from the previous batch. As with the individual carbon mesh anode reactors, the electrode-pairs were connected to individual channels of the VSP potentiostat in a standard configuration with the anodes as the WE and were controlled using EC-Lab software.

Acetate respiration modeling

Acetate respiration modeling was carried out in the same way for two carbon mesh anode and two graphite anode MEC reactors. Solutions were prepared with various concentrations of sodium acetate, 5 mM $NaHCO_3$, and HCl was used to adjust the pH to 7. The solutions were sparged with N_2 for a minimum of 30 minutes to eliminate most of the DO and were then pumped through the individual MEC reactors at a rate of 2.3 mL/min (1 h HRT). The experiments were carried out at 30 °C. The polarization curves used for modeling the relationship between anode potential, current production, and acetate concentration were generated using 3-cycle CV from -0.5 to 0 V vs. Ag/AgCl at a sweep rate of 1 mV/s. Three cycles were necessary because charging of the biofilm due to uptake of substrate prior to the first cycle results in a much higher peak current during the first cycle. At high acetate concentrations, the second cycle also peaked slightly higher, but after the third cycle any additional cycles followed the same curve as the third cycle, so this cycle was selected as the best representation of the ARB's steady-state

respiratory capabilities at a particular acetate concentration and anode potential. The CV technique was preceded by at least 30 min of OCV and 5 min of CA at midpoint potential.

The amperometric data from the anodic (positive direction) sweep of the CV was used for fitting the BVM modeling parameters K_1, K_2, and α in Microsoft Excel using non-linear least squares estimation. Other research into anode respiring biofilms in MECs based on polarization curves have used the anodic scan (Lee et al. 2009) the cathodic (negative direction) scan (Yoho et al. 2014) or both the anodic and cathodic scan (Torres et al. 2008b). To test the predictive capability of the BVM model the K_1, K_2, and α parameters that were estimated by fitting polarization curve data from a high acetate concentration CV (250 or 500 mg/L sodium acetate) were applied to polarization curve data from lower acetate experiments and the acetate concentration was estimated using non-linear least squares estimation.

3.2 Results

3.2.1 Carbon mesh anode results

Column reactor

Current production in the column reactor began to increase steadily after 2 days of inoculation. However, it was observed that two of the electrode-pairs consistently outperformed the others. If the electrode-pairs were numbered from the top, the second and fourth electrode-pairs consistently produced 15% - 30% more current than the other electrode-pairs, even after the biofilms were stable and mature. The additional performance seemed to be possibly related to the symmetry of the system and the position of those electrode pairs relative to the others, so the experiments described in section 3.1.2 were carried out to characterize whether or not there were interactions between the electrode pairs through the external circuit or through the solution. Figure 13 shows the current response of four of the electrode-pairs (E1, E2, E3, and E5) poised at midpoint potential while a fifth electrode-pair (E4) was put through a series of electrochemical techniques. All of the electrode-pairs were connected to the potentiostat in the CE to ground configuration, so that it was possible for E4 to influence the other electrode pairs both through the external circuit and through the bulk liquid. A second experiment investigated whether an interaction took place when the external circuit of each electrode-pair was isolated from the others. E1, E2, E3, and E5 were connected in the standard configuration to separate channels and OCV was used to monitor the response of anode potential to a series of electrochemical techniques run on E4 (results shown in Appendix A, Figure 49). Interactions between electrode-pairs were observed during both experiments, with the effect being strongest between electrode pairs in close proximity to one another, which indicates that interaction was occurring at least in part through the bulk liquid. These interactions are likely due to

electrical fields which have been observed to allow working electrodes within the same fluid channel in multi-electrode systems to exert an influence over one another depending on their relative positions, even at very low applied potentials (Contento and Bohn 2015). An MEC with multiple working electrodes and a single cathode was also used by Torres et al. (2008a) to evaluate the effects of proton transport limitations on anode biofilm respiration, and no interaction effects were reported, perhaps because the configuration of the WE's positions relative to one another differed significantly from that of the column reactor.

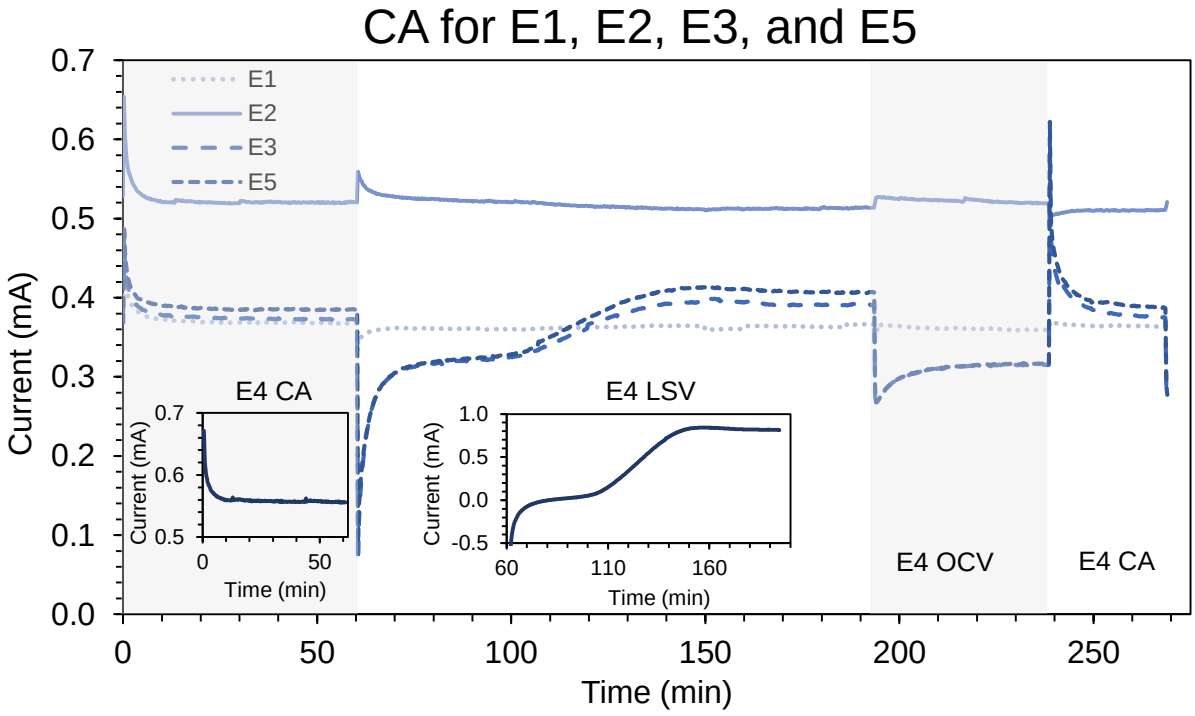

Figure 13: Current response of electrode pairs 1, 2, 3, and 5 poised at midpoint potential to changes in current and anode potential of electrode-pair 4 (data or technique shown in insets).

Individual electrode-pair reactors

After two of the electrode-pairs were transferred to individual reactors, cyclic voltammetry experiments were carried out to determine the relationships between acetate (substrate) concentration, anode potential, and current production. Figure 14 shows the results of performing CV experiments with sodium acetate concentrations of 0, 50, 250, and 500 mg/l. In the figure it can be clearly seen that over the same anode potential range the current response does differ at different substrate concentrations, with peak current at an anode potential of 0 V vs Ag/AgCl of 0.19 mA, 0.24 mA, 0.33 mA, and 0.40 mA, respectively. The correlation between peak current and acetate concentration was somewhat linear, with an R^2 value of 0.949 and an increase of about 0.04 mA per 100 mg of sodium acetate. E_{KA} values were -0.32 V vs.

Ag/AgCl for all of the concentrations except for 0 mg/L sodium acetate which had an E_{KA} of -0.26 V vs. Ag/AgCl.

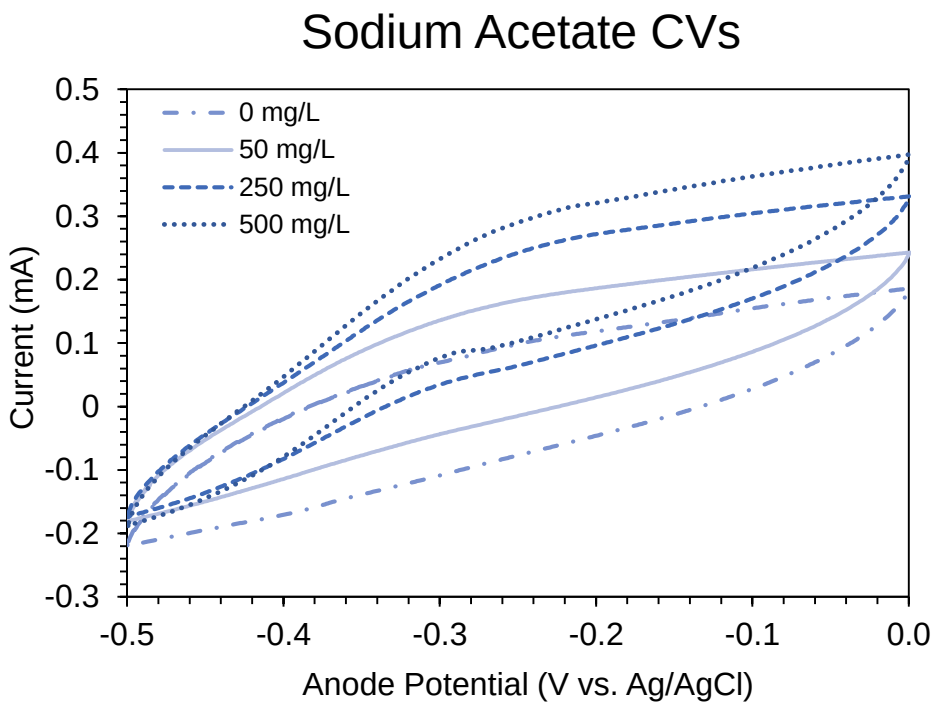

Figure 14: Third cycle CVs from a carbon mesh anode MEC at various acetate concentrations.

The data from the CV experiments was then used to test the fit of the BVM model and estimate the parameters. In this case, the fit was not ideal because the current production did not plateau at higher anode potentials as expected. In the anodic sweeps of the CV curves shown in Figure 14, though the rate of increase in current decreases above an anode potential around -0.25 V vs. Ag/AgCl, it does not plateau as is typically seen in bio-anode polarization curves (Torres et al. 2008b). This indicates that not all of the current measured was biologically catalyzed, and that the polarization curves obtained from the CV experiments are characterizing other phenomenon in addition to the respiration of the anode biofilm, such as capacitance of the electrode material and the biofilm. The difference between the anodic and cathodic sweeps could also be related to capacitive effects, which are discussed in further detail at the end of this section. Another possibility is that the scan rate was too fast for the biofilm current production to reach steady-state, although a sweep rate of 1 mV/s, as was used here, is typically slow enough for such a characterization (Torres et al. 2010).

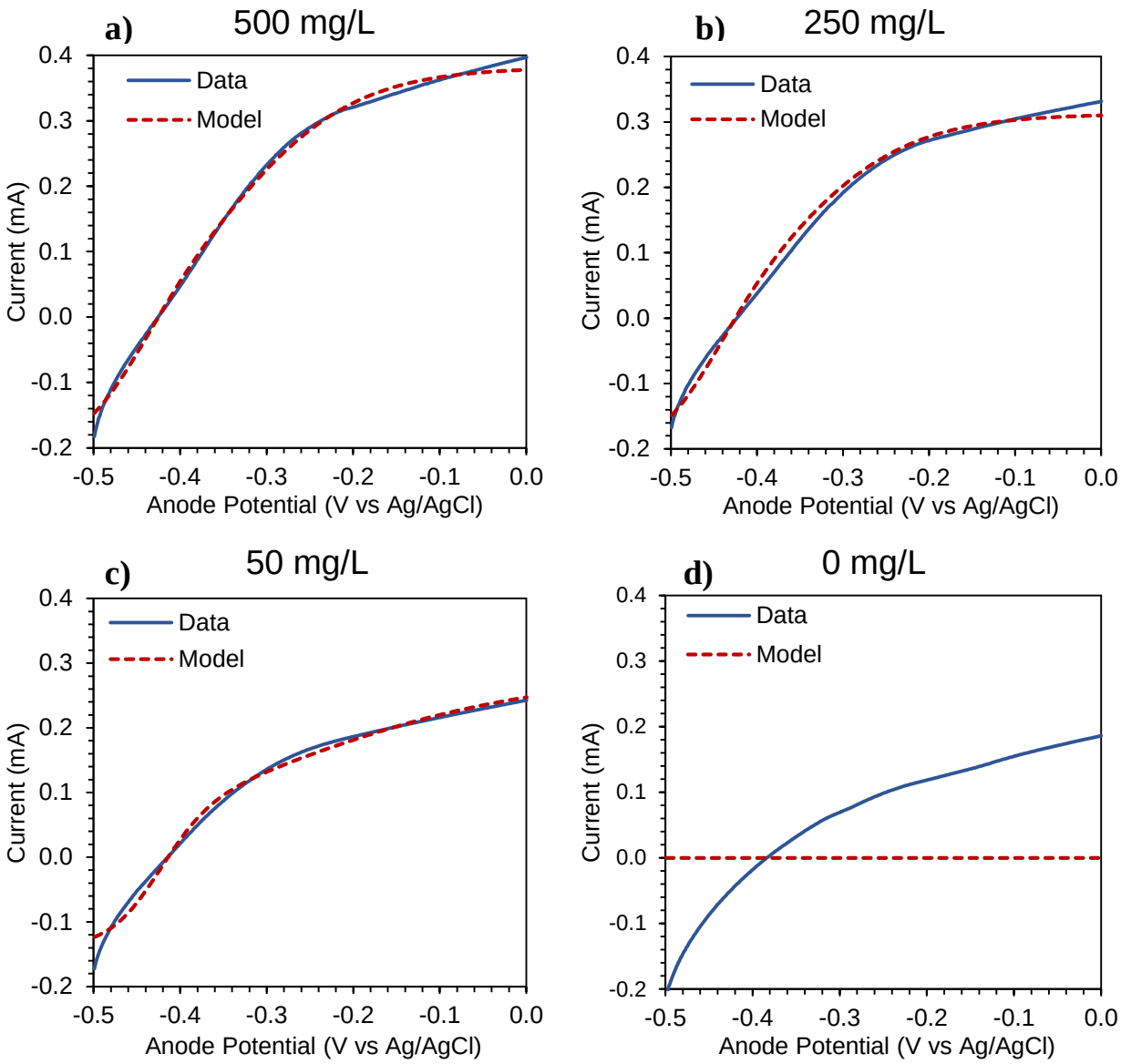

Figure 15: BVM modeling of sodium acetate CV data using a literature value for K_M and fitting K_1, K_2, and α.

Figure 15 shows the BVM model's fit for each of the anodic sweeps shown in Figure 14 when the K_1, K_2, and α parameters are estimated using non-linear least-squares estimation. For the data from the 25, 250, and 500 mg/L CVs, the model fits the data reasonably well, but there are portions of the curves that do not align well, for example at high anode potentials for the 500 mg/L data (Figure 15a) and 250 mg/L data (Figure 15b). The model does not fit the data at all for the 0 mg/L CV (Figure 15d), possibly because of capacitance effects or because endogenous respiration is not accounted for in the model, which therefore assumes that with no added substrate, no respiration will occur. The estimated parameters K_1, K_2, and α at each acetate concentration are shown in Table 1. Though the parameters should be characteristic to a particular biofilm, they do not remain constant at different acetate concentrations. This could be due to

other environmental conditions having an effect, such as solution conductivity, or it could be due to the effect of capacitance. Temperature and pH were controlled to be the same for each experiment, however solution electroconductivity for each acetate concentration varied from about 400 µS/cm to 950 µS/cm.

Table 1: Summary of BVM model fitting results for Acetate CV data

	Sodium acetate concentration:			
Parameters	**500 mg/L**	**250 mg/L**	**50 mg/L**	**0 mg/L**
K_1	3.920	2.974	3.291	5.295
K_2	1.842	2.639	2.816	0.000
α	0.638	0.777	0.826	0.331
Acetate prediction		73.4 mg/L	24.05 mg/L	10.9 mg/L

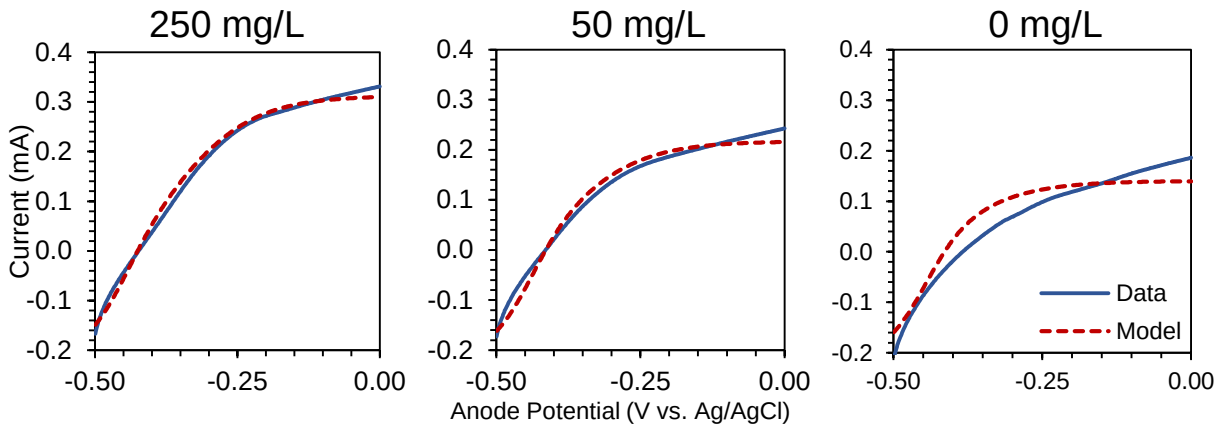

Figure 16: Comparison of data and BVM model prediction using fitted parameters from 500 mg/L sodium acetate CV data.

When the predictive capability of the model was tested, the acetate concentration was underestimated for 250 mg/L and 50 mg/L of sodium acetate, but over predicted for 0 mg/L. These results are also summarized in Table 1, and the fit of the model when the estimated K_1, K_2, and α from the 500 mg/L CV were used to estimate lower concentrations of acetate are shown in Figure 16. A summary of the BVM model fitting results for a second carbon mesh anode MEC is available in Appendix A, Table 6.

Anode and biofilm capacitance

The effects of capacitance of both the carbon mesh anode material and the biofilm were also investigated. Figure 17 shows CVs of an uninoculated carbon mesh anode and a carbon mesh biofilm anode with no substrate present. The increasing current response as the scan rate increases is typical of a capacitive effect, and the effect was greater for the biofilm anode, indicating that the biofilm itself is contributing to

capacitance. A comparison of the 1 mV/s CVs for the inoculated and bare carbon mesh is provided in Figure 18.

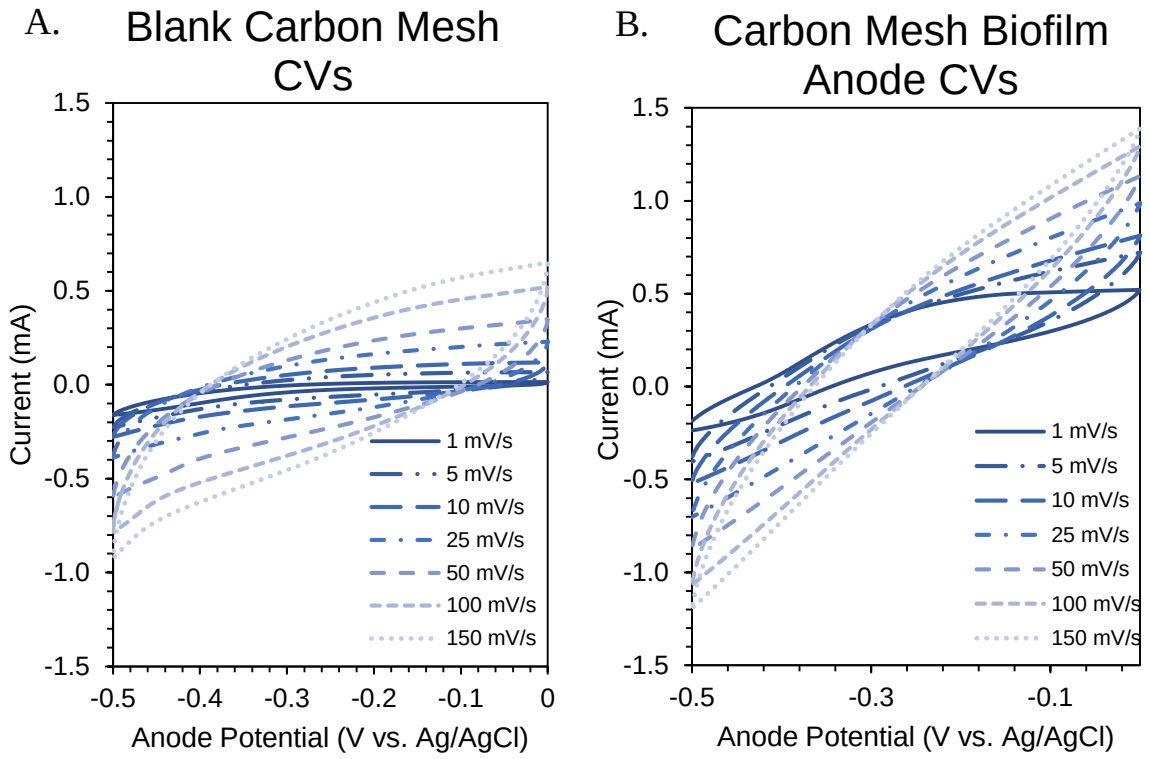

Figure 17: Cyclic voltammograms of carbon mesh electrodes before (A) and after (B) growth of a biofilm.

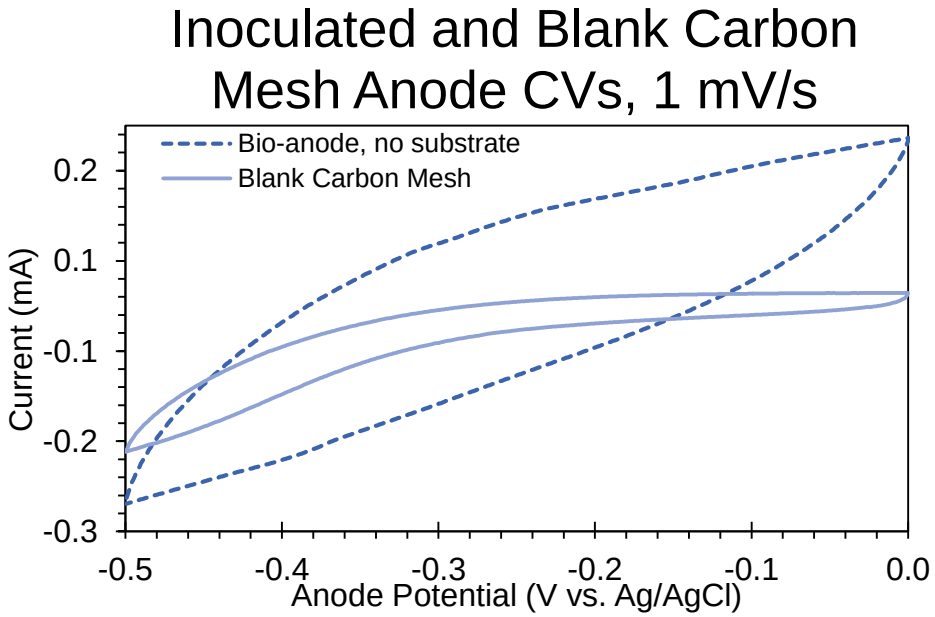

Figure 18: Comparison of a 1 mV/s CV for blank carbon mesh and carbon mesh with an anode respiring biofilm attached.

Electrode-solution interfaces have been shown to behave like capacitors because of the interaction between the charge of the electrode surface and the ions in the solution in the immediate vicinity. This is characterized as electrical double layer (EDL) capacitance and the current caused by the charging of a capacitor is referred to as charging current (Bard and Faulkner 2001). The high specific surface area of the carbon mesh likely contributes to the charging current because of the greater interfacial area between the electrode and the solution. Unlike EDL capacitance, which is non-faradaic, electrochemical pseudocapacitance causes faradaic charging through reversible redox reactions at the electrode surface (Conway and Pell 2003). The additional charging current in the biofilm anode CVs is likely contributed by pseudocapacitance of the biofilm due to the presence of redox mediators that are a part of the apparatus for bacterial respiration and EET.

Equation 23

$$C = \frac{I}{dV/dt}$$

Where:
$C = capacitance$
$I = peak\ current\ of\ anodic\ sweep$
$dV/dt = anode\ potential\ scan\ rate$

The CV data shown in Figure 17 was used to calculate the capacitance of the carbon mesh and the biofilm at each scan rate using Equation 23. The capacitance was normalized to electrode area (geometric area, not specific surface area) to obtain the specific capacitance. The results are shown in Table 2. The capacitance of the biofilm anode shows a higher dependence on scan rate, decreasing by more than 98% from a 1 mV/s sweep to a 150 mV/s sweep, compared to only a 70% decrease for the carbon mesh. This data would tend to support the theory that the carbon mesh primarily has EDL capacitance while the biofilm adds pseudocapacitance. For and EDL capacitor, current should vary directly with sweep rate because it is surface-controlled. Conversely, electrochemical pseudocapacitance is limited by is expected to vary proportionally with the square root of the scan rate (Augustyn et al. 2014).

Table 2: Sweep rate dependent specific capacitance of carbon mesh and anode respiring biofilm

	Specific capacitance	
Sweep rate (mV/s)	Carbon mesh	Bio-anode
1 mV/s	1920 μF/cm^2	69500 μF/cm^2
5 mV/s	1770 μF/cm^2	19280 μF/cm^2
10 mV/s	1590 μF/cm^2	10800 μF/cm^2
25 mV/s	1220 μF/cm^2	5270 μF/cm^2
50 mV/s	931 μF/cm^2	3030 μF/cm^2
100 mV/s	694 μF/cm^2	1730 μF/cm^2
150 mV/s	579 μF/cm^2	1240 μF/cm^2

3.2.2 Graphite plate anode results

The graphite anode MECs were inoculated after the characterization of the carbon mesh anode MECs was completed with the expectation that the lower specific surface area would reduce the amount of charging current from EDL capacitance during CV experiments and provide a better fit to the BVM model. As can be seen from the results of CV experiments at different acetate concentrations in Figure 19, the shape of the curve for the anodic sweep is shaped very differently than those from the carbon mesh anode reactors. Though the upper portion of the curve is still not flat, it was found that the predictive capability of the BVM model was significantly better for the graphite anode MECs than for the carbon mesh MECs.

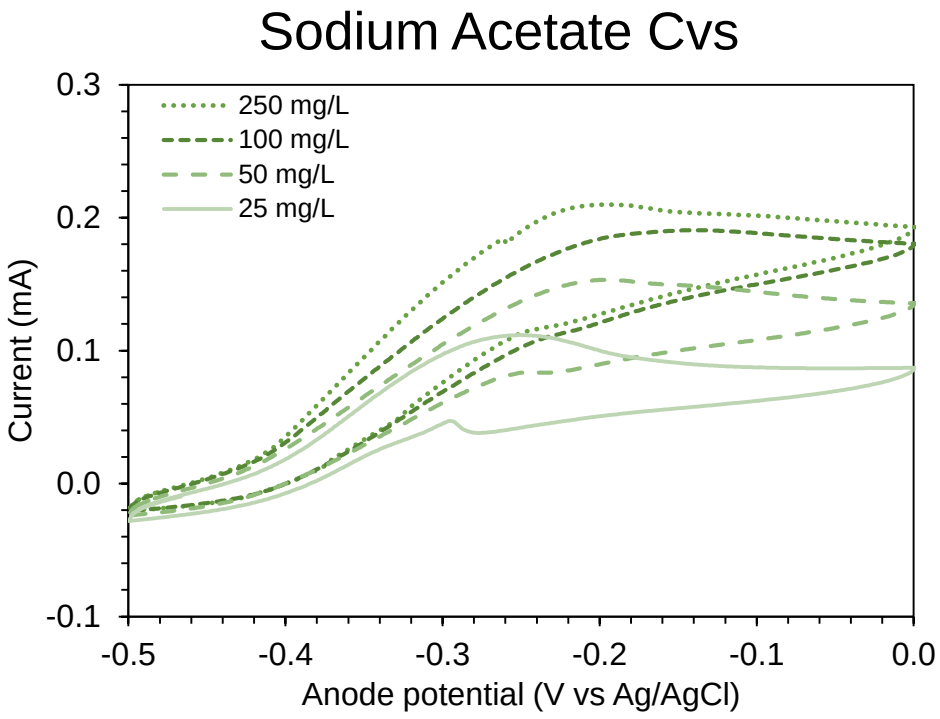

Figure 19: Cyclic voltammetry data for a graphite anode MEC at various sodium acetate concentrations. The third of three 1 mV/s cycles is shown.

The anodic and cathodic sweeps still do not align, indicating that steady-state current is not being reached at a 1 mV/s scan rate, which could be due to the charging current resulting from EDL capacitance and pseudocapacitance. The differences in the shape of the CV curves in Figure 19 compared to those in Figure 14 could be caused by a variety of factors. EDL capacitance could be one reason. The relative ages of the MECs could also be a factor. The slight hump visible in both the anodic and cathodic portions of the curve, especially for the lowest acetate concentration, has been found to be characteristic of less mature biofilms (Yoho et al. 2014), and the carbon mesh biofilms were more than a year old at the time of the characterization presented in section 3.2.1, while the graphite anode biofilms were only about two months old.

The BVM model fit for the anodic sweep of the CVs at different acetate concentrations is shown in Figure 20, and the fitted parameters for each concentration, as well as acetate concentration predictions, are summarized in Table 3. The predictions were more accurate than with the carbon mesh anode MECs, though they under predicted the acetate concentration for the MEC reactor data shown here. A second graphite anode MEC was also characterized, and the results are summarized in Appendix A, Table 7. For the second MEC, higher acetate concentrations were overestimated, while lower concentrations were underestimated. Figure 21 shows the BVM model fit for the acetate concentration estimations.

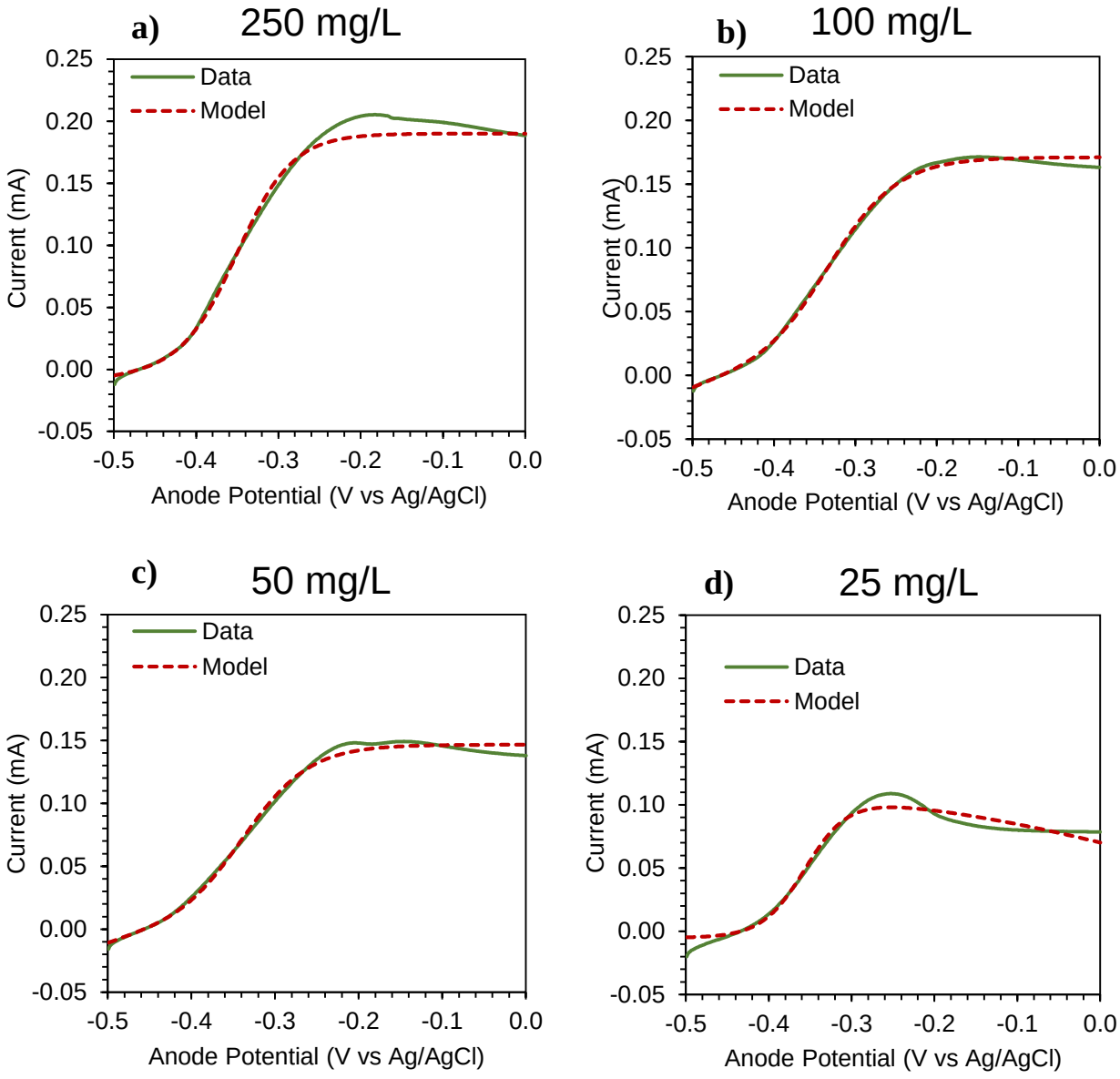

Figure 20: BVM modeling of sodium acetate CV data using a literature value for K_M and fitting K_1, K_2, and α.

Table 3: Summary of BVM model fitting results for Acetate CV data when K_1, K_2, and α are estimated

	Sodium acetate concentration:			
Parameters	**250 mg/L**	**100 mg/L**	**50 mg/L**	**25 mg/L**
K_1	37.02913	25.92399	26.5699	0.086523
K_2	0	0.303275	0	39.51097
α	0.224574	0.389889	0.3518	1.154418
Acetate prediction		78.2 mg/L	47.5 mg/L	16.2 mg/L

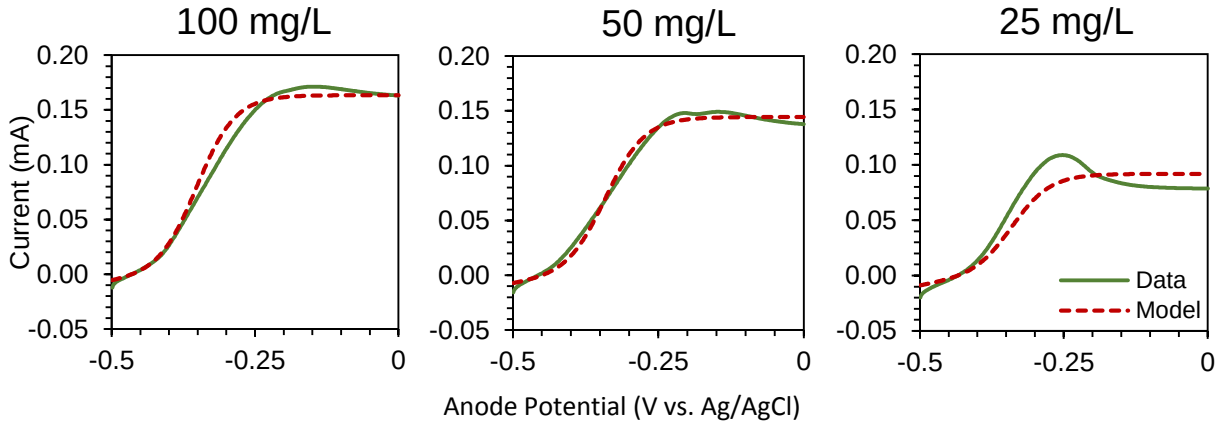

Figure 21: Comparison of data and BVM model prediction using fitted parameters from 250 mg/L sodium acetate CV data and estimating acetate concentration for data from lower concentration CVs.

As discussed in section 2.3.2, K_2 is expected to be significantly larger than one, which was not the case for the fitted K_2 parameters obtained for sodium acetate concentrations of 50 mg/L or higher. If the electrochemical reaction is much faster than the biochemical reaction, then K_1 will approach zero, so a high value for K_1 suggests that the opposite is true. Additionally, the transfer coefficient α should be very close to a value of 0.5. From Table 3 it can be seen that the fitted parameters obtained do not meet these criteria. Hamelers et al. (2011), the developers of the BVM model, fitted all three parameters for a number of different biofilm anodes, some with different anode materials and some maintained at a different anode potential for an extended period of time preceding the experiments, and estimated α values were consistently very close to 0.5.

When the parameter estimation was repeated by estimating only K_1 and K_2 and setting α equal to 0.5, the plausibility of the estimated K_1 and K_2 values improved markedly, without appreciably changing the fit or predictions of the BVM model, as shown in Figure 22, Figure 23, and Table 4. Because the fit of the model to the data was nearly the same, it is likely that the parameters in Table 4 are more accurate representations of the associated biochemical and electrochemical processes.

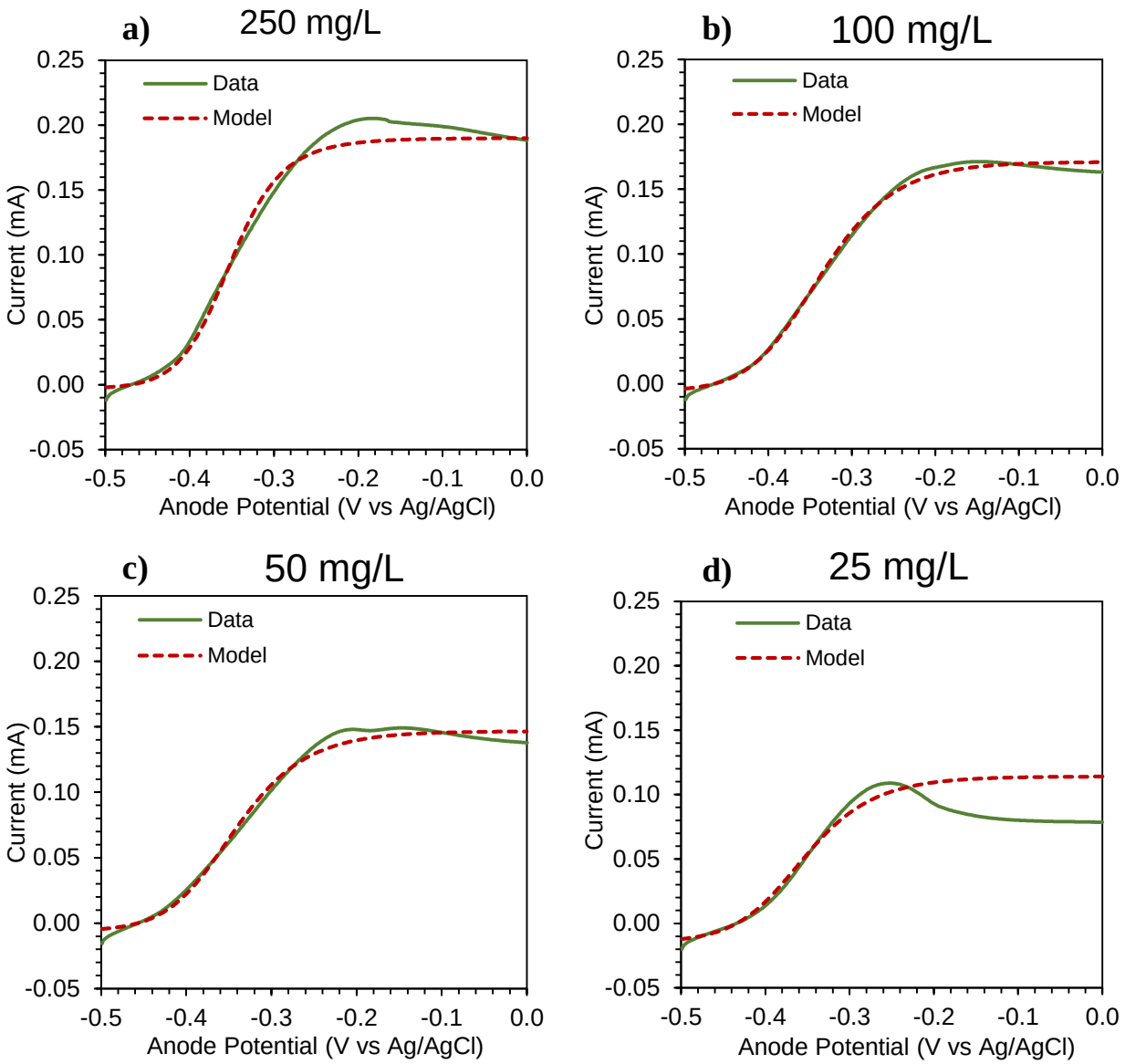

Figure 22: BVM modeling of the CV data shown in Figure 20, but using literature values for both K_M and α and fitting only K_1 and K_2.

Table 4: Summary of BVM model fitting results for Acetate CV data when α is fixed at 0.5

	Sodium acetate concentration:			
Parameters	**250 mg/L**	**100 mg/L**	**50 mg/L**	**25 mg/L**
K_1	3.145	11.260	9.197	6.492
K_2	67.111	34.248	32.742	13.566
α	0.500	0.500	0.500	0.500
Acetate prediction		78.2 mg/L	47.5 mg/L	16.2 mg/L

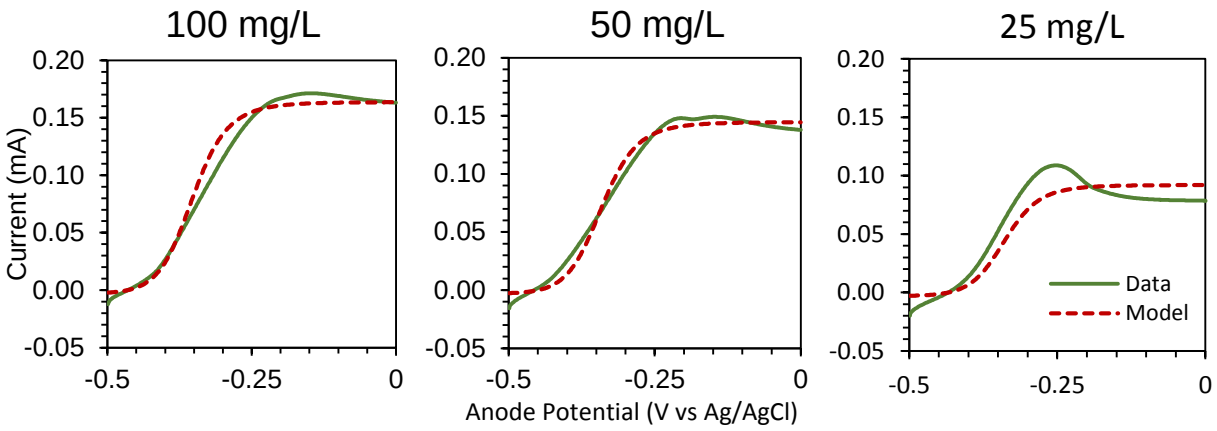

Figure 23: Comparison of data and BVM model prediction using fitted parameters from 250 mg/L sodium acetate CV data and $\alpha = 0$.

3.3 Discussion

The results of the MEC biofilm respiration kinetics characterizations indicate that the method of using the BVM model to predict substrate concentration based on anode biofilm polarization curves holds some promise for application as a BOD biosensor. However, there is much more work remaining to make such an application feasible.

The three-cycle CV takes 50 minutes to run, so the response time is comparable to other MFC and MEC biosensors. It is longer than the 5 to 11 minutes reported by Moon et al. (2004), but much shorter than the response times reported for the only biosensor study with a range exceeding 1000mg/L BOD, which required up to 20 h, and within a response time of 5 h only had a range of up to 320 mg/L (Modin and Wilén 2012).

The accuracy of the BVM model predictions clearly need to be improved. For the graphite plate anode MECs, the deviation of the predictions from the true values ranged from 5% to 35%. This is inferior to the accuracy of the sensor developed by Di Lorenzo et al. (2009), which was able to closely match COD measurements made using the standard methods for unknown samples of real wastewater.

The upper limit of the range that can be measured by fitting voltammetry data to the BVM model has not yet been quantified. However, due to the fact that there are few rate-limitations on anode biofilm respiration in an MEC and the method does not depend on a linear relationship between current or charge and substrate concentration, the upper limit could be expected to be higher than many previously reported ranges for MFC-based BOD sensors, such as the 100 mg/L BOD limit reported by Chang et al. (2004), the 250 mg/L limit reported by Kim et al. (2003), or the 500 mg/L limit reported by Di Lorenzo et al. (2009).

3.3.1 Operational failures

The amount of voltage applied to the electrodes in an MEC must be carefully controlled not only to achieve the desired anode potential, but also to avoid damage to both the biofilm and the electrode materials. In the course of this study, problems were occasionally encountered where an incorrect setup or a faulty reference electrode caused much higher than normal voltages to be applied to the MECs. For a biosensor based on an MEC, it would be very important to design a control system that limits the applied voltage to within a range that is safe for the biofilms and the electrodes.

The first attempt to inoculate five carbon mesh anodes in the column reactor failed when CA was performed with the standard configuration selected in the control software while the electrodes were actually connected to the potentiostat in the CE to ground configuration. As shown in Figure 24, severe damage was caused to both the stainless steel cathodes and the carbon mesh of the anodes. The cathodes were oxidized in places, with spots of rust appearing, while some of the carbon from the anodes dispersed into the bulk liquid. Some of the electrode pairs were more damaged than others, as evidenced by the carbon mesh anode in the bottom left of the image. The biofilms also did not recover even after an extended period of time with the correct control settings for the CE to ground configuration.

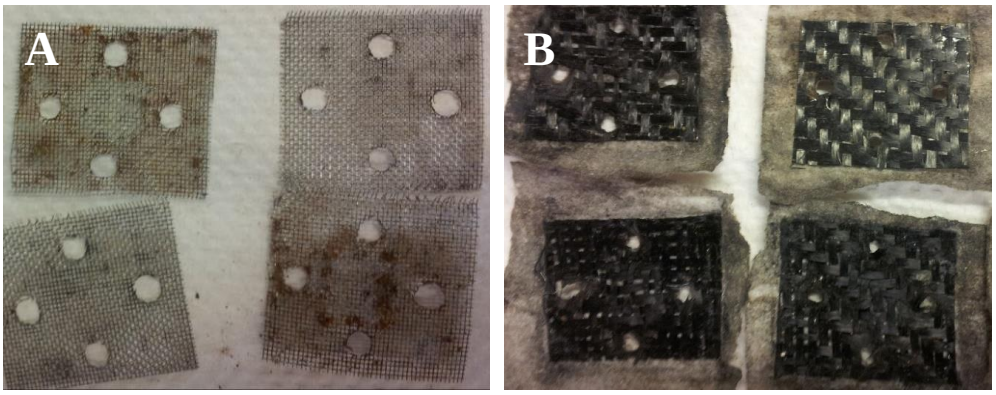

Figure 24: Damage to the A) stainless steel cathodes and B) carbon mesh anodes.

The Ag/AgCl reference electrodes were also sometimes problematic. Because the reference electrodes were used as a reference potential for all other potentials in the system, they had a large role in determining the amount of voltage applied to the MEC electrodes. The electrodes have a porous glass frit (typically vycor® or coralpor®) at the interface between the electrolyte inside the reference and the bulk liquid to provide connectivity between the interior and exterior solutions while minimizing ion transport. The frits are prone to fouling in the presence of dissolved organic matter, which increases the resistance in the connectivity of the two solutions and causes the potential of the reference electrode to drift. The reference electrodes had to be replaced or refurbished frequently, becoming fouled within a span of two

weeks to several months. The connection between the interior and exterior solutions can also be broken entirely if gas bubbles become entrapped at the inner or outer surface of the frit. Damage similar to that shown in Figure 24 occurred to some carbon mesh anode and some graphite anode MECs because of bubble entrapment at the tip of the reference electrodes.

Having a reference potential is very important for maintaining and controlling an MEC. During this study, cathode potential was found to vary both with applied voltage and substrate concentration. With the anode poised at midpoint potential, the cathode potential would be lower (higher cell potential) than at low substrate concentrations. A biosensor based on a two-electrode MEC controlled based on cell potential would be much less effective, and would lose one of the major advantages that MECs have over MFCs, control of the limits placed on respiration by anodic affinity for electrons (anode potential). Therefore, in order for a BOD biosensor based on an MEC to be viable, a reference electrode with long-term stability and reliability in water with a high content of organic molecules must be found or developed.

3.3.2 Performance comparison of anode materials and treatment

The results discussed in sections 3.2.1 and 0 show that anode material can have an effect on the shape of polarization curves generated with CV. However, while graphite anodes produced better prediction of acetate concentration by the BVM model, the anode biofilms grown on graphite performed less well in terms of current production, peaking 43% lower in a 250 mg/L sodium acetate CV, and were more susceptible to damage. In addition to the CVs presented in Figure 19, CV data was collected for a 500 mg/L sodium acetate concentration, and an experiment to collect CV data for 0 mg/L sodium acetate was also planned. However, the peak current of the 500 mg/L CV was less than for the 250 mg/L CV that preceded it. In addition, what appeared to be gas bubbles appeared under the biofilm surface. The bubbles grew for a couple of days before breaking free by tearing the biofilm, as shown in Figure 25. Because of this, the 0 mg/L acetate CVs were never carried out and the 500 mg/L CV data was not used.

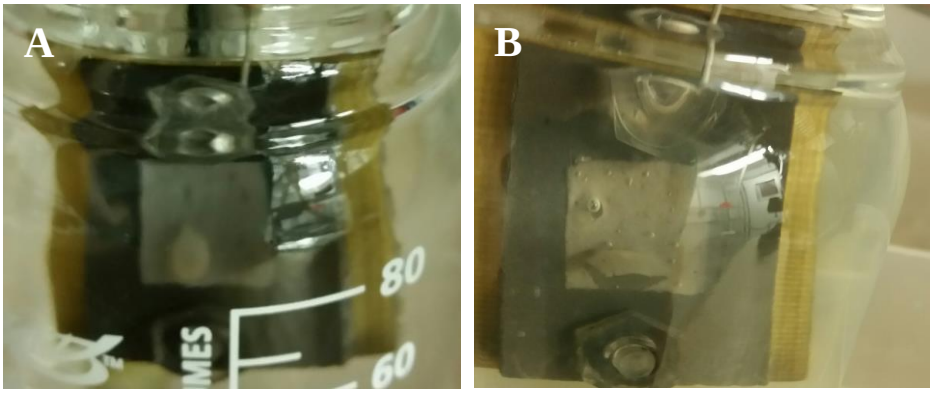

Figure 25: Damage to one of the graphite anode MEC biofilms A) immediately after and B) three days after 3-cycle CV experiments at five different sodium acetate concentrations.

In addition to the material of the anode, the presence or lack of contaminants on the surface prior to inoculation had a large effect on the rate of growth and maturation of a new anode respiring biofilm. Before the second time that carbon mesh anodes were inoculated in the column reactor, they were heat treated (450 °C for 1 h) to burn off any surface contaminants. The first time carbon mesh anodes had been inoculated the carbon mesh had not been heat treated, and the anode biofilms took much longer to start producing current and it took much longer for the current production to stabilize. Similarly, some of the graphite anodes were sanded with fine-grit sandpaper prior to inoculation and then buffed smooth with lint-free paper, while others were not. After several weeks, those that had not been sanded were only producing about 5 to 10% of the current that the sanded anodes were producing after the same amount of time.

3.3.3 Study limitations

One of the most evident limitations of this study is the use of acetate as the only substrate for the characterization of the respiration kinetics of an anode biofilm. Acetate is a very readily biodegradable substrate. In order to be effective as a BOD sensor, the ARB in an MEC must have a response to a wide spectrum of different substrates. While the MECs were maintained with a synthetic wastewater for fuel, which consisted of a complex mixture of organic compounds, the ability of the anode biofilms to respire on a more complex mixed substrate was not addressed.

In addition to substrate concentration and anode potential, other environmental conditions such as solution pH, electroconductivity, and temperature can also have a significant impact on microbial respiration rates. The effect of temperature was demonstrated by Di Lorenzo et al. (2009), who observed that a decrease in temperature from 30 °C to 20 °C resulted in a 96% decrease in the current generated by their SCMFC biosensor respiring on real wastewater. In order for an MEC biosensor for BOD to be practical, the effects of these other environmental conditions on anode biofilm respiration must also be characterized.

Another possible issue with using an MEC as a BOD biosensor is that the model parameters used to estimate the substrate concentration are specific to the microbial community and structure of the anode biofilm, which can change over time. Periodic recalibration might be necessary for an MEC based BOD biosensor.

3.3.4 Future work

In order to further the development of an MEC biosensor, the limitations of this study discussed in the previous section must be addressed in future work.

The respiration kinetics of the MEC biofilms should be characterized under a much wider range of environmental conditions, including the ranges of pH, electroconductivity, and temperature that are common at wastewater treatment facilities. Additionally, respiration should be characterized for real wastewater and a broader spectrum of substrates.

To address the issue of polarization curves being influenced by charging current in addition to biologically catalyzed current, additional methods for generating the polarization curves should be explored. If charging current or other factors are preventing the current from reaching steady-state during a 1 mV/s CV or LSV, as evidenced by the non-alignment of the anodic and cathodic scans of the CVs presented in section 3.2, then methods that poise the anode potential for a slightly longer time, perhaps two to five minutes, before recording current might alleviate the problem and generate polarization curves that better fit the BVM model and allow more accurate prediction. This would be similar to the method used by Hamelers et al. (2011). Chronoamperometry was used to maintain an anode potential for two minutes before the current was measured and the anode potential was stepped down by 0.050 V and the process repeated until a minimum current was reached.

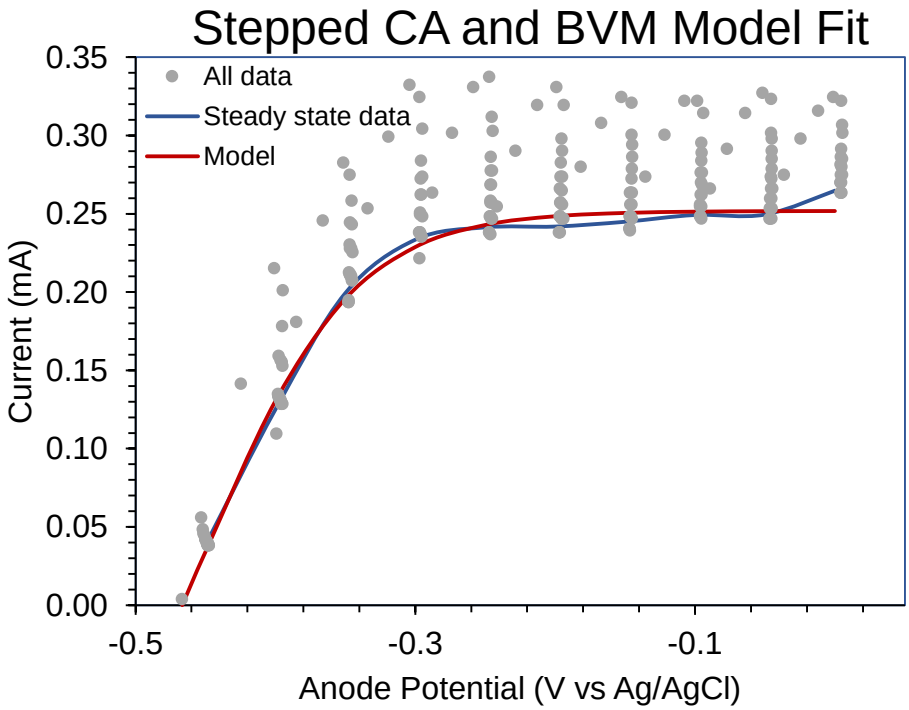

Figure 26: An example of voltammetric data collected using stepped CA. The steady-state data represents the average current over the last 50 s of each step.

An example of how data from a stepped CA experiment can be fit to the BVM model is shown in Figure 26. This experiment was conducted using the control system described in Chapter 4. Starting at OCV, the anode potential was increased to -0.45 V vs. Ag/AgCl, and then increased in steps of 0.05 V until 0 V,

with each anode potential step lasting for three minutes. Data was collected every ten seconds, and the last five measurements at each step were averaged to obtain a value for the steady-state current at each anode potential. When the steady-state data is fit to the BVM model by setting α equal to 0.5 and estimating K_1 and K_2, the resulting values are 2.68 and 1.41, respectively. When comparing the steady-state data to all of the data, it is clear that it takes some time for the current to reach steady-state and that this method can be used to differentiate charging current from biologically catalyzed current.

Compared to using CV to generate polarization curves, stepped CA could also potentially reduce response times, depending on how many potential steps are performed. A three-cycle CV from -0.5 to 0 V vs. Ag/AgCl takes 50 minutes, while the data shown in Figure 26 can be collected in about 30 minutes.

Chapter 4: Control System Development

In order to use an MEC as a biosensor it is necessary to correlate the signal (current output) with the variable to be detected (such as concentration of substrate as BOD). The two major components necessary for this are a good model and a portable and inexpensive control system capable of performing basic electrochemical techniques, such as OCV, CA, and LSV and/or CV. A significant amount or work has been done on the topic of modeling the kinetics of anode biofilms (Hamelers et al. 2011; Marcus et al. 2007; Pinto et al. 2011; Strycharz et al. 2011). However, equipment that is typically used in laboratories to grow and characterize anode biofilms in MECs is not appropriate for a biosensor application due to being bulky and prohibitively expensive. The purpose of this work was to develop a suitable control and data acquisition system for an MEC biosensor.

4.1 Methods

The development of a control and data acquisition system for an MEC sensor included both software and hardware development. The system was based around the use of a microcontroller board called Arduino Uno. Advantages of the Arduino, pictured in Figure 27 below, include low cost and small size.

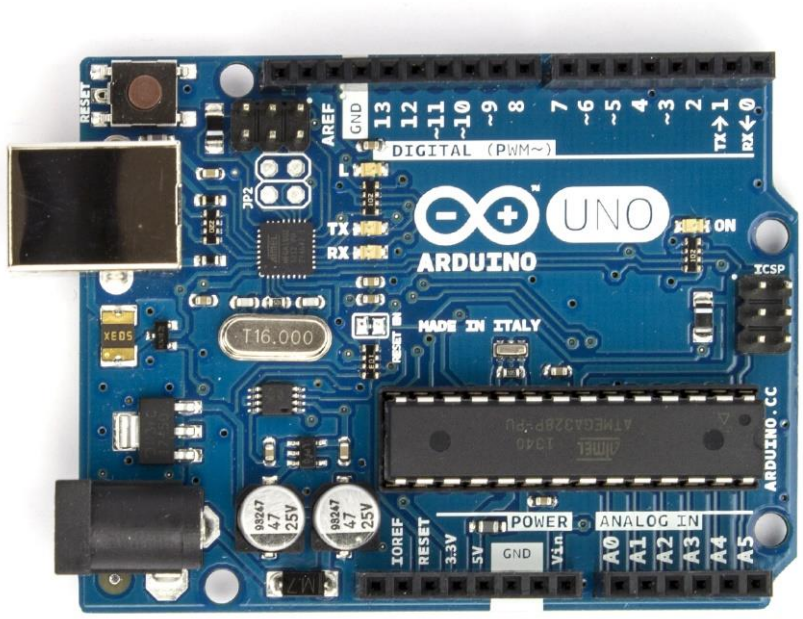

Figure 27: The Arduino Uno Microcontroller.

4.1.1 Hardware development

The primary requirements for the hardware to be able to perform the necessary electrochemical techniques are the ability to control the amount of voltage applied to the electrodes and the ability to

measure anode potential, cell potential, and current. In order to control the applied voltage, a simple voltage divider circuit was employed. A diagram of the circuit is shown in Figure 28. The sum of the voltage drops around the loop containing R_1 and R_3 must equal V_1, so if the resistance value of R_3 increases, the voltage drop across R_3 will increase and the drop across R_1 will decrease, resulting in a higher voltage between *A* and *B* (anode and cathode). Furthermore, when current is flowing from the anode to the cathode, there will be a measurable voltage drop across R_2, which can be used to calculate current based on Ohm's Law.

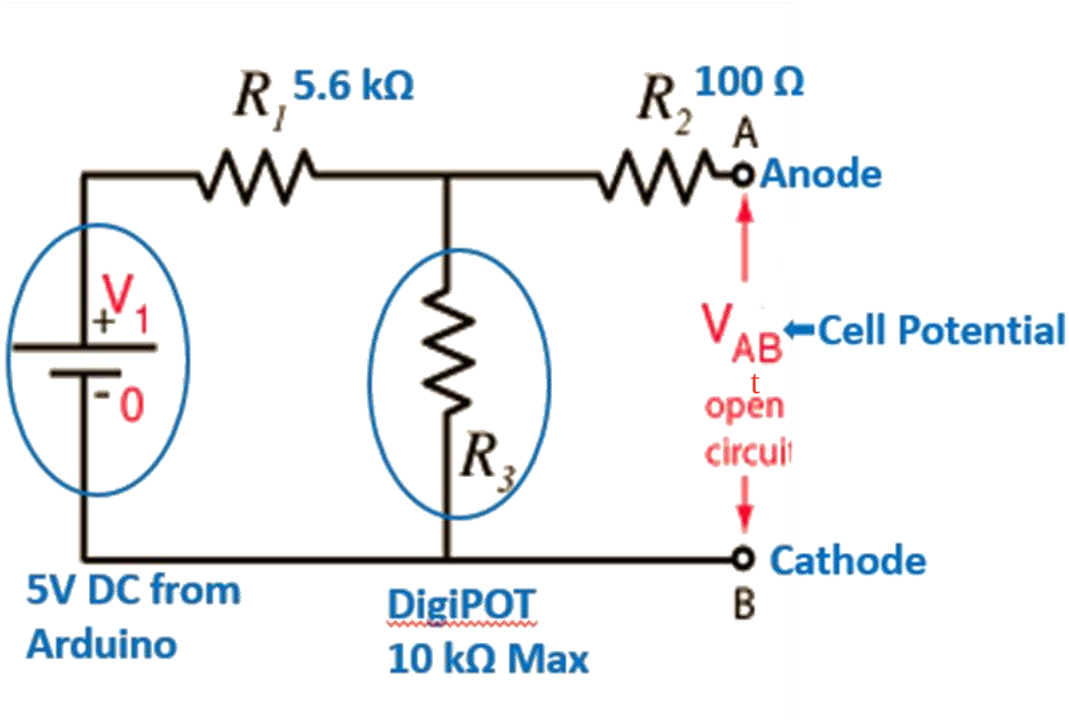

Figure 28: Diagram of an individual voltage divider circuit. Note that the values shown for the resistors represent the values used in the final design.

By placing a variable resistor at R_3, the cell potential, and therefore the anode potential, can be controlled by adjusting the resistor to apply more or less voltage. In order to obtain a useful measurement for anode potential, it was necessary to have a stable, known reference potential for comparison. An Ag/AgCl reference electrode was used for this purpose.

Figure 29 and Figure 30 show the initial prototype of the control system, which combined two voltage dividers with an Arduino Uno microcontroller board to control and collect data from two anode-cathode pairs contained in a single reactor. This prototype made use of dial-type potentiometers, which allowed the voltage applied to the electrode-pairs to be manually adjusted. The circuit was built on a breadboard using jumper wires.

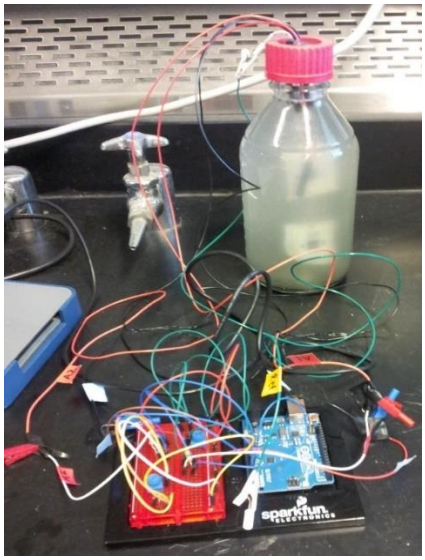

Figure 29: The initial prototype of the control system.

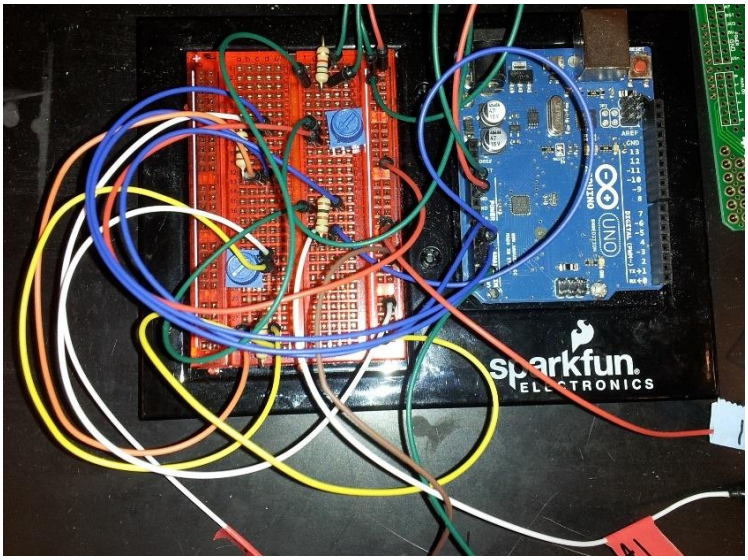

Figure 30: Close-up of the first prototype.

The next major improvement to the prototype was replacement of the dial-type potentiometers with digital potentiometers (digiPots) which can be programmatically controlled. The chosen digiPots had a maximum resistance of 10 kΩ, and the resistance could be set by the Arduino through seral-peripheral interface (SPI) communication by sending a number from 0 – 255 which would set the wiper to one of 256 tap points along the resistor. Having a variable resistor that could be controlled programmatically dramatically improved the ability of the system to reliably control anode potential. Figure 31 shows the prototype after the addition of the digiPots.

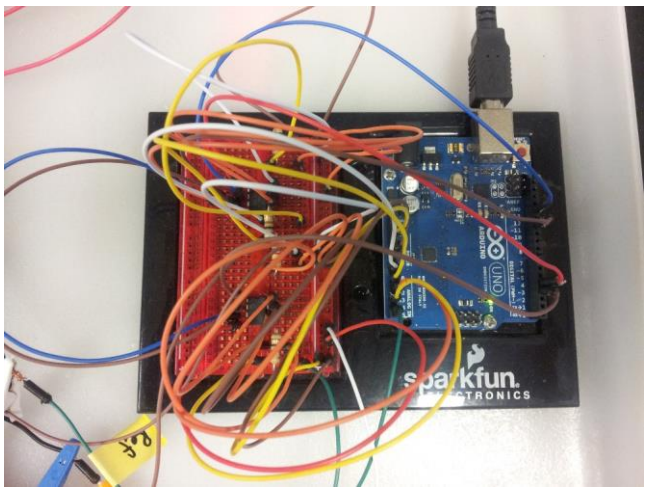

Figure 31: The prototype after the switch to digiPots.

Two major problems still existed with this version of the prototype. First, the acquired data was very noisy, and second, the data was very low resolution. In order to address these two issues, a custom printed circuit board (PCB) was designed to eliminate the need for jumper-wires and an external 16 bit analog-to-digital converter (ADC) was added to the system. The PCB was designed to be an Arduino shield, meaning it has pins extending from the bottom that plug into the headers on the Arduino board. The 16 bit ADC dramatically improved the resolution of the data compared to the Arduino Uno's on-board 10 bit ADC, and also added the capability to take differential readings, meaning the anode voltage could be directly compared to the reference electrode voltage to determine anode potential, and the voltage drop across the 100 Ω resistor could be directly obtained for determination of current. The PCB and external ADC, which came in the form of a breakout-board (Adafruit Industries), can be seen in Figure 32 and Figure 33. The improvement in the data due to these two upgrades can be clearly seen in the data presented in the results section. One final improvement was the addition of a metal–oxide–semiconductor field-effect transistor (MOSFET), which acts as a digital switch that can open the circuit to allow for a true OCV mode. A schematic of the circuit and the layout of the PCB are included in Appendix B.

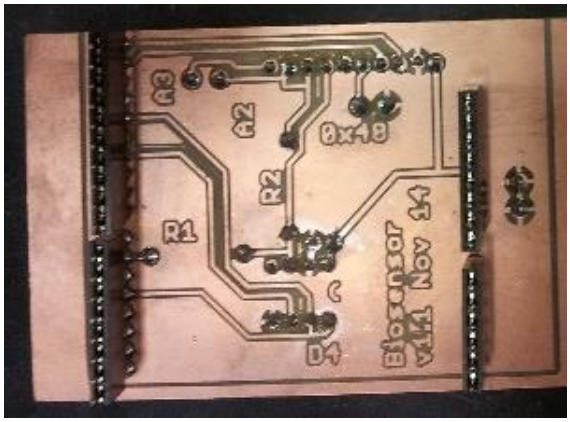

Figure 32: PCB shield, bottom view. Though it could only control a single electrode-pair, the switch to a PCB was a major upgrade over the breadboard and jumper-wire prototypes.

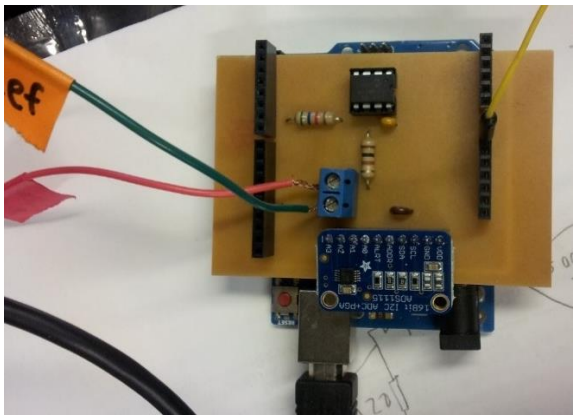

Figure 33: Another major upgrade came at the same time as the switch to a PCB was the addition of a four channel 16 bit external ADC. This image shows the ADC plugged into the top of the PCB shield.

A later version of the PCB was developed to include a waterproof temperature sensor (Adafruit Industries) which will be used with a data logger shield (Adafruit Industries) to collect data in a field study at a wastewater treatment plant. The data logger allows the system to collect data without being connected to a computer by saving it to an SD card.

4.1.2 Software development

The code to run the Arduino is called a 'sketch', and can be uploaded to the Arduino via USB, which also provides the power for the Arduino when it is connected to a computer. The Arduino can also be powered by an outlet or a battery. Sketches for four different electrochemical techniques were created for this project. In addition, a very simple script in python was created to receive the serial port communications from the Arduino and display the data and log it to a file. Examples of the sketches and the python script are included in Appendix B.

The first sketch that was created was for performing CA, where the anode potential is poised at a chosen value while the current output is measured. Initially, the manual dial potentiometers were used to control anode potential, but with the addition of the digiPots, it could be done by the sketch. Though updates were made as the hardware components of the system were changed, the basic functionality of the CA sketch did not change after the addition of the digiPots. Every ten seconds, the sketch monitors anode potential based on the readings from the ADC, and if it has dropped too low, the tap point of the digiPot is incremented up by one value to increase the applied voltage. If the anode potential is too high, the digiPot is incremented downwards by one. If the anode potential is within 0.5 mV of the desired anode potential, no change is made. Once per minute data including current (in mA), anode potential (V), and cell potential (V) is sent through serial communication to a computer running the python sketch which displays the values, and appends them to the current data file every 15 minutes.

The second sketch was for performing LSV, where the anode potential increased at a constant rate from a minimum potential up to a maximum while the current response is measured. This sketch works by setting a target value for the anode potential which increases at a set rate, for example, an increase of 2 mV every 2 s for a scan rate of one mV/s. The anode potential is checked once per second and if the value is below the current target, then the digiPot is incremented to increase the applied voltage. In this sketch, the digiPot is never allowed to increment downwards until the maximum value is reached and the LSV is finished.

The purpose of the third sketch is to perform cyclic voltammetry, where the anode potential is increased at a constant rate, and once it reaches the desired maximum, it is decreased back to the minimum at the same rate. This sketch works much in the same way as the LSV sketch. However, currently the transition from the upward (anodic) scan to the downward (cathodic) scan is too slow, and the sketch would need to be improved further in order to collect useful data.

The final sketch was developed for use in a field study. Based on the findings discussed in Chapter 3, stepped CA was chosen to provide data that could be used to generate a polarization curve of steady-state

current at each anode potential. Using a method similar to that used in the CA sketch, the anode potential is increased in steps, first to the nearest 0.05 V vs Ag/AgCl, and thereafter by 0.05 V increments until 0 V vs. Ag/AgCl is reached. Each anode potential increment is held for three minutes. The sketch runs on approximately a 2 h cycle, with 20 minutes of pseudo-OCV where the minimum amount of voltage is applied, followed by 30 minutes of stepped CA, 20 minutes of pseudo-OCV, and 50 minutes of CA at midpoint potential.

4.2 Results

Overall, though improvements can still be made, the performance of the system is acceptable and meets the goals that were set for its development. The performance of the system progressively improved with each software improvement and hardware upgrade. The results for the initial prototype with manually adjustable potentiometers pointed to what improvements needed to be made. Figure 34and Figure 35 show some of the first data collected during inoculation of the MEC as the anode biofilm was just beginning to grow and produce current. Figure 34 clearly shows how difficult it was to keep the anode potential at a desired value using a manually adjustable potentiometer.

From these figures, it is clear that the resolution was very poor, especially for the current measurements, as can be seen in Figure 35.

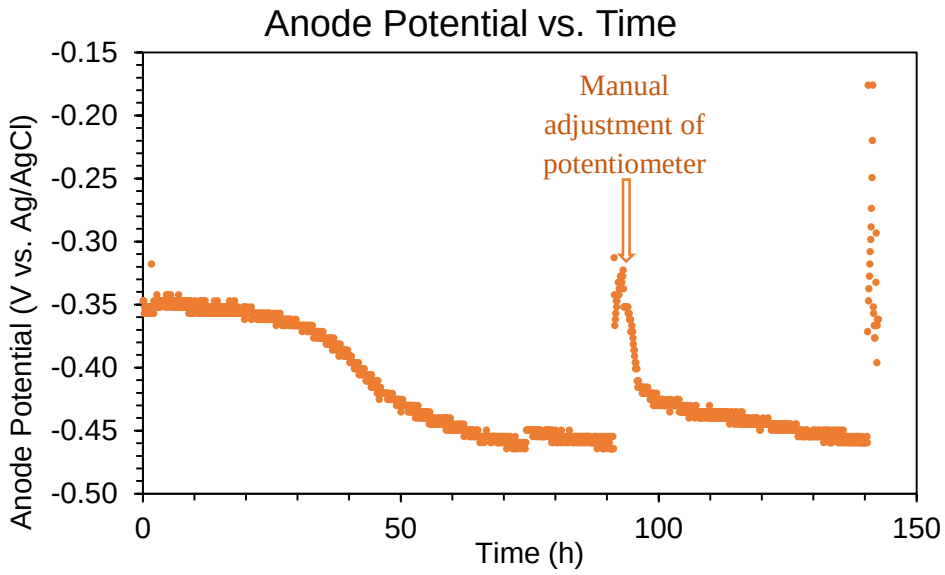

Figure 34: An example of some of the early anode potential data collected during inoculation with the initial prototype. The resolution limit of ~0.01 V for voltage measurements can be clearly seen.

Figure 36 shows how the resolution was improved by a change in the code which told the Arduino to use its internal reference range of 1.1 V instead of its external 5V reference range for the voltage

measurements. Because the Arduino's 10 bit on-board ADC can only divide the reference range into 1024 digital values, this change improved the resolution from about 0.1 mA to 0.02 mA. However, this also resulted in a reported voltage of 1.1 for any measured voltage that was 1.1 V or greater.

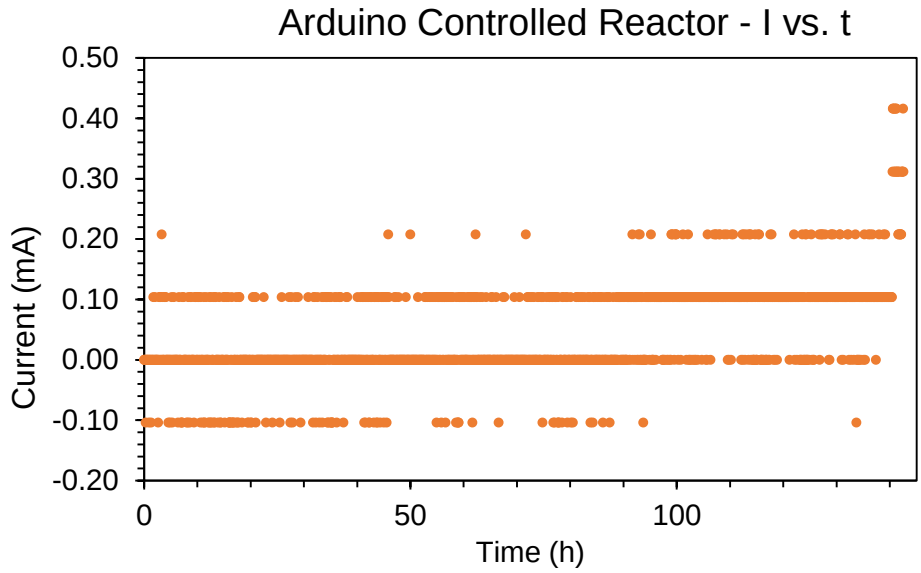

Figure 35: An example of current data collected during inoculation by the initial prototype. Again the 0.1 mA resolution limit of the current measurements can be clearly seen.

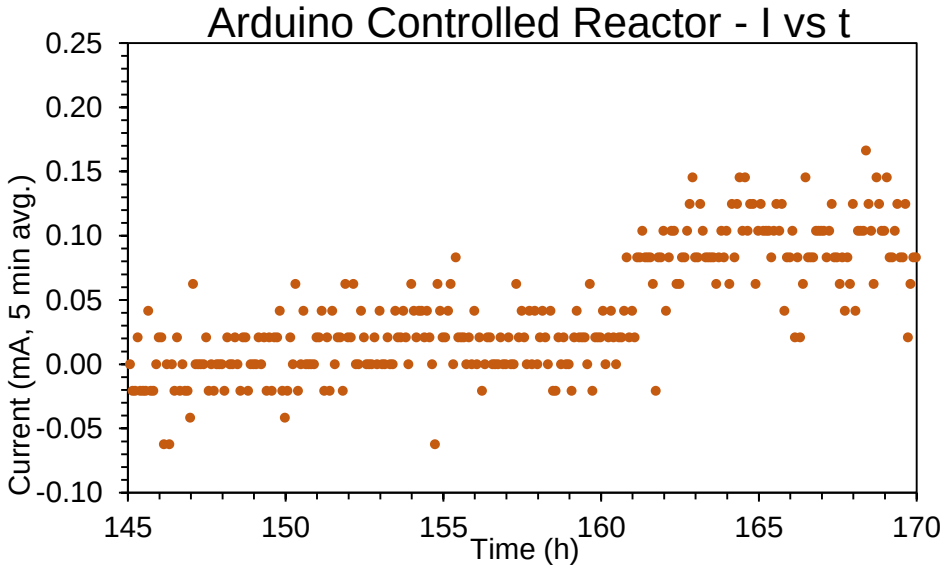

Figure 36: Current data collected during inoculation after a software improvement increased the resolution of current readings to ~0.02 mA.

Figure 37 shows data collected after the digiPots replaced the dial potentiometers. By comparing this figure with Figure 34, it is clear how much this upgrade improved the ability to control anode potential.

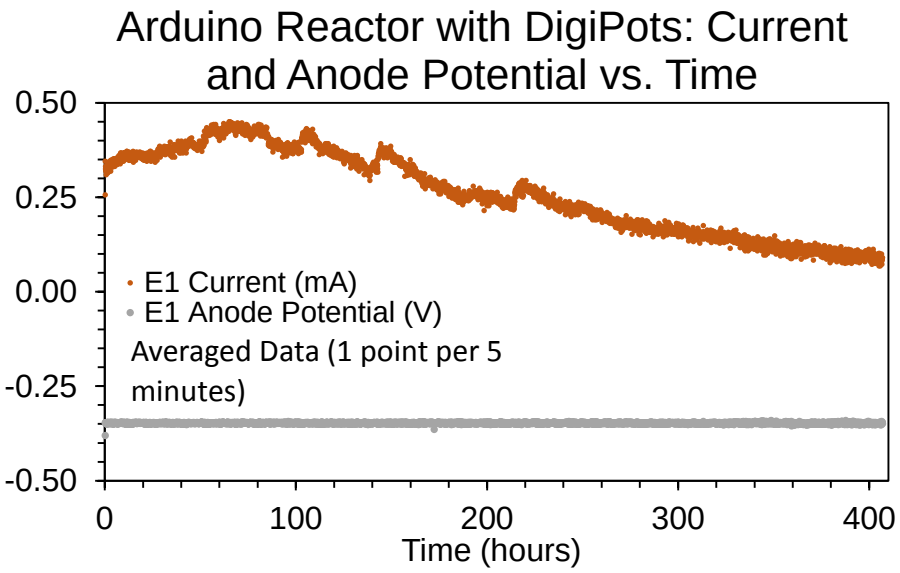

Figure 37: This plot shows both anode potential and current after the first major hardware improvement. When compared with Figure 34, it is evident that the switch from manually adjustable potentiometers to digiPots greatly improved the ability to set the anode potential to a desired value.

However, as shown by the current data in Figure 37 and Figure 38, the addition of the digiPots did not reduce the amount of noise in the data.

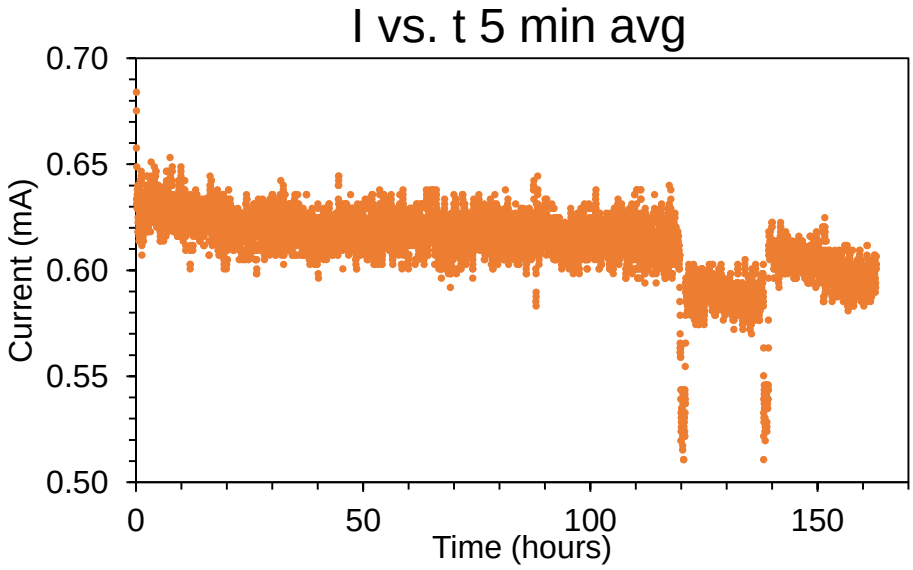

Figure 38: This data shows the amount of noise in the collected current data. At this point, by changing the value of the resistor used to measure the current, the resolution had been increased to 0.01 mA, though this is not reflected in the plot, which shows averaged data.

It was not until the first PCB shield prototype was developed and the 16 bit ADC was added that both resolution improvement and noise reduction were achieved, as shown in Figure 39.

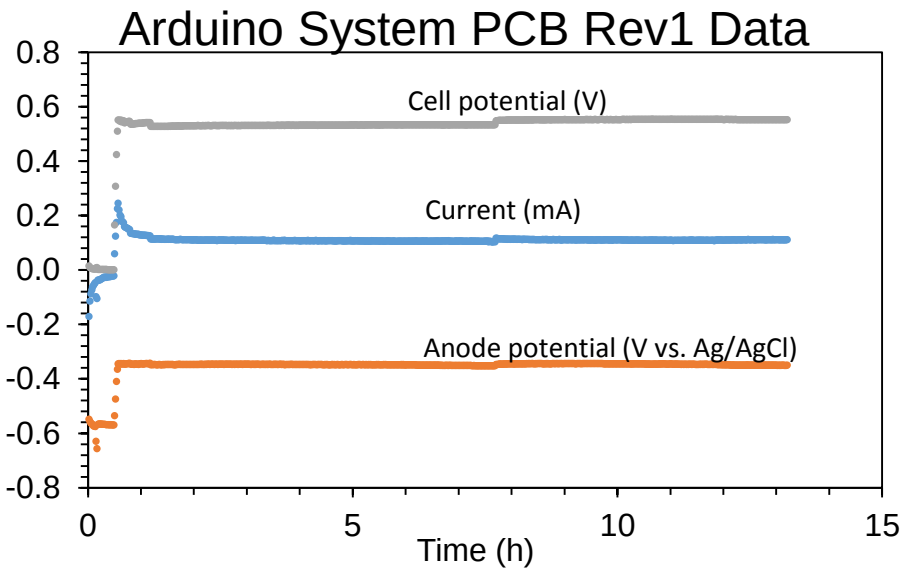

Figure 39: This plot shows raw current, anode potential, and cell potential data after the switch to a PCB and the addition of an external 16 bit ADC.

The development of the LSV sketch began after the addition of the digiPots. The first attempt worked by incrementing the digiPot upwards at a set rate, starting from the 0 tap point. This method did result in roughly the expected shape for the current vs. potential curve, as shown in Figure 40. However, because the scan rate for anode potential was not constant, the data points are more bunched in some parts of the range than others, resulting in a pseudo-LSV.

Figure 41 shows all of the data collected during this initial attempt at performing LSV. There were two anode/cathode pairs together in a single MEC reactor, one above the other. The LSV was run on the top pair, designated as E2. From E2's anode potential data in Figure 41, it is clear that the sweep was not linear. It is also interesting to note the response in E1's anode potential as E2's potential increased. At this time in the development of the prototype, there was no mechanism built into the circuit to allow for OCV, so both electrode-pairs were electrically connected through the cathodes, which were both connected to ground. During the pseudo-LSV on E2, E1 was connected, but with the tap point of the digiPot in its voltage divider set to 0. This interaction between the electrode-pairs is not desirable and could potentially affect the results. Later LSVs were performed with the other electrode-pair disconnected from the circuit to prevent interaction. Initially this was done by disconnecting the wires, but later it will be done with a MOSFET switch or a relay.

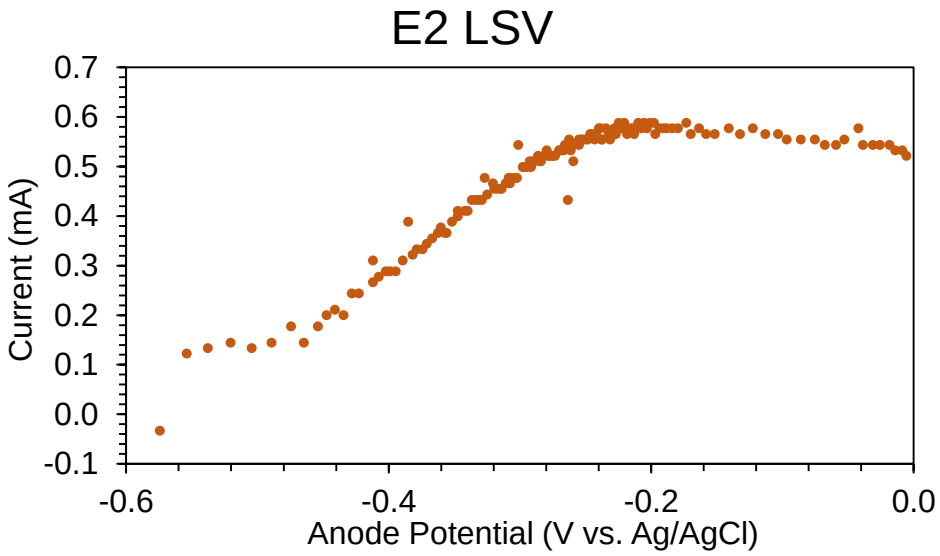

Figure 40: Data from the initial attempt to perform LSV.

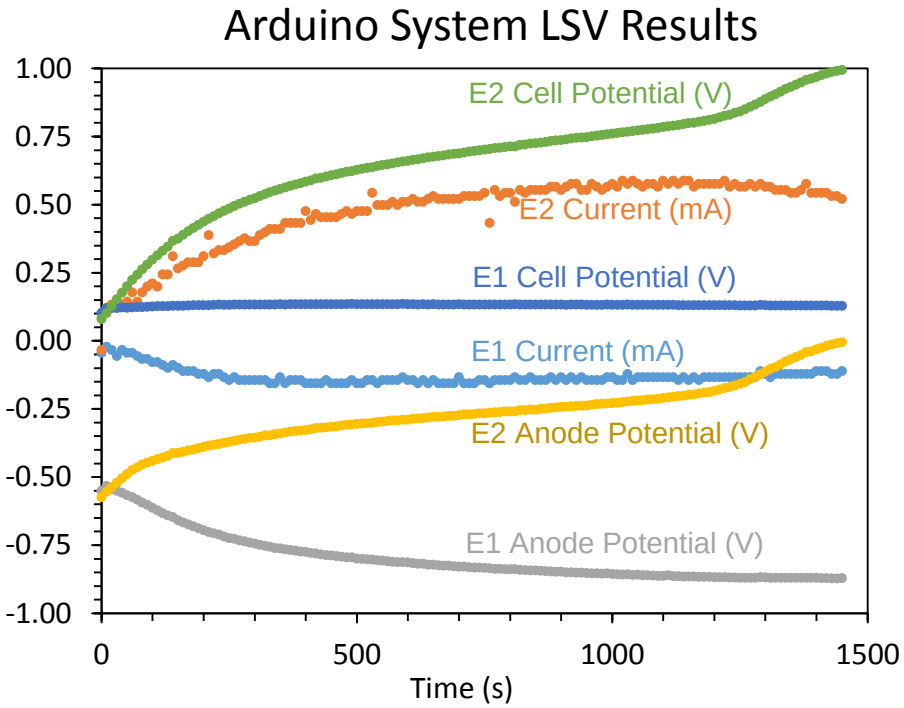

Figure 41: This plot shows all of the data collected for both electrode-pairs in a single reactor, during the initial attempt to perform LSV on the top electrode-pair (E2). It is clear that E2's anode potential scan rate was not linear.

The method previously described in the Software development section was developed after the pseudo-LSV to correct the non-linearity of the anode potential scan rate. The results are shown in Figure 42 and Figure 43 below. The linearity of the anodic sweep was greatly improved. However, because this was

before the development of the PCB and the addition of the 16 bit ADC, the voltammetric data is still very noisy.

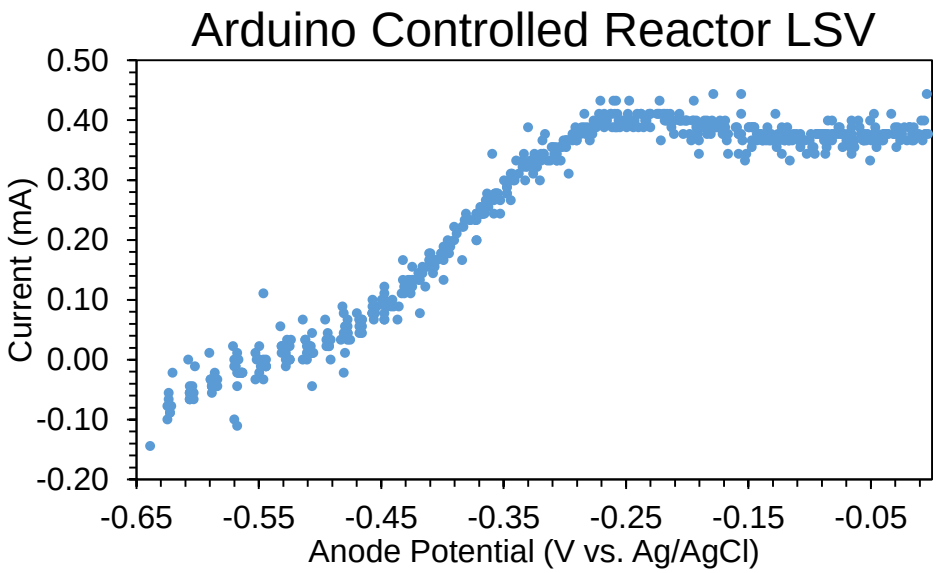

Figure 42: Raw data from the first LSV completed using the method described in the Software Development section above.

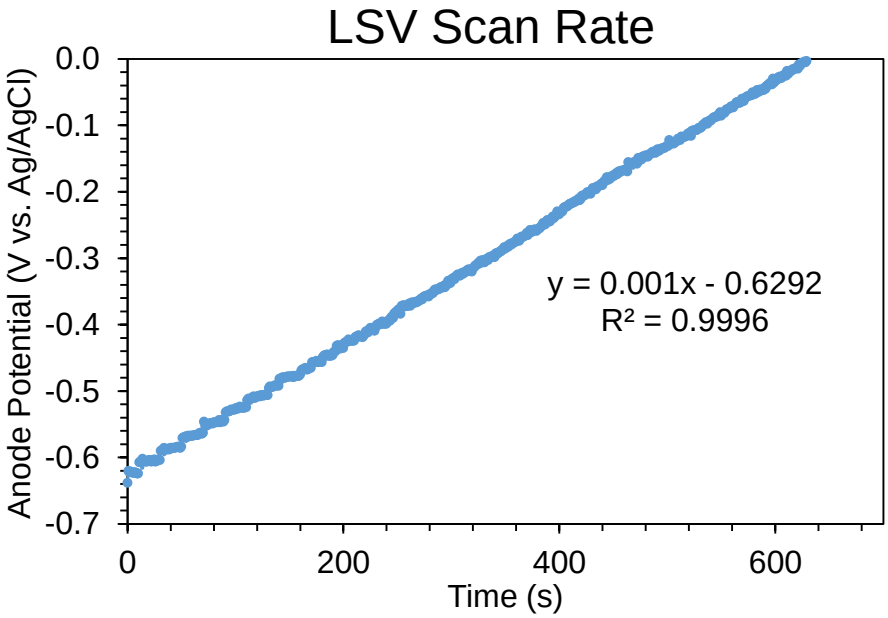

Figure 43: Anode potential scan rate for an LSV completed using the method described in the Software Development section. The scan rate is much more linear compared to the data in Figure 41 from the pseudo-LSV.

Acceptable LSV results were finally obtained by using the first PCB prototype and 16 bit ADC and the same method described in the Software Development section. Figure 44 shows the raw data for such an LSV. Compared with Figure 42, it is clear that the data has much less noise. The data shown in Figure 44

is suitable for fitting to a model. The fit for the Butler-Volmer Monod model developed by Hamelers et al. (2011)is also shown on the plot.

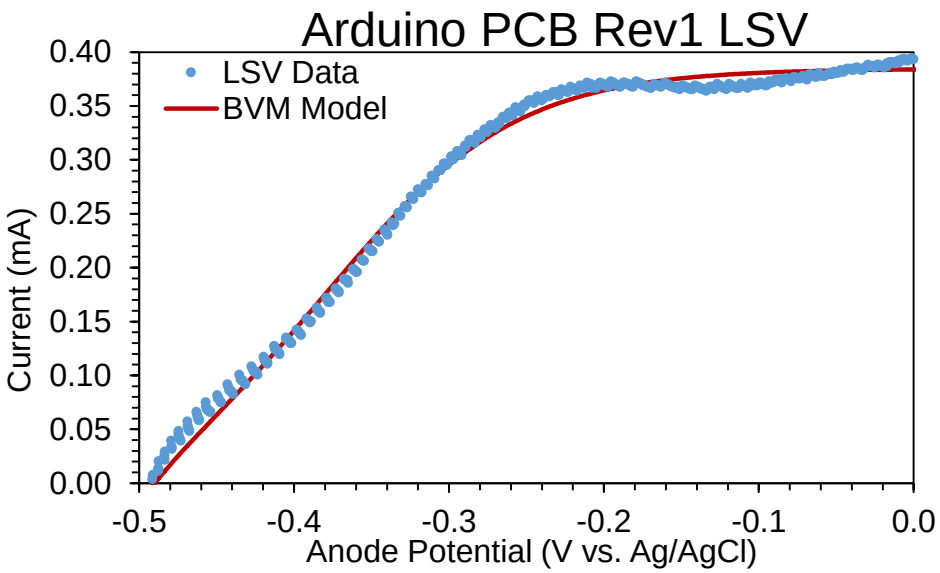

Figure 44: Raw LSV data collected using the first PCB prototype and 16 bit ADC and the fit of the BVM model.

Figure 45 below shows the anodic scan rate for the LSV.

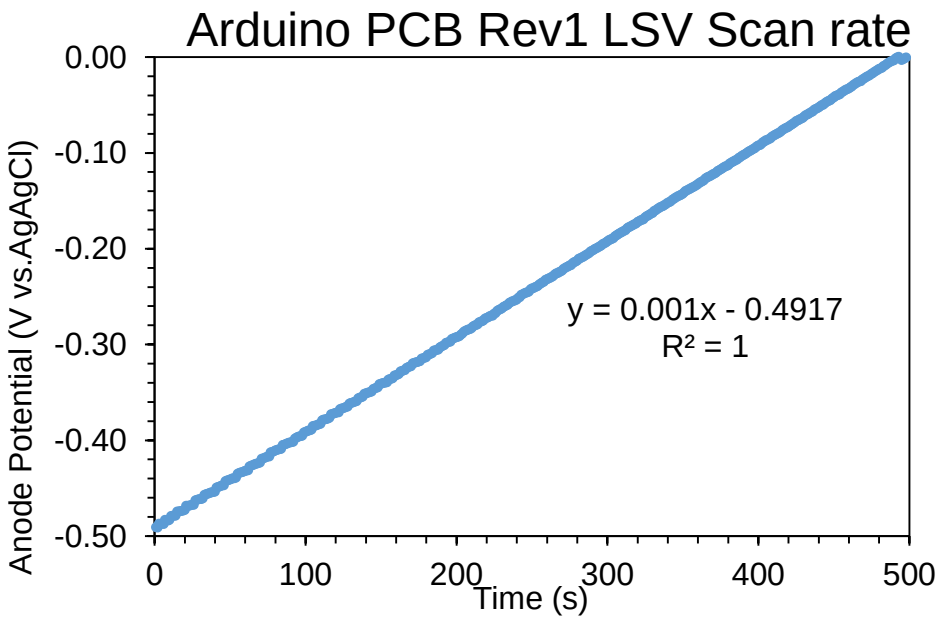

Figure 45: Anodic scan rate for an LSV performed with the first PCB prototype.

The final electrochemical technique that was attempted with the control system prototype was CV. Unfortunately, the method described in the Software Development section has not yielded usable results, as can be seen in Figure 46.

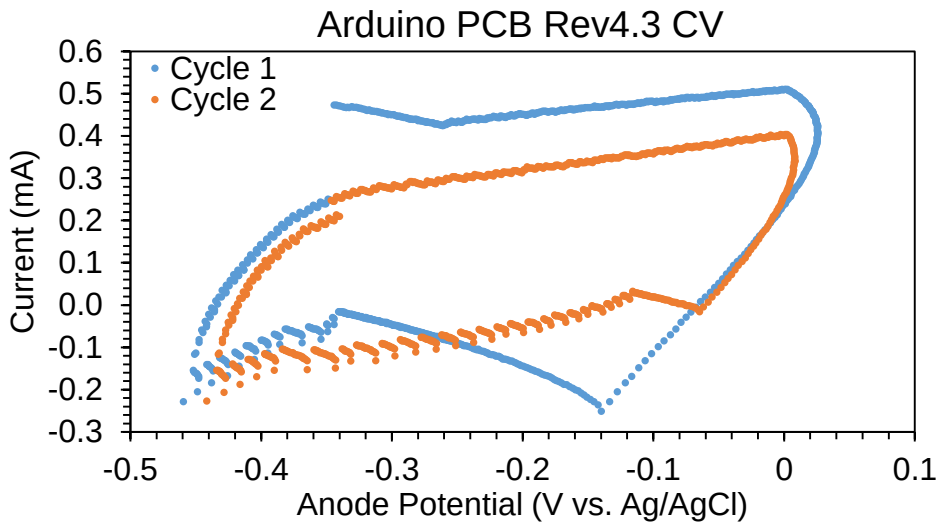

Figure 46: CV results with the PCB prototype.

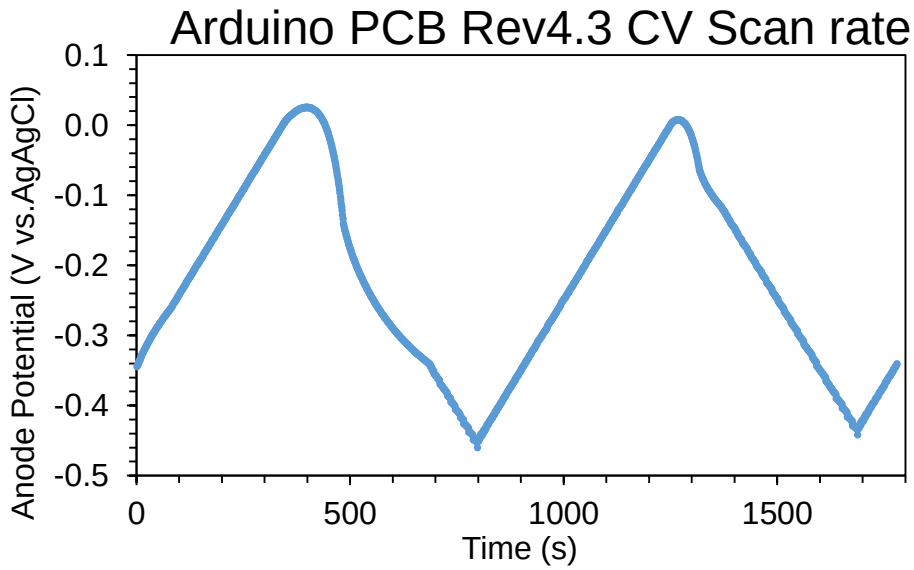

Figure 47: Anode potential scan rate for an attempted CV with the PCB prototype. The peaks of the anode potential should form a sharp point and occur at 0 V. This plot shows that the Anode potential drops much too slowly during this portion of the CV.

Figure 47 shows the anode potential scan rate during the CV, and the lack of sharp peaks during the switch from an anodic scan to a cathodic scan indicates that this transition occurred much too slowly. This is due to the system not having a way to forcibly draw the anode potential down, but could potentially be fixed by dramatically increasing the rate at which the digiPot can increment downwards. However, since the LSV or stepped CA data should be sufficient for modeling purposes, the capability to perform CV is not really necessary.

4.3 Discussion

Though there are still many improvements that can be made, the system that has been developed meets the goals that were set for this project and has all of the required capabilities to control an MEC and collect data for monitoring and modeling its behavior. Furthermore, the resulting system small and portable, and is incredibly inexpensive when compared with typical laboratory electrochemical instrumentation.

4.3.1 Future work

Future improvements to the system will include expanding the PCB to contain two voltage dividers capable of controlling two electrode-pairs and adding other sensors for pH, dissolved oxygen, electroconductivity, and temperature. These improvements will expand the capabilities of the system well beyond what a typical laboratory potentiostat can typically do. They will also greatly enrich the modeling of the data, as environmental conditions such as temperature and pH can greatly impact the behavior of an anode biofilm. These improvements will add significantly to the overall cost of the system, because switching to the Arduino Mega, a microcontroller board with many more input/output pins than the Uno, will probably be necessary. In addition, a waterproof temperature sensor costs about $9 and each of the other probes costs about $140. A user-friendly graphical user interface for the system is also under development.

A prototype of an MEC probe and control system is also being prepared for installation at a wastewater treatment plant in Urbana, IL as part of a field study to test the concept and collect stepped-CA, CA, and temperature data from a primary clarifier. This system will be housed in a waterproof junction box and powered by an electrical outlet using a 9 V DC power adapter.

4.3.2 Cost comparison

The cost of the current prototype is about $43. If all of the improvements discussed in the Future Work section are implemented, the cost could approach $500. However, a single channel for a laboratory potentiostat (which would be capable of controlling a single electrode-pair) can cost $6,000 to $8,000, and even an inexpensive potentiostat built for a field study by Friedman et al. (2012) had a total cost $600. The prototype system does not have all of the same capabilities as a potentiostat, is slightly less user-friendly, and can’t compare in terms of resolution and accuracy of data, however, the prototype system described in this chapter is sufficient for the purpose for which it was designed and provides hundreds to thousands of dollars in cost savings as well as adding portability and the potential to collect additional types of data.

4.3.3 Components and materials

The components used to build the hardware system are inexpensive and readily available. Table 5 provides a summary of the components and materials used. The total cost of the hardware is $63.65 if a data logger shield is used. If the system can be connected to a computer, the cost is only $43.40.

Table 5: Hardware components and materials

Component	Description/Function	Qty	Cost
Arduino Uno R3	A microcontroller board that can run basic code, interact with sensors and integrated chipsets (ICs), send data to a computer, power other small devices, and measure small voltages	1	$25.00
Microchip Technology 8-pin Digital Potentiometer- 10 kΩ	An IC with a variable resistor which can receive commands from the Arduino using SPI. The resistance is varied by positioning the wiper along 256 tap points.	1	$1.15
16 bit ADC breakout board	Converts analog voltage signals to digital signals. Has 4 analog inputs and can take single-ended or double-ended (differential) readings.	1	$14.95
PCB stock	Copper-clad board which can be etched or milled to create a custom PCB	1	~$0.50
Screw terminals	Soldered on to the PCB to provide connections for wires going to the anode, cathode, and reference electrode	2	$0.95
Fixed resistor – 5.6 kΩ	Part of the voltage divider circuit	1	$0.30
Fixed resistor – 100 Ω	Used to create a measurable drop in voltage which can be used to calculate current.	1	$0.30
0.1 µF Capacitor	Needed for stable operation of the digiPot IC	1	$0.25
Data logger shield	Saves data to an SD card when the Arduino is not connected to a computer	1	$19.95

Chapter 5: Conclusions

The work encompassed in this thesis can be categorized into two parts: 1) the test of the BVM model's predictive capability based on a kinetic characterization of MEC biofilm respiration for biofilms grown on two types of anode materials, and 2) the development of an inexpensive control and data acquisition system capable of carrying out basic electrochemical techniques. Both parts were undertaken with the broader goal of developing an inexpensive and reliable real-time or near real-time BOD sensor based on an MEC which could be deployed at wastewater treatment plants to allow for better process monitoring and optimization, potentially saving the plants money and increasing treatment effectiveness. There is also the possibility that such a sensor could help to increase automation at wastewater treatment plants and make smaller decentralized plants more feasible in both the developed and developing world.

The MEC biofilms were characterized by collecting voltammetry data from the anodic sweep of a third-cycle CV at different concentrations of acetate. The voltammetry data was then fit to the BVM model to determine the model's kinetic parameters for a particular biofilm. The parameters did not remain consistent at different substrate concentrations and were not always close to expected values. However, when the predictive capability of the BVM model was tested, the results showed that this approach could be useful with some additional fine tuning of the electrode materials and the electrochemical technique used to collect the voltammetry data.

The biofilms in the graphite plate anode MECs appear to be prone to damage when repeated CVs are carried out, while this kind of damage was not observed for the carbon mesh anode MECs. However, the data from the graphite plate anode MECs fit the BVM model better and resulted in better predictive capability of the model. The effects of both EDL capacitance and pseudocapacitance may be responsible for the shortfalls of the fit and predictive capability with both anode materials, but especially for the carbon mesh because of its high specific surface area. The problem of capacitance resulting in the measured current including both biologically catalyzed current and charging current could be addressed by ensuring that only steady-state current is measured. Future work will include investigation of using stepped CA to generate polarization curves rather than CV. If each step in potential is maintained long enough to reach steady-state, then the measured current will not include any charging current. Such a technique should improve the fit and predictive capability of the model regardless of which anode material is used.

The development of the control and data acquisition system resulted in an inexpensive system capable of performing CA, LSV, and stepped CA. The system can be connected to a computer for direct collection of data, or it can be used with a data logger shield and powered by the electrical grid for field

applications. Future work should focus on adding the capability to monitor other parameters such as pH and electroconductivity, adding the capability to measure OCV, and making the system more user-friendly by developing a graphical user interface. Work is already underway to use the control system for a field study at an Urbana, IL wastewater treatment plant to collect CA and stepped CA data from a primary clarifier.

There is much at stake in maintaining and expanding access to sanitation around the world, and the ability to monitor, optimize, or even automate the processes with inexpensive sensors for important wastewater quality parameters such as BOD, pH, temperature, and DO could go a long way in helping to make smaller, less expensive, and community managed wastewater treatment facilities more viable. While this study did not produce a fully developed sensor ready for deployment at wastewater treatment plants, it has shown that a model-based approach to developing a BOD sensor is worth pursuing in further research.

References

An L, Niu H, Zeng H. 1998. A new biosensor for rapid oxygen demand measurement. Water Environment Research 70(5):1070-1074.

ASCE. 2013. 2013 Report Card for America's Infrastructure: Wastewater. American Society of Civil Engineers.

Augustyn V, Simon P, Dunn B. 2014. Pseudocapacitive oxide materials for high-rate electrochemical energy storage. Energy & Environmental Science 7(5):1597-1614.

Bard AJ, Faulkner LR. 2001. Electrochemical methods : fundamentals and applications. New York: Wiley.

Chang IS, Jang JK, Gil GC, Kim M, Kim HJ, Cho BW, Kim BH. 2004. Continuous determination of biochemical oxygen demand using microbial fuel cell type biosensor. Biosensors and Bioelectronics 19(6):607-613.

Chang IS, Moon H, Jang JK, Kim BH. 2005. Improvement of a microbial fuel cell performance as a BOD sensor using respiratory inhibitors. Biosensors and Bioelectronics 20(9):1856-1859.

Chee G-J, Nomura Y, Ikebukuro K, Karube I. 2000. Optical fiber biosensor for the determination of low biochemical oxygen demand. Biosensors and Bioelectronics 15(7–8):371-376.

Chee G-J, Nomura Y, Karube I. 1999. Biosensor for the estimation of low biochemical oxygen demand. Analytica Chimica Acta 379(1–2):185-191.

Contento N, Bohn P. 2015. Electric field effects on current–voltage relationships in microfluidic channels presenting multiple working electrodes in the weak-coupling limit. Microfluidics and Nanofluidics 18(1):131-140.

Conway BE, Pell WG. 2003. Double-layer and pseudocapacitance types of electrochemical capacitors and their applications to the development of hybrid devices. Journal of Solid State Electrochemistry 7(9):637-644.

Di Lorenzo M, Curtis TP, Head IM, Scott K. 2009. A single-chamber microbial fuel cell as a biosensor for wastewaters. Water Research 43(13):3145-3154.

Donovan C, Dewan A, Peng H, Heo D, Beyenal H. 2011. Power management system for a remote sensor powered by a sediment microbial fuel cell. Journal of Power Sources 196(3):1171-1177.

Eaton AD, Clesceri LS, Greenberg AE, Franson MAH, editors. 1995. Standard methods for the examination of water and wastewater. Washington, DC: American Public Health Association.

El-Naggar MY, Wanger G, Leung KM, Yuzvinsky TD, Southam G, Yang J, Lau WM, Nealson KH, Gorby YA. 2010. Electrical transport along bacterial nanowires from Shewanella oneidensis MR-1. Proceedings of the National Academy of Sciences 107(42):18127-18131.

Fang C, Min B, Angelidaki I. 2011. Nitrate as an Oxidant in the Cathode Chamber of a Microbial Fuel Cell for Both Power Generation and Nutrient Removal Purposes. Applied Biochemistry and Biotechnology 164(4):464-474.

Friedman ES, Rosenbaum MA, Lee AW, Lipson DA, Land BR, Angenent LT. 2012. A cost-effective and field-ready potentiostat that poises subsurface electrodes to monitor bacterial respiration. Biosensors and Bioelectronics 32(1):309-313.

Gil G-C, Chang I-S, Kim BH, Kim M, Jang J-K, Park HS, Kim HJ. 2003. Operational parameters affecting the performannce of a mediator-less microbial fuel cell. Biosensors and Bioelectronics 18(4):327-334.

Gorby YA, Yanina S, McLean JS, Rosso KM, Moyles D, Dohnalkova A, Beveridge TJ, Chang IS, Kim BH, Kim KS and others. 2006. Electrically conductive bacterial nanowires produced by Shewanella oneidensis strain MR-1 and other microorganisms. Proceedings of the National Academy of Sciences 103(30):11358-11363.

Hamelers HVM, ter Heijne A, Stein N, Rozendal RA, Buisman CJN. 2011. Butler–Volmer–Monod model for describing bio-anode polarization curves. Bioresource Technology 102(1):381-387.

Kang K, Jang J, Pham T, Moon H, Chang I, Kim B. 2003. A microbial fuel cell with improved cathode reaction as a low biochemical oxygen demand sensor. Biotechnology Letters 25(16):1357-1361.

Karube I, Matsunaga T, Mitsuda S, Suzuki S, Tadashi Matsunaga Ib. 2009. Microbial electrode BOD Sensors. Biotechnology and Bioengineering 102(3):659-672.

Kaur A, Ibrahim S, Pickett CJ, Michie IS, Dinsdale RM, Guwy AJ, Premier GC. 2014. Anode modification to improve the performance of a microbial fuel cell volatile fatty acid biosensor. Sensors and Actuators B: Chemical 201(0):266-273.

Kaur A, Kim JR, Michie I, Dinsdale RM, Guwy AJ, Premier GC. 2013. Microbial fuel cell type biosensor for specific volatile fatty acids using acclimated bacterial communities. Biosensors and Bioelectronics 47(0):50-55.

Kenward AY, Daniel; Raja, Urooj. 2013. Sewage Overflows from Hurricane Sandy. Princeton, New Jersey.

Kim B-H, Kim H-J, Hyun MS, Park DH. 1999a. Direct Electrode Reaction of Fe(3)-Reducing Bacterium , Shewanella putrefaciens. J. Microbiology and Biotechnology 9(2):127-131.

Kim B, Chang I, Cheol Gil G, Park H, Kim H. 2003. Novel BOD (biological oxygen demand) sensor using mediator-less microbial fuel cell. Biotechnology Letters 25(7):541-545.

Kim BH, Park HS, Kim HJ, Kim GT, Chang IS, Lee J, Phung NT. 2004. Enrichment of microbial community generating electricity using a fuel-cell-type electrochemical cell. Applied Microbiology and Biotechnology 63(6):672-681.

Kim HJ, Hyun MS, Chang IS, Kim BH. 1999b. A microbial fuel cell type lactate biosensor using a metal-reducing bacterium, Shewanella putrefaciens. Journal of Microbiology and Biotechnology 9(3):365-367.

Kim HJ, Park HS, Hyun MS, Chang IS, Kim M, Kim BH. 2002. A mediator-less microbial fuel cell using a metal reducing bacterium, Shewanella putrefaciens. Enzyme and Microbial Technology 30(2):145-152.

Kim M-N, Kwon H-S. 1999. Biochemical oxygen demand sensor using Serratia marcescens LSY 4. Biosensors and Bioelectronics 14(1):1-7.

Kumlanghan A, Liu J, Thavarungkul P, Kanatharana P, Mattiasson B. 2007. Microbial fuel cell-based biosensor for fast analysis of biodegradable organic matter. Biosensors and Bioelectronics 22(12):2939-2944.

Lee H-S, Torres CsI, Rittmann BE. 2009. Effects of Substrate Diffusion and Anode Potential on Kinetic Parameters for Anode-Respiring Bacteria. Environmental Science & Technology 43(19):7571-7577.

Liu H, Logan BE. 2004. Electricity Generation Using an Air-Cathode Single Chamber Microbial Fuel Cell in the Presence and Absence of a Proton Exchange Membrane. Environmental Science & Technology 38(14):4040-4046.

Liu H, Ramnarayanan R, Logan BE. 2004. Production of Electricity during Wastewater Treatment Using a Single Chamber Microbial Fuel Cell. Environmental Science & Technology 38(7):2281-2285.

Liu J, Björnsson L, Mattiasson B. 2000. Immobilised activated sludge based biosensor for biochemical oxygen demand measurement. Biosensors and Bioelectronics 14(12):883-893.

Liu J, Mattiasson B. 2002. Microbial BOD sensors for wastewater analysis. Water Research 36(15):3786-3802.

Logan BE. 2008a. Introduction. Microbial Fuel Cells: John Wiley & Sons, Inc. p 1-11.

Logan BE. 2008b. Voltage Generation. Microbial Fuel Cells: John Wiley & Sons, Inc. p 29-43.

Lovley DR, Phillips EJP. 1988. Novel Mode of Microbial Energy Metabolism: Organic Carbon Oxidation Coupled to Dissimilatory Reduction of Iron or Manganese. Applied and Environmental Microbiology 54(6):1472-1480.

Marcus A, Torres CI, Rittmann BE. 2007. Conduction-based modeling of the biofilm anode of a microbial fuel cell. Biotechnology and Bioengineering 98(6):1171-1182.

Min B, Logan BE. 2004. Continuous electricity generation from domestic wastewater and organic substrates in a flat plate microbial fuel cell. Environmental Science & Technology 38(21):5809-5814.
Modin O, Wilén B-M. 2012. A novel bioelectrochemical BOD sensor operating with voltage input. Water Research 46(18):6113-6120.
Moon H, Chang I, Kang K, Jang J, Kim B. 2004. Improving the dynamic response of a mediator-less microbial fuel cell as a biochemical oxygen demand (BOD) sensor. Biotechnology Letters 26(22):1717-1721.
Myers CR, Nealson KH. 1988. Bacterial Manganese Reduction and Growth with Manganese Oxide as the Sole Electron Acceptor. Science 240(4857):1319-1321.
Nakamura H, Suzuki K, Ishikuro H, Kinoshita S, Koizumi R, Okuma S, Gotoh M, Karube I. 2007. A new BOD estimation method employing a double-mediator system by ferricyanide and menadione using the eukaryote Saccharomyces cerevisiae. Talanta 72(1):210-216.
Nielsen LP, Risgaard-Petersen N, Fossing H, Christensen PB, Sayama M. 2010. Electric currents couple spatially separated biogeochemical processes in marine sediment. Nature 463(7284):1071-1074.
Park DH, Zeikus JG. 2000. Electricity Generation in Microbial Fuel Cells Using Neutral Red as an Electronophore. Applied and Environmental Microbiology 66(4):1292-1297.
Pell M, Nyberg F. 1989. Infiltration of wastewater in a newly started pilot sand-filter system: I. Reduction of organic matter and phosphorus. Journal of Environmental Quality 18(4):451-457.
Pham TH, Jang JK, Chang IS, Kim BH. 2004. Improvement of cathode reaction of a mediatorless microbial fuel cell. Journal of Microbiology and Biotechnology 14(2):324-329.
Pinto RP, Srinivasan B, Escapa A, Tartakovsky B. 2011. Multi-Population Model of a Microbial Electrolysis Cell. Environmental Science & Technology 45(11):5039-5046.
Pirbadian S, Barchinger SE, Leung KM, Byun HS, Jangir Y, Bouhenni RA, Reed SB, Romine MF, Saffarini DA, Shi L and others. 2014. Shewanella oneidensis MR-1 nanowires are outer membrane and periplasmic extensions of the extracellular electron transport components. Proceedings of the National Academy of Sciences 111(35):12883-12888.
Preininger C, Klimant I, Wolfbeis OS. 1994. Optical Fiber Sensor for Biological Oxygen Demand. Analytical Chemistry 66(11):1841-1846.
Puig S, Serra M, Coma M, Balaguer MD, Colprim J. 2011. Simultaneous domestic wastewater treatment and renewable energy production using microbial fuel cells (MFCs). Water Science and Technology 64(4):904-909.
Qian Z, Tan TC. 1998. RESPONSE CHARACTERISTICS OF A DEAD-CELL BOD SENSOR. Water Research 32(3):801-807.
Rabaey K, Rozendal RA. 2010. Microbial electrosynthesis — revisiting the electrical route for microbial production. Nat Rev Micro 8(10):706-716.
Rabaey K, Verstraete W. 2005. Microbial fuel cells: novel biotechnology for energy generation. Trends in Biotechnology 23(6):291-298.
Rastogi S, Rathee P, Saxena TK, Mehra NK, Kumar R. 2003. BOD analysis of industrial effluents: 5 days to 5 min. Current Applied Physics 3(2–3):191-194.
Reguera G, McCarthy KD, Mehta T, Nicoll JS, Tuominen MT, Lovley DR. 2005. Extracellular electron transfer via microbial nanowires. Nature 435(7045):1098-1101.
Reguera G, Nevin KP, Nicoll JS, Covalla SF, Woodard TL, Lovley DR. 2006. Biofilm and Nanowire Production Leads to Increased Current in Geobacter sulfurreducens Fuel Cells. Applied and Environmental Microbiology 72(11):7345-7348.
Ren H, Tian H, Lee H-S, Park T, Leung FC, Ren T-L, Chae J. 2015. Regulating the respiration of microbe: A bio-inspired high performance microbial supercapacitor with graphene based electrodes and its kinetic features. Nano Energy 15(0):697-708.
Richter H, Nevin KP, Jia H, Lowy DA, Lovley DR, Tender LM. 2009. Cyclic voltammetry of biofilms of wild type and mutant Geobacter sulfurreducens on fuel cell anodes indicates possible roles of

OmcB, OmcZ, type IV pili, and protons in extracellular electron transfer. Energy & Environmental Science 2(5):506-516.
Riedel K, Lehmann M, Tag K, Renneberg R, Kunze G. 1998. Arxula adeninivorans Based Sensor for the Estimation of BOD. Analytical Letters 31(1):1-12.
Riedel K, Renneberg R, Kühn M, Scheller F. 1988. A fast estimation of biochemical oxygen demand using microbial sensors. Applied Microbiology and Biotechnology 28(3):316-318.
Riedel K, Uthemann R. 1994. Sensor BOD, a new cumulative parameter. Wasserwirtsch Wassertech(2):35-28.
Rimboud M, Pocaznoi D, Erable B, Bergel A. 2014. Electroanalysis of microbial anodes for bioelectrochemical systems: basics, progress and perspectives. Physical Chemistry Chemical Physics 16(31):16349-16366.
Roller SD, Bennetto HP, Delaney GM, Mason JR, Stirling JL, Thurston CF. 1984. Electron-transfer coupling in microbial fuel cells: 1. comparison of redox-mediator reduction rates and respiratory rates of bacteria. Journal of Chemical Technology and Biotechnology. Biotechnology 34(1):3-12.
Snider RM, Strycharz-Glaven SM, Tsoi SD, Erickson JS, Tender LM. 2012. Long-range electron transport in Geobacter sulfurreducens biofilms is redox gradient-driven. Proceedings of the National Academy of Sciences 109(38):15467-15472.
Sonawane JM, Marsili E, Ghosh PC. 2014. Treatment of domestic and distillery wastewater in high surface microbial fuel cells. International Journal of Hydrogen Energy 39(36):21819-21827.
Srikanth S, Marsili E, Flickinger MC, Bond DR. 2008. Electrochemical characterization of Geobacter sulfurreducens cells immobilized on graphite paper electrodes. Biotechnology and Bioengineering 99(5):1065-1073.
Strycharz SM, Malanoski AP, Snider RM, Yi H, Lovley DR, Tender LM. 2011. Application of cyclic voltammetry to investigate enhanced catalytic current generation by biofilm-modified anodes of Geobacter sulfurreducens strain DL1 vs. variant strain KN400. Energy & Environmental Science 4(3):896-913.
Tan TC, Wu C. 1999. BOD sensors using multi-species living or thermally killed cells of a BODSEED microbial culture. Sensors and Actuators B: Chemical 54(3):252-260.
Torres C, Kato Marcus A, Rittmann B. 2007. Kinetics of consumption of fermentation products by anode-respiring bacteria. Applied Microbiology and Biotechnology 77(3):689-697.
Torres CI, Kato Marcus A, Rittmann BE. 2008a. Proton transport inside the biofilm limits electrical current generation by anode-respiring bacteria. Biotechnology and Bioengineering 100(5):872-881.
Torres CI, Marcus AK, Lee H-S, Parameswaran P, Krajmalnik-Brown R, Rittmann BE. 2010. A kinetic perspective on extracellular electron transfer by anode-respiring bacteria. FEMS Microbiology Reviews 34(1):3-17.
Torres CI, Marcus AK, Parameswaran P, Rittmann BE. 2008b. Kinetic Experiments for Evaluating the Nernst−Monod Model for Anode-Respiring Bacteria (ARB) in a Biofilm Anode. Environmental Science & Technology 42(17):6593-6597.
van Loosdrecht MCM, Brdjanovic D. 2014. Anticipating the next century of wastewater treatment. Science 344(6191):1452-1453.
Velling S, Tenno T. 2009. Different calibration methods of a microbial BOD sensor for analysis of municipal wastewaters. Sensors and Actuators B: Chemical 141(1):233-238.
WHO/UNICEF. 2013. Progress on Sanitation and Drinking Water: 2013 Update. Geneva, Switzerland: World Health Organization
Xu G-H, Wang Y-K, Sheng G-P, Mu Y, Yu H-Q. 2014. An MFC-Based Online Monitoring and Alert System for Activated Sludge Process. Sci. Rep. 4.
Yang Z, Suzuki H, Sasaki S, Karube I. 1996. Disposable sensor for biochemical oxygen demand. Applied Microbiology and Biotechnology 46(1):10-14.
Yoho RA, Popat SC, Torres CI. 2014. Dynamic Potential-Dependent Electron Transport Pathway Shifts in Anode Biofilms of Geobacter sulfurreducens. ChemSusChem 7(12):3413-3419.

Yu C, Twigg CM, Sadik OA, Shiqiong T. A self-powered adaptive wireless sensor network for wastewater treatment plants; 2011 21-25 March 2011. p 356-359.

Appendix A: MEC Characterization

A.1 Reactor Designs

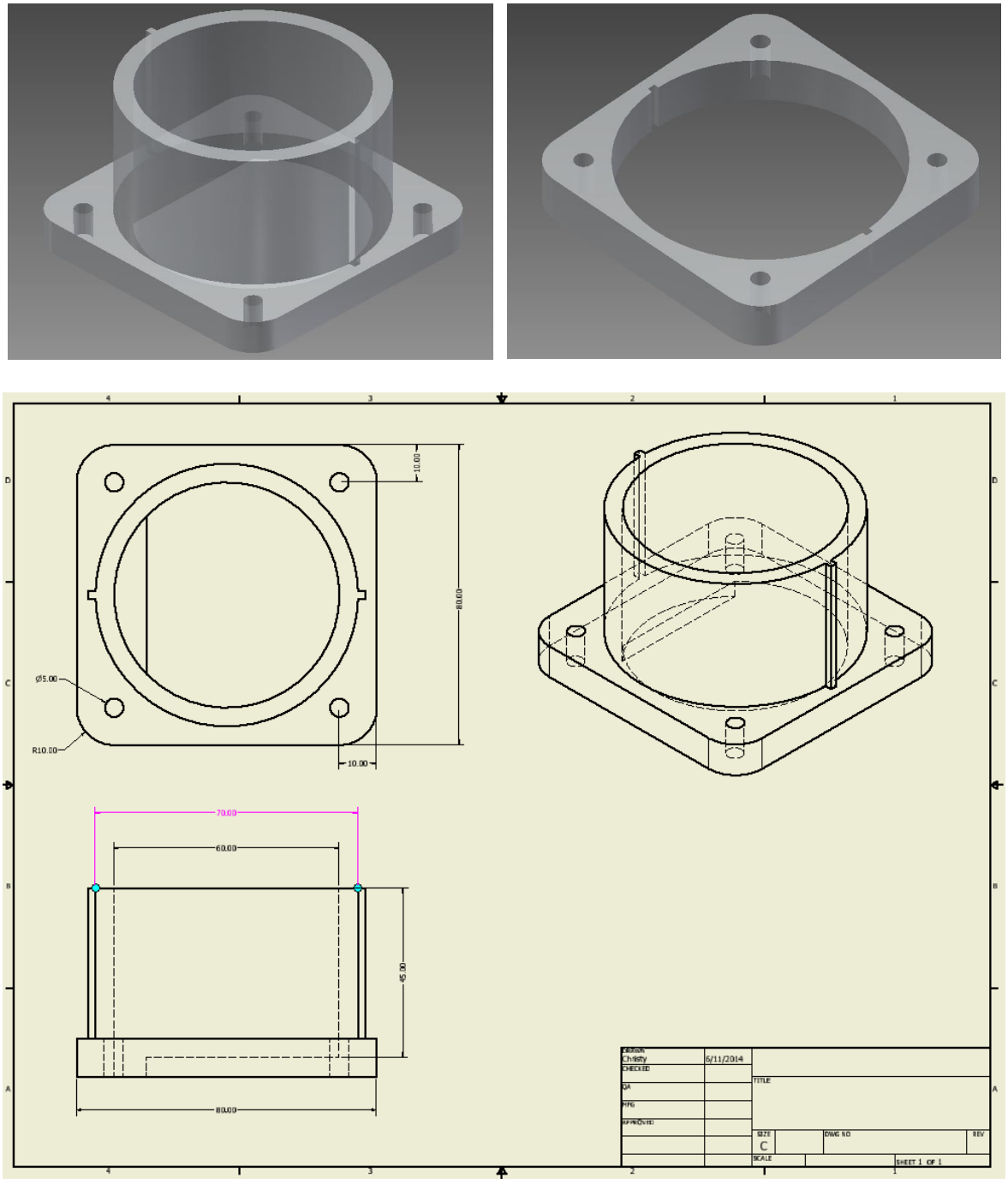

Figure 48: Renderings and design drawings for modular multiple WE MEC reactor.

A.2 Additional data and figures

A.2.1 Carbon mesh anode results

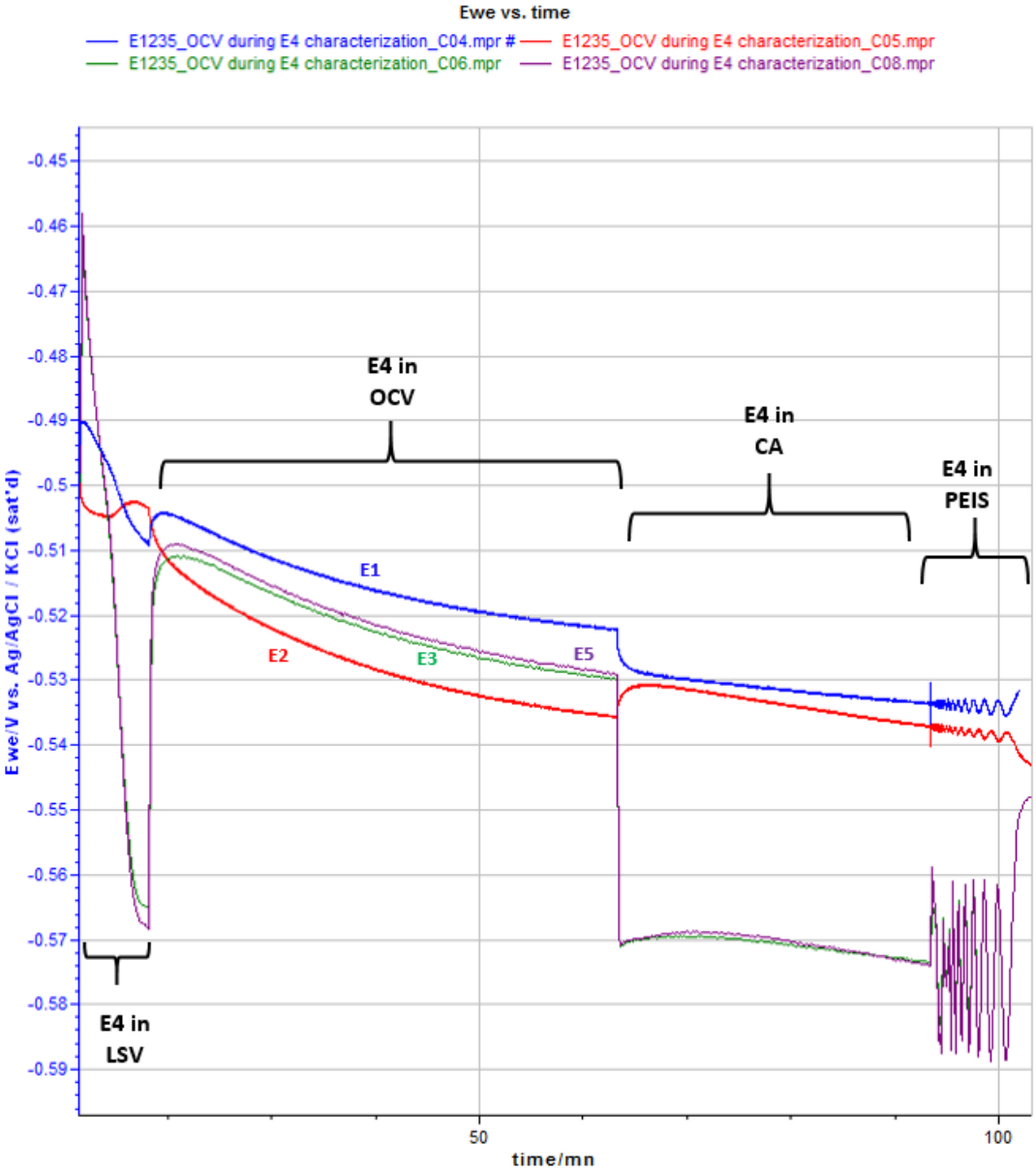

Figure 49: Anode potential response of electrode-pairs E1, E2, E3, and E5 in OCV to a series of electrochemical techniques performed on E4.

Table 6: Summary of BVM model fitting results for a second carbon mesh anode MEC.

	Sodium acetate concentration:			
Parameters	**500 mg/L**	**250 mg/L**	**50 mg/L**	**0 mg/L**
K_1	4.402895	4.379024	3.754817	5.295191
K_2	1.421722	1.972184	2.441506	0
α	0.630747	0.67906	0.767914	0.331044
Acetate prediction		131.2 mg/L	30.6 mg/L	13.5 mg/L

A.2.2 Graphite plate anode results

Table 7: BVM model fitting results for a second graphite anode MEC, which are comparable to those presented in section 3.2.

	Sodium acetate concentration:			
Parameters	**250 mg/L**	**100 mg/L**	**50 mg/L**	**25 mg/L**
K_1	2.904566	6.552285	8.562944	8.562944
K_2	45.26796	34.92795	16.29614	16.29614
α	0.5	0.5	0.5	0.5
Acetate prediction		123.5 mg/L	43.6 mg/L	17.6 mg/L

Appendix B: Control system development

B.1 Schematics

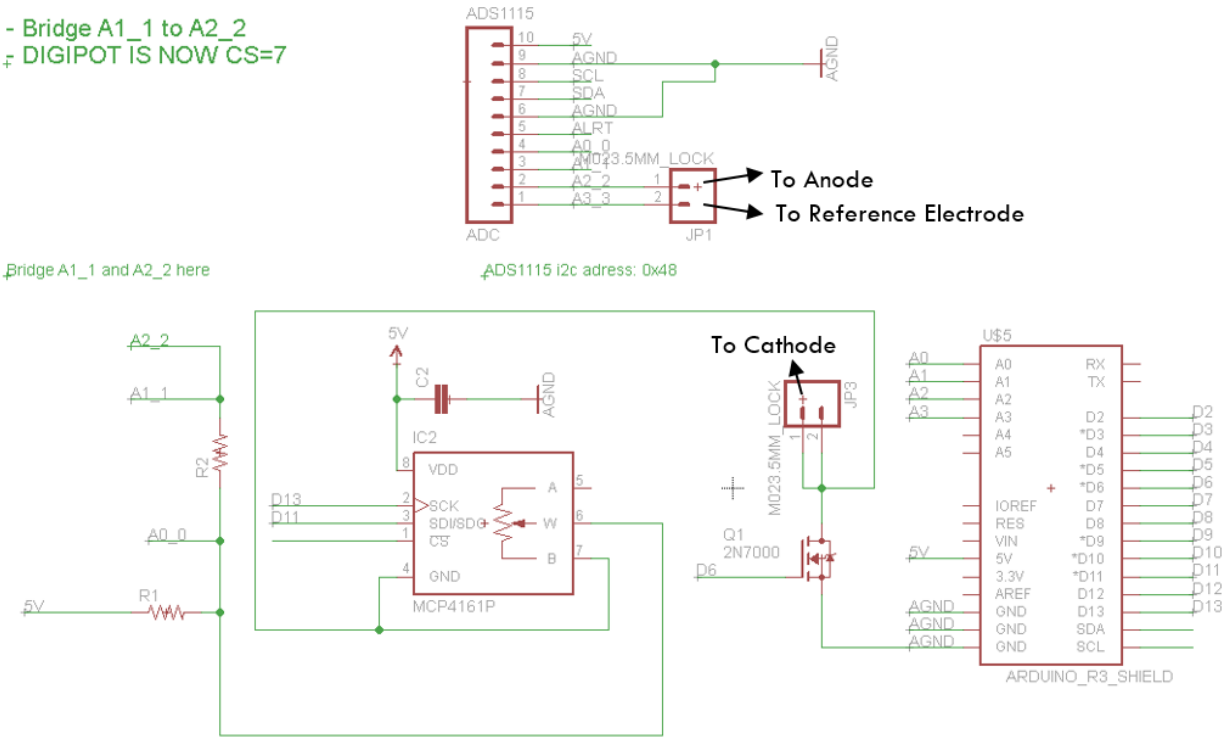

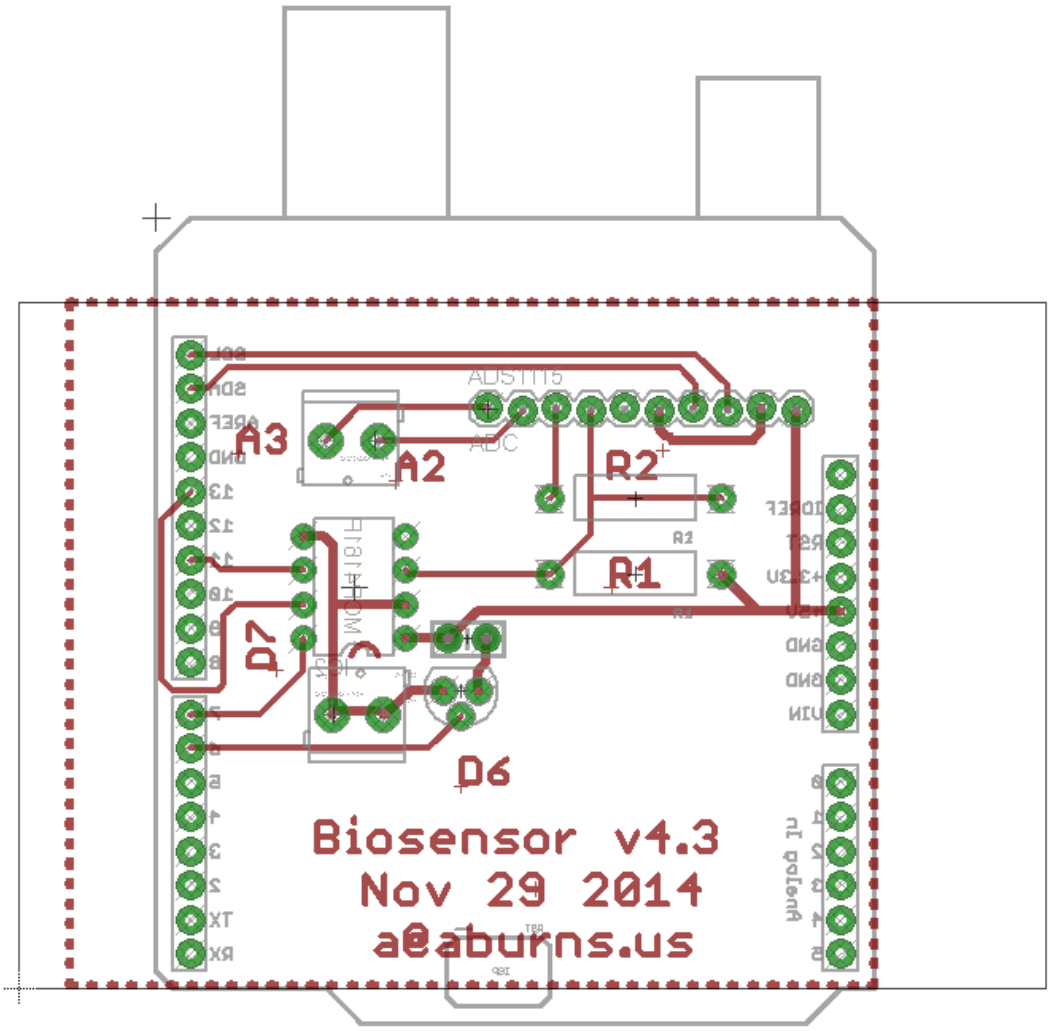

B.2 Code

B.2.1 Chronoamperometry

```
/*
 set_potential_v4_3.ino

 Measures current while holding the anode potential close to a specified value

 ================================================================
 ***** ONLY WORKS WITH CIRCUIT VERSION 4.3 **********
 ================================================================

 30 minutes in open circuit mode .
 During off mode, log all of the same data as the other part of the sketch.

 Changes:
 - Using only one digital pot now - removed #2 (Analog 2 & 3)
 - Added ADS1115 library + code
 - Changed digipot cs pin to D7
 - Fixed issue with digitpot CS pin
```

```
 - Removed code for 2nd digipot

 Last modified: 12/8/14 - Adam Burns - burns7@illinois.edu
 */
#include <Wire.h>
#include <Adafruit_ADS1015.h>

Adafruit_ADS1115 ads;
#include <SPI.h>
int power1state = LOW;
boolean offState = true;
const int Power1 = 6; // power control for MCP4161 #1 to D6
unsigned long offDuration = 300000; // off mode for 30 mins (1,800,000ms)

int csPin1 = 7; //Chip select Digital Pin 7 for digital pot #1
int trans_sig = 0; // Value sent to digipot
int cnt = 0;
double current=0;
double vol_nor=0;
double cell_vol=0;
int numOfDigits = 5;

#define DEBUG 0 // set to 1 to print debug data to serial monitor

void setup()
{
  Serial.begin(9600);
  SPI.begin();
  ads.begin();
  pinMode(csPin1, OUTPUT);
  pinMode(Power1, OUTPUT);
  digitalWrite(Power1, LOW);

  delay(200);

  // Reset digipot to 0
  digitalWrite(Power1, HIGH);
  delay(200);
  digitalWrite(csPin1, HIGH);
  delay(200);
  digitalWrite(csPin1, LOW);
  SPI.transfer(0);
  SPI.transfer(0);
  digitalWrite(csPin1,HIGH);
  delay(200);

  // Setting digipot to 0 again in case 1st attempt failed
  digitalWrite(csPin1, LOW);
  SPI.transfer(0);
  SPI.transfer(0);
  digitalWrite(csPin1, HIGH);
  delay(200);
  digitalWrite(Power1, LOW);
  delay(200);

  // The ADC input range (or gain) can be changed via the following
  // functions, but be careful never to exceed VDD +0.3V max, or to
  // exceed the upper and lower limits if you adjust the input range!
  // Setting these values incorrectly may destroy your ADC!
  //                                                                ADS1015  ADS1115
  //                                                                -------  -------
  // ads.setGain(GAIN_TWOTHIRDS);  // 2/3x gain +/- 6.144V  1 bit = 3mV      0.1875mV
(default)
```

```
  ads.setGain(GAIN_ONE);        // 1x gain   +/- 4.096V  1 bit = 2mV      0.125mV
  // ads.setGain(GAIN_TWO);        // 2x gain   +/- 2.048V  1 bit = 1mV      0.0625mV
  // ads.setGain(GAIN_FOUR);       // 4x gain   +/- 1.024V  1 bit = 0.5mV    0.03125mV
  //  ads.setGain(GAIN_EIGHT);          //  8x  gain     +/-  0.512V    1  bit  =  0.25mV
0.015625mV
  //  ads.setGain(GAIN_SIXTEEN);       //  16x  gain    +/-  0.256V    1  bit  =  0.125mV
0.0078125mV
  //
  //ADC Range: +/- 6.144V (1 bit = 0.1875mV)
  //
  //analogReference(INTERNAL);
}

void setPot(int pin, int value)//function currently unused
{
  digitalWrite(pin, LOW);
  SPI.transfer(0);
  SPI.transfer(value);
  digitalWrite(pin,HIGH);
}


void loop()
{
  cnt ++;

  if(offState==true){
    unsigned long currentMillis = millis();
    if((currentMillis>offDuration) && (offState==true))
    {
      power1state=HIGH;
      offState=false;
      digitalWrite(Power1,power1state);
      delay(150); // delay for stabilization
    }
  }

  float multiplier = 0.125F; // ADS1115  1x gain   +/- 4.096V (16-bit results) 0.125mV
  double vol_nor;
  double current;
  double cell_vol;



  /*-------- changed to using ads1115 --------------------
   read1 = analogRead(A0);
   delay(7);
   read2 = analogRead(A1);
   delay(7);
   read5 = analogRead(A4);
   double vol = (read1 - read2) * 1.0 /1023 * 1.1;
   double current = vol / 97 * 1000; //Ohm's Law to calculate current based on drop
across 97 ohm resistor
   double vol_nor = (read1 - read5) * 1.0 / 1023 * 1.1; // calculate anode potential
(A0) vs reference electrode (A4)
   double cell_vol = read1 * 1.0 / 1023 * 1.1;
   */
  if(offState==false){
    if (vol_nor < -0.352) trans_sig ++;
    else if (vol_nor > -0.342 && trans_sig >0) trans_sig --;
  }

  digitalWrite(csPin1, LOW);
```

```
  SPI.transfer(0);
  SPI.transfer(trans_sig);
  digitalWrite(csPin1, HIGH);
  delay(200); // let the state change stabilize



  double vol = ads.readADC_Differential_0_1();
  vol=vol*multiplier; //reading in mV
  current = ((vol)/(98.2)); // ohm law

  vol_nor = ads.readADC_Differential_2_3();
  vol_nor= (vol_nor * multiplier)/1000;

  cell_vol = ads.readADC_SingleEnded(1);
  cell_vol=(cell_vol * multiplier)/1000;



#if DEBUG
  Serial.println();
  Serial.print("trans_sig: ");
  Serial.println(trans_sig);
  Serial.print("current: ");
  Serial.print(current, numOfDigits);
  Serial.print(",  annode potential:");
  Serial.print(vol_nor, numOfDigits);
  Serial.print(",  Cell vol:");
  Serial.print(cell_vol, numOfDigits);
  Serial.print(",  vol_drop:");
  Serial.print(vol, numOfDigits);
  Serial.println();
#endif


  /*--------------- only using one digital pot -----------------
   //setPot(csPin2, trans_sig2); // set pot #2
   delay(200); // let the state change stabilize
   read3 = analogRead(A2);
   delay(7);
   read4 = analogRead(A3);
   delay(7);
   read5 = analogRead(A4);
   double vol_nor2 = (read3 - read5) * 1.0 / 1023 * 1.1;
   double vol2 = (read3 - read4) * 1.0 /1023 * 1.1;
   double current2 = vol2 / 97 * 1000;
   double cell_vol2 = read3 * 1.0 / 1023 * 1.1;
   if (vol_nor2 < -0.352) trans_sig2 ++;
   else if (vol_nor2 > -0.342 && trans_sig2 >0) trans_sig2 --;

   digitalWrite(csPin2, LOW);
   SPI.transfer(0);
   SPI.transfer(trans_sig2);
   digitalWrite(csPin2, HIGH);  //-- moved to setPot function - 11/5/14 - AJB

   #if DEBUG
   Serial.println();
   Serial.print("trans_sig2: ");
   Serial.println(trans_sig2);
   #endif
   ------------------------------------------------------*/

  if (cnt == 6){
```

```
    //Printing
    cnt = 0;
    Serial.print(current, numOfDigits);
    Serial.print("  ");
    //Serial.print(current2, numOfDigits);
    //Serial.print("  ");
    Serial.print(vol_nor, numOfDigits);
    Serial.print("  ");
    //Serial.print(vol_nor2, numOfDigits);
    // Serial.print("  ");
    Serial.println(cell_vol, numOfDigits);
    //Serial.print("  ");
    //Serial.println(cell_vol2, numOfDigits);
  }

  delay(10000);

}
```

B.2.2 Linear Sweep Voltammetry

```
/*
lsv_sep_22.ino

 measures current while increasing anode potential at a set rate (1mV/s)

 Start in open circuit mode for 30 minutes, then run LSV

 ================================================
 ***ONLY WORKS ON CIRCUIT V4.3********
 ================================================

 Changes:
 - Moved digital pot communication to end of loop
 - Added ADS1115 library + code
 - Changed SPI CS pin for digipot to D7
 - MOSFET between cathod + digipot & GND - pin D6
 - Read from the ADC after changing the digipot trans_sig

 Last modified: 12/8/14 - Adam Burns - burns7@illinois.edu
 */

#include <SPI.h>
#include <Wire.h>
#include <Adafruit_ADS1015.h>

Adafruit_ADS1115 ads;
int power1state = LOW;
int power2state = LOW;
boolean offState = true;
const int Power1 = 6; // power control for MCP4161 #1 to D6
const int Power2 = 5; // power control for MCP4161 #2 to D5
unsigned long offDuration = 300000; // off mode for 30 mins (1,800,000ms)
int numOfDigits = 5;

int csPin1 = 7; //Chip select Digital Pin 7 for digital pot #1
int csPin2 = 3; //Chip select D3 for digital pot #2
/*
int vol_before_resistor; //Analog Pin 2
 int vol_after_resistor;  //Analog Pin 3
```

```
 int vol_reference;       //Analog Pin 4 *///no longer used
int trans_sig = 0;
int cnt = 0;
int resistor = 98.2; // R2 resistance in Ohms
int lsv_finished = 0;

double target_value;
//double tol = 0.001;
#define DEBUG 0 // set to 1 to print debug data to serial monitor


void setup()
{
  Serial.begin(9600);
  SPI.begin(); //Init SPI
  ads.begin();

  // The ADC input range (or gain) can be changed via the following
  // functions, but be careful never to exceed VDD +0.3V max, or to
  // exceed the upper and lower limits if you adjust the input range!
  // Setting these values incorrectly may destroy your ADC!
  //                                                                ADS1015  ADS1115
  //                                                                -------  -------
  // ads.setGain(GAIN_TWOTHIRDS);  // 2/3x gain +/- 6.144V  1 bit = 3mV      0.1875mV
(default)
  ads.setGain(GAIN_ONE);        // 1x gain   +/- 4.096V  1 bit = 2mV      0.125mV
  // ads.setGain(GAIN_TWO);        // 2x gain   +/- 2.048V  1 bit = 1mV      0.0625mV
  // ads.setGain(GAIN_FOUR);       // 4x gain   +/- 1.024V  1 bit = 0.5mV    0.03125mV
  //  ads.setGain(GAIN_EIGHT);          //  8x  gain     +/-  0.512V    1  bit  =  0.25mV
0.015625mV
  //  ads.setGain(GAIN_SIXTEEN);       //  16x  gain    +/-  0.256V    1  bit  =  0.125mV
0.0078125mV
  //

  pinMode(csPin1, OUTPUT);
  pinMode(csPin2, OUTPUT);

  pinMode(Power1, OUTPUT);
  pinMode(Power2, OUTPUT);
  digitalWrite(Power1,HIGH);
  digitalWrite(Power2, LOW);
  delay(200);

  // Reset digipot to 0
  digitalWrite(csPin1, LOW);
  SPI.transfer(0);
  SPI.transfer(0);
  digitalWrite(csPin1, HIGH);
  delay(200);

  // Setting digipot to 0 again in case 1st attempt failed
  digitalWrite(csPin1, LOW);
  SPI.transfer(0);
  SPI.transfer(0);
  digitalWrite(csPin1, HIGH);
  delay(200);
  digitalWrite(Power1, LOW);
  //analogReference(INTERNAL);
  //delay(offDuration); // stay open for 30 minutes
  //digitalWrite(Power2, HIGH); // power on anode #2
}

void loop()
```

```
{

  if(offState==true){
    unsigned long currentMillis = millis();
    if((currentMillis>offDuration) && (offState==true))
    {
      power1state=HIGH;
      power2state=HIGH;
      offState=false;
      digitalWrite(Power1,power1state);
      digitalWrite(Power2,power2state);
      delay(150); //allow current to stabilize
    }
  }

  float multiplier = 0.125F; // ADS1115  1x gain   +/- 4.096V (16-bit results) 0.125mV
  double vol_nor;
  double current;
  double cell_vol;

  if (cnt==0){
    target_value=vol_nor;
  }
  Serial.print(trans_sig);
  Serial.print("      ");
  Serial.print(current, 10);
  Serial.print("  ");
  Serial.print(vol_nor, 10);
  Serial.print("  ");
  Serial.print(cell_vol, 10);
  Serial.println("  ");


  if(offState==false){
    cnt ++;
    if (cnt % 2 == 0 && cnt != 0)
    {
      target_value += 0.002;
      if (target_value > 0)
      {
        lsv_finished = 1;
      }
    }

    if (lsv_finished == 0)
    {
      if (cnt < 10) target_value = vol_nor;
      else {
        if (cnt % 1 ==0)
        {
          if (vol_nor < target_value)
          {
            trans_sig ++;
            if(trans_sig > 255){
              trans_sig = 255;
            }
            digitalWrite(csPin1, LOW);
            SPI.transfer(0);
            SPI.transfer(trans_sig);
            digitalWrite(csPin1, HIGH);
            delay(100); //allow voltage to stabilize
          }
        }
```

```
      }
    }
    else {
      trans_sig = 0;
      digitalWrite(csPin1, LOW);
      SPI.transfer(0);
      SPI.transfer(trans_sig);
      digitalWrite(csPin1, HIGH);
    }
  }

  double vol=ads.readADC_Differential_0_1();
  vol=vol * multiplier;

  current = ((vol)/(98.2));

  vol_nor = ads.readADC_Differential_2_3();
  vol_nor= (vol_nor * multiplier)/1000;

  cell_vol = ads.readADC_SingleEnded(1);
  cell_vol=(cell_vol * multiplier)/1000;

#if DEBUG
  Serial.println();
  Serial.print("trans_sig: ");
  Serial.print(trans_sig);
  Serial.print(",  current: ");
  Serial.print(current, numOfDigits);
  Serial.print(",  annode potential:");
  Serial.print(vol_nor, numOfDigits);
  Serial.print(",  Cell vol:");
  Serial.print(cell_vol, numOfDigits);
  Serial.print(", Cnt: ");
  Serial.println(cnt);
  Serial.print(", Target: ");
  Serial.println(target_value, numOfDigits);
#endif


  delay(1000);
}
```

B.2.3 Python code

```
from serial import Serial
from serial.tools import list_ports
import os
import datetime

baud = 9600

#Scan USB ports, and find the serial connection to the Arduino
port_list = list_ports.comports()
for line in port_list:
if('usb' in line[2].lower()):
chosenPort = line[0]
ser = Serial(chosenPort,baud)

dt=str(datetime.datetime.now().strftime("%y-%m-%d_%H%M"))
```

```
myfile = open(dt + ".txt", "w")

iteration = 0
while(True):
l = ser.readline()
print(l)
myfile.write(l)
iteration += 1
if(iteration % 12 == 0):
myfile.flush()
os.fsync(myfile.fileno())
```

B.2.4 Field study code

```
#include <SD.h>

/*
  Measures current while holding the anode potential close to a specified value
Logs data to SD card

~2 h cycle:

        20 minutes in open offstate (digiPot at tap pt 0).
              During off mode, log data once per min

       Stepped CA up to 0V vs Ag/AgCl, increments of 0.05 V
              3 min at each potential, data every 10 s

       20 min offstate

       50 min midpoint CA
              data once per min

*/

#include <Adafruit_ADS1015.h>
#include <DallasTemperature.h>
#include <OneWire.h>
#include <RTClib.h>

#include <SPI.h>
#include <Wire.h>


//Pins
#define ONE_WIRE_BUS 5
#define csPin1 7
#define Power1 6
#define SDpin 10
#define redLED 3
#define greenLED 4



//Constant Variables
#define MULTIPLIER 0.125F         // ADS1115  1x gain   +/- 4.096V (16-bit results)
0.125mV
#define RESISTANCE 98.2         // The value of the intrenal resistor
#define TOLERANCE 0.0           // The tolerance of the scan rate.
```

```
#define probeRate 5000 //60000         // Number of millis seconds between consecutive
probe reaadings
#define offDuration 1800000              // The amount of time the program will wait
affter setup to begin the experiment (30 min)
#define numOfDigits 5           // The nuber of didgits a the ADC reading will print
#define digiPotAdjRate 10       /* The number of ADCreads that are taken before
                                   adjusting the digiPotValue*/


//Global Varibles
Adafruit_ADS1115 ads;
OneWire oneWire(ONE_WIRE_BUS); // Temperature probe data line (yellow wire)
DallasTemperature sensors(&oneWire);

//Logfile Varibles
File logfile; // log file

//RTC Varible
RTC_DS1307 RTC; // Real Time Clock object
DateTime now;

//double vol  = 0;
double current=0;
double anodePotential=-.5;
double cell_vol=0;

double target_value = 0;

int digiPotValue = 0; // Value sent to digipot

boolean offState = true;
boolean lsvState = false;
boolean setPotentialState = false;
boolean firstTime = true;
boolean lsvIsNext = true;
boolean targetReached = true;
int cnt = 0;


void readADC();
void printADCreadings(int digits);
void logADCreadings(int digits);
void writeDigiPotValue();

//New COde for'

unsigned long changeTime = 0;
unsigned long lsvIntervalTime = 180000; //3min
unsigned long setPotentialDuration = 1800000; // 30min

void error(){
 while (true){
   digitalWrite(redLED, HIGH);
   delay(500);
   digitalWrite(redLED, LOW);
   delay(500);
 }
}

void setup() {
    //Serial.begin(9600);   // increased baud rate to catch all incoming data
    SPI.begin();
```

```
// ==================== ADC Initilization ========================
    ads.begin();
    ads.setGain(GAIN_ONE); // 1x gain,  +/- 4.096V, 1 bit = 0.125mV

    pinMode(csPin1, OUTPUT);
    pinMode(Power1, OUTPUT);
    pinMode(SDpin, OUTPUT);
    pinMode(redLED, OUTPUT);
    pinMode(greenLED, OUTPUT);
    digitalWrite(redLED, HIGH);
    digitalWrite(greenLED, HIGH);

    delay(200);
    digitalWrite(Power1, LOW);
    delay(200);
    digitalWrite(Power1, HIGH);


    // Temp Probe initilization
    sensors.begin(); // IC Default 9 bit (change to 12 if issues exist)

    digitalWrite(csPin1, HIGH);
    delay(200);

    // Reset digipot to 0 twice.
    writeDigiPotValue();
    delay(200);
    writeDigiPotValue();
    delay(200);

    //digitalWrite(Power1, LOW);
    delay(200);
    digitalWrite(redLED, LOW);
    digitalWrite(greenLED, LOW);

// ==================== SD Initilization ========================
    //Serial.print("SD initialization ");
    // see if the card is present and can be initialized:
    if (!SD.begin(10,11,12,13)) {
        //Serial.println("Card init. failed!");
    }
    digitalWrite(greenLED, HIGH);
    char filename[15];
    strcpy(filename, "BIOLOG00.TXT");
    for (uint8_t i = 0; i < 100; i++) {
        filename[6] = '0' + i/10;
        filename[7] = '0' + i%10;
        // create if does not exist, do not open existing, write, sync after write
        if (!SD.exists(filename)) {
          //Serial.println("cant create file");
          error();
          break;
        }
    }
    digitalWrite(greenLED, LOW);
    logfile = SD.open(filename, FILE_WRITE);
    if( ! logfile ) {

        //Serial.print("Couldnt create ");

        //Serial.println(filename);
        error();
  }
```

```
    //Serial.print("Writing to ");
    //Serial.println(filename);


    Wire.begin();
    if (!RTC.begin()) {
        logfile.println("RTC failed");
        error();
        //Serial.println("RTC failed");
    }
    //Serial.println("RTC initialized");

    logfile.println("experiment,date,time,current,anodePotential,cell_vol,temperature
[C]");

    //Serial.println("date,time,current,anodePotential,cell_vol,temperature [C]");
    //RTC.adjust(DateTime(__DATE__, __TIME__));


    //Serial.println("Setup End");
}

void loop() {
    unsigned long currentMillis = millis();
    if(offState)
    {
        if(currentMillis%10000 ==0)
        {
            readADC();
            cnt++;//printADCreadings(4);
            if((currentMillis>changeTime+offDuration) && (offState==true))
            {

                offState=false;
                if(lsvIsNext)
                {
                   cnt = 0;
                   lsvIsNext = false;
                   lsvState = true;
                   firstTime =true;
                }
                else
                {
                    changeTime = currentMillis + setPotentialDuration;
                    setPotentialState = true;
                    lsvIsNext = true;
                }

                target_value = anodePotential;
                digitalWrite(Power1,HIGH);
                //Serial.println();
                //Serial.println("OffState End");
            }
        }
    }
    else if(lsvState)
    {
        if(currentMillis%2000 == 0)
        {
            readADC();
            if(currentMillis%10000 == 0)
            {
                //Serial.println();
```

```
                //Serial.print("CA: ");
                //Serial.print(target_value);
                //Serial.print(", ");
                printADCreadings(5);
                logfile.print("CA: ");
                logfile.print(target_value);
                logfile.print(",");
                logADCreadings(5);
            }
            if(currentMillis > changeTime && targetReached == true)
            {
                if(target_value > 0)
                {
                    lsvState = false;
                    changeTime = currentMillis;
                    offState = true;
                    digiPotValue = 0;
                    writeDigiPotValue();
                    //Serial.println("LSV END");
                    //digitalWrite(Power1,LOW);
                }
                else{
                    if(firstTime)
                    {
                        double base_value = -.6;
                        while(target_value != base_value)
                        {
                            base_value += .05;
                            if(anodePotential < base_value)
                            {
                              target_value = base_value;
                            }
                        }
                        firstTime = false;
                    }
                    else
                    {
                        target_value+= .05;
                    }
                    changeTime = currentMillis + lsvIntervalTime;
                    targetReached = false;
                }
            }
            if(lsvState){
                if  (anodePotential  <(target_value-.005)  &&  digiPotValue  <  255)
digiPotValue ++;
                else  if  (anodePotential  >  (target_value+.005)  &&  digiPotValue  >0)
digiPotValue --;
                else if(targetReached == false)
                {
                    changeTime = currentMillis + lsvIntervalTime;
                    targetReached = true;
                }


                writeDigiPotValue();
            }
        }
    }
    else if(setPotentialState)
    {
        if(currentMillis%10000 == 0)
        {
```

```
            readADC();
            cnt++;
            if(currentMillis > changeTime)
            {

                    setPotentialState = false;
                    offState = true;
                    changeTime = currentMillis;
                    digiPotValue = 0;
                    writeDigiPotValue();
                    //Serial.println("SetPotential END");
                    //digitalWrite(Power1,LOW);
            }
            if(setPotentialState)
            {
                if (anodePotential  < -0.352 && digiPotValue < 255) digiPotValue ++;
                else if (anodePotential > -0.342 && digiPotValue >0) digiPotValue --;
                writeDigiPotValue();
            }
        }
    }
    if(cnt == 6 && (offState || setPotentialState))
    {
        //Serial.println();
        if(offState)
        {
            //Serial.print("offstate, ");
            logfile.print("offstate,");
        }
        else
        {
            //Serial.print("midpoint, ");
            logfile.print("midpoint,");
        }
        printADCreadings(5);
        logADCreadings(5);
        cnt = 0;
    }

}

void readADC()
{
    double vol = (ads.readADC_Differential_0_1()) * MULTIPLIER; // Voltage reading
    current = ((vol) / (RESISTANCE)); // ohm's law
    anodePotential = ((ads.readADC_Differential_2_3()) * MULTIPLIER) / 1000;
    cell_vol = ((ads.readADC_SingleEnded(1)) * MULTIPLIER) / 1000;
    sensors.requestTemperatures();
}

void writeDigiPotValue()
{
    if (digiPotValue > 255)
    {
        digiPotValue = 255;
        //Serial.println(" ERROR: Digipot exceeding max value (255)");
    }

    if(digiPotValue < 0)
    {
        digiPotValue = 0;
        //Serial.println(" ERROR: Digipot has fallen bellow the  min value (0)");
    }
```

```
    digitalWrite(csPin1, LOW);
    SPI.transfer(0);
    SPI.transfer(digiPotValue);
    digitalWrite(csPin1, HIGH);
}

void printADCreadings(int digits)
{
    //Serial.print("digiPotValue: ");
    //Serial.print(digiPotValue);
    //Serial.print(",  current: ");
    //Serial.print(current, digits);
    //Serial.print(",  annode potential:");
    //Serial.print(anodePotential, digits);
    //Serial.print(",  Cell vol:");
    //Serial.print(cell_vol, digits);
    //Serial.print(",  Temp:");
    //Serial.println(sensors.getTempCByIndex(0));
}

void logADCreadings(int digits)
{
    now = RTC.now();
    // log time
    logfile.print(now.month(), DEC);
    logfile.print("/");
    logfile.print(now.day(), DEC);
    logfile.print("/");
    logfile.print(now.year(), DEC);
    logfile.print(",");
    logfile.print(now.hour(), DEC);
    logfile.print(":");
    logfile.print(now.minute(), DEC);
    logfile.print(":");
    logfile.print(now.second(), DEC);
    logfile.print(",");
    logfile.print(current,digits);
    logfile.print(",");
    logfile.print(anodePotential, digits);
    logfile.print(",");
    logfile.print(cell_vol, digits);
    logfile.print(",");
    logfile.print(sensors.getTempCByIndex(0), digits);
    logfile.println();
    logfile.flush();

}
```